Manuel Hündler, BSc

Isolating the iron storage protein ferritin from human brain tissue and characterizing its iron core via electron microscopic techniques

MASTER'S THESIS

to achieve the university degree of
Master of Science

Master's degree program:
Biochemistry and Molecular Biomedical Sciences

submitted to

Graz University of Technology

Supervisor
Assoz. Prof. Priv.-Doz. Mag. Dr.rer.nat., Gerd Leitinger

Gottfried Schatz Research Center for Cell Signaling, Metabolism and Aging
Divison of Cell Biology, Histology and Embryology

Research Unit Electron Microscopic Techniques
Co-Supervisor: Mariella Sele, MSc

Graz, January 2019

AFFIDAVIT

I declare that I have authored this thesis independently, that I have not used other than the declared sources/resources, and that I have explicitly indicated all material which has been quoted either literally or by content from the sources used. The text document uploaded to TUGRAZonline is identical to the present master‘s thesis.

Graz, 25th of January

Location, Date

Signature

Danksagung

Zuallererst möchte ich meinem Betreuer Gerd und seinem gesamten Team danken. Danke dafür, dass ihr mich so herzlich aufgenommen habt und immer ein offenes Ohr hattet, wenn es mal Probleme gab. Ein herzlicher Dank an Elisabeth und Lissi für ihre Expertise bei Einschulungen und ihre scheinbar „unendliche“ Geduld. Etwaige Fragen blieben nie unbeantwortet. Vielen Dank lieber Gerd für die Betreuung der Arbeit, und dass ich mich zu jeder Zeit an dich wenden konnte. Ich habe mich immer als vollwertiges Teammitglied gefühlt.

Im Speziellen möchte ich meiner Zweit-Betreuerin Mariella danken. Danke für den respektvollen und professionellen Umgang. Ohne deine zahlreichen Tipps und Anmerkungen wäre diese Arbeit sicher nicht das geworden, was sie jetzt ist. Ich konnte dich immer um Rat fragen, wenn ich mal am Schlauch stand. Unsere Diskussionen haben meine Sichtweise auf gewisse Dinge nachhaltig beeinflusst. Danke auch für die zahlreichen Ratschläge abseits dieser Masterarbeit.

Ich möchte Karin Kornmüller und ihrem Team danken. Ihr habt euch für meine Arbeit extra viel Zeit genommen und unterstützen mich mit hilfreichen Vorschlägen, die zur Verbesserung der Methode beigetragen haben.

Einen großen Dank möchte ich auch Verena Kohler aussprechen. Ohne deine Erfahrung und Mithilfe wäre dieses hervorragende Ergebnis nie zustande gekommen.

Einen herzlichen Dank all den Leuten der Zellbiologie Arbeitsgruppen. Ich habe mich bei euch immer willkommen gefühlt und kann mit Fug und Recht behaupten, dass ich die meiste Zeit in eurem Labor verbracht habe. Diese Zeit war gefüllt mit Fleiß, Respekt, Hilfsbereitschaft, „Verdächtigungen“ und vor allem Spaß. Bei euch war Lächeln an der Tagesordnung.

Ein riesengroßes Dankeschön an meine gute Freundin Margarita. Du hast mir die nötige Kraft und vor allem Rückhalt gegeben, wenn mein Leben mal nicht so verlaufen ist, wie ich es mir vorgestellt habe. Danke für deine offene Art. Manchmal benötigt man einfach einen nachdrücklichen Schubs in die richtige Richtung. Ich habe mich bei dir immer geborgen und verstanden gefühlt. Danke für die wundervolle Zeit, ohne dich wäre Graz einfach nur eine Stadt gewesen!!

Vielen Dank auch an meine Freunde Nici, Max, Lisa, Simon, Eva, Sophie, Lilli und Natascha. Ihr habt diese Zeit zu der besten gemacht, die ich bisher erlebt habe. Der Spaß stand bei euch an oberster Stelle.

Zu guter Letzt möchte ich meine Eltern und Großeltern danken. Ihr habt mich bei allem unterstützt, was ich erreichen wollte. Ihr habt mir Geborgenheit und viele schöne Momente geschenkt. Ohne euch wäre ich nie so weit gekommen. Ihr habt mir die beste Kindheit ermöglicht, die man sich wünschen kann. Danke dass ihr immer für mich da seid und an mich glaubt!!

Abstract

Iron accumulation in the human brain has been associated with neurodegenerative diseases like Alzheimer disease. The iron storage protein ferritin is of special interest, as its amount and iron load is directly affected by an alteration of intracellular iron level. Today it is commonly excepted that ferritin molecules isolated from different tissues have iron cores of different average size. However, little is known if there are differences in the distribution of ferritin iron load between brain regions and if neurodegenerative diseases could be linked to an alteration of that distribution.

A purification procedure capable of isolating all ferritin species from different brain regions would offer unprecedented insight in their iron load distribution and could contribute in elucidating the appearance of neurodegenerative diseases.

A method was established with pig brain tissue that enabled almost complete isolation of ferritin, in a purity that made reliable identification of its iron core possible. The final purification procedure was then tested on human brain tissue and included homogenization of the tissue sample with the Turrax Homogenizer, heat treatment of the resulted supernatant and protein separation with density gradient centrifugation using a linear glycerine gradient. Once isolated, the iron cores of the ferritin molecules were rendered visible with transmission electron microscopy (TEM) and then automatically identified, counted and geometrically measured. Subsequently, the ferritin iron load distribution was highlighted by generating histograms.

The established purification procedure was capable of isolating almost all ferritin species with an excellent purity, which could be proved with Native-Page and with TEM using negative stained samples. The mean maximal diameter of the ferritin iron core was 4,8 ± 2,1 nm for frontal cortex samples and 5,2 ± 2,2 nm for occipital cortex samples.

The introduced method is capable of isolating ferritin molecules out of brain tissue with an excellent purity in a short period of time (4 days from tissue disruption until the pure concentrated sample). Hence, it can be used for analysing even higher sample numbers, which are commonly required for a statistical relevant statement.

Zusammenfassung

Vermehrte Eisenanreicherung im Gehirn wird mit neurodegenerativen Erkrankungen, z.B. Alzheimer assoziiert. Hierbei kommt dem Eisenspeicherprotein Ferritin besonderes Augenmerk zu, da dessen Gehalt und Eisenbeladung direkt mit der intrazellulären Eisenkonzentration im Zusammenhang steht. Die Tatsache, dass Ferritin Moleküle, die aus verschiedenen Geweben isoliert wurden, unterschiedliche Eisenkerngrößen aufweisen, wird heute als gegeben angesehen. Allerdings besteht wenig Wissen darüber, ob es Unterschiede in der Ferritin Eisenbeladungsverteilung zwischen verschiedenen Gehirnregionen gibt und ob mögliche Änderungen dieser Verteilung mit neurodegenerativen Erkrankungen zusammenhängen. Ein Reinigungsverfahren, das geeignet ist alle Ferritin Spezies aus verschiedenen Gehirnregionen zu isolieren, würde neue Einblicke in dessen Eisenbeladungsverteilung ermöglichen und würde dazu beitragen das Auftreten von neurodegenerativen Erkrankungen aufzuklären.

Es wurde eine Methode auf Basis von Schweinehirnen etabliert, die eine fast vollständige Isolierung von Ferritin erzielte und zwar in einer Reinheit, die eine zuverlässige Identifizierung dessen Eisenkerne möglich machte. Das finale Reinigungsverfahren wurden anschließend auf menschliches Gehirngewebe übertragen und war wie folgt aufgebaut: Homogenisierung der Gewebeprobe mittels Turrax Homogenisator, eine Hitzebehandlung des gewonnenen Überstandes und eine anschließende Proteinseparation mittels Dichtegradientenzentrifugation, die auf einen linearen Gradienten aufbaute. Nach erfolgter Isolierung, konnten die Eisenkerne der Ferritin Moleküle mittels Transmissionselektronenmikroskopie sichtbar gemacht werden, worauf dessen automatisierte Identifikation, Zählung und geometrische Vermessung folgte. Die Ferritin Eisenbeladungsverteilung wurde anschließend über Histogramme aufgezeigt.

Das hier etablierte Reinigungsverfahren ermöglichte uns fast alle Ferritin Spezies in einer exzellenten Reinheit zu isolieren, welche mittels Native-Page und TEM unter der Verwendung von Negativkontrast aufgezeigt werden konnte. Es konnte ein mittlerer, maximaler Eisenkerndurchmesser von 4,8 ± 2,1 nm in Proben vom Frontallappen und 5,2 ± 2,2 nm in Proben vom Occipitallappen nachgewiesen werden.

Die eingeführte Methode ermöglicht eine schnelle Isolierung (4 Tage vom Gewebeaufschluss bis zur reinen, konzentrierten Probe) von Ferritin aus Gehirngewebe in einer exzellenten Reinheit. Daher kann sie auch für eine größere Probenzahl herangezogen werden, die als Basis für statistisch relevante Aussagen benötigt wird.

List of abbreviations

AD	Alzheimer disease
ALS	amyotrophic lateral sclerosis
APP	amyloid precursor protein
BSA	bovine serum albumin
CCD	charged coupled device
DAB	diaminobenzidine
DDM	diaminodiphenylmethane
DGC	density gradient centrifugation
DMT1	divalent metal transporter 1
DTT	dithiothreitol
ECL	enhanced chemiluminescence system
EDS	energy dispersive X-ray spectrometer
EDTA	ethylenediaminetetraacetic acid
EELS	electron energy loss spectroscopy
ER	endoplasmic reticulum
FPN	ferroportin
Ft	ferritin
FTD	frontotemporal dementia
HAADF	high annular dark field
IRE	iron response element
IRP	iron response protein
LIP	labile iron pool
MAMs	mitochondria associated membranes
P-/ TBST	phosphate-/ Tris buffered saline with Tween®
PD	Parkinson disease
PVDF	poly-vinylidene
SAXS	small angle X-ray spectroscopy
SDS-Page	sodium dodecyl sulfate polyacrylamide gel electrophoresis
SEC	size exclusion chromatography
SEM	scanning electron microscopy
TCA	trichloroacetic acid
TDP-43	TAR DNA binding protein 43
TEM	transmission electron microscopy
Tf	transferrin
TFR-1	transferrin receptor 1
UTR	untranslated region

Content table

1 Introduction

Iron is an essential element for all living organisms. It is capable of providing several physiological functions: it is involved in oxygen transport, respiration, lipid metabolism, gene regulation and DNA-synthesis [1], [2]. Most of the iron can be found in the blood, tightly bound to hemoglobin [3]. A big proportion of the remaining iron is securely stored in ferritin, the major iron storage protein [4]. These proteins serve as an iron reservoir, ensuring supply for metabolic processes and functioning as a buffer in case of iron deficiency [5]. However, both its excess and deficiency have severe consequences for human physiology [2], [6] and iron therefore offers an interesting field of study.

1.1 Role of iron in the human brain

Iron plays an important role in human brain development and is involved in many metabolic processes, that when altered can lead to cognitive impairment. Prior the 1970`s, it was thought that neurological alterations during brain development are primarily caused by anaemia and its adverse effect on cerebral oxygenation. Newer findings show that low brain iron concentrations (independently of anaemia) can influence the cerebral energy metabolism through loss of cytochromes and inefficient ATP production and electron transport. Moreover, iron deficiency acutely effects the synthesis of myelin, monoamine neurotransmitter and their receptors, as iron is a cofactor of the involved enzymes [7], [8]. Various studies showed, that iron concentrations differ between different brain regions. Most iron is found in the globus pallidus, putamen, substantia nigra and red nucleus [9], [10].

1.2 Current research & motivation

As one of the first, Fleming et. al demonstrated that brain samples from Alzheimer patients contain more ferritin and iron than brain samples from healthy controls [11]. Thus, iron accumulation may be associated with neurodegenerative diseases [10]. To get further insight, current research tries to answer the following questions: how is the intracellular iron level regulated and how is it transported to other cells [6], [12]–[14]; how is iron incorporated into the ferritin shell [15]–[18] and how is iron released from the iron core, when needed [3], [5].

It is already known that ferritin being isolated from various tissue samples have different iron loading [19], [20], which is in good correlation with the finding that different brain regions have different iron contents [9], [10]. However, little is known if there are differences in the distribution of ferritin iron levels between different brain regions and if neurodegenerative diseases, like Alzheimer could be linked to an alteration of that distribution. The easiest way to enable analysis of ferritin iron loading distribution is to isolate all possible ferritin variants, from apo-ferritin with missing iron core to ferritin molecules with highest iron load.

So far, the most used purification procedure for ferritin is based on the publication of Linder et al. [21]. They utilized the heat stability and the relatively high molecular weight (separation with size exclusion chromatography) of ferritin. Other groups used a similar purification procedure with slight modifications: they added an acidic precipitation step (pH= 4,6 - 4,8) [4], [11], [22]–[24], or combined the heat precipitation with methanol precipitation [25], [26]. Highest purity could be reached by including a polishing step in the purification procedure (preparative electrophoresis [22]–[24], [27] or anion exchange chromatography [28], [29]). Only two groups were found to use ultracentrifugation for purifying ferritin [30], [31]. However, their described procedures were time consuming, as one is based on two ultracentrifugation runs, using different gradients, while the other needed a subsequent step (size exclusion chromatography). To our knowledge, we were the first who achieved sufficient ferritin purity with a short heat precipitation step and only one ultracentrifugation run, making use of a linear density gradient.

Isolated ferritin was the subject of several studies: a lot of research ran into structural characterization of the protein shell and its tissue related composition, thereby elucidating the functions of the two subunits [17], [27]–[29]; other groups focused on stability tests and subjected the ferritin molecules to heat [23], [32], [33], acidic pH [33]–[36] and chaotropic agents [32], [33], [37]. Wang and Fei showed the general function of ferritin in vivo: they described neuroprotective and even immunological properties [38], [39]. However, only a few publications were found concerning the determination of the mean ferritin iron core size in different tissue samples [19], [20], and even less data was available towards analysis of ferritin iron load distribution in dependence of neurodegenerative diseases.

This master thesis provides a method for an efficient isolation of ferritin out of different brain regions, which enables further analysis of their iron load distribution. The purification procedure was established with pig brains and once it met our requirements, transferred to human brain tissue. Two samples of the frontal cortex and two of the occipital cortex were analyzed from three different brains. The purification procedure included a fast heat precipitation step and a subsequent separation of the protein mixture by density gradient centrifugation using a linear glycerin gradient. The pooled ferritin fractions were visualized to detect differences in their iron load with transmission electron microscopy. Automated identification, count and geometric measurement of the ferritin iron cores were done with the CellProfiler™ program and the iron load distribution statistically evaluated with SPSS®.

1.3 Background

Since iron resorption from diet is very poor (10 - 15 % of total iron intake), human physiology is geared towards iron retention. Nevertheless, the human body is vulnerable to significant iron loss, caused either by an injury or menstrual bleeding [3]. That is may be the reason, why excess of iron is stored in ferritin molecules. Another reason is that unbound iron ions, also known as the “labile iron pool (LIP)”, are toxic for the human body [6]. Hence, there are several regulation mechanisms, with a complex connection to

each other, keeping the LIP on a constant level. An overview about this complex regulation process is given in the following sections and rendered visible in Figure 1.

As free iron is toxic, it must be transported in a secure bound state. This is accomplished with transferrin (Tf), a glycoprotein transporter, which circulates in the blood until it is recognized by transferrin receptor-1 (TFR-1). Cells with embedded TFR-1 on their surface then take up the Tf-TFR-1 complex by receptor mediated endocytosis. Once internalized, the evolved endosome is acidified, which facilitates iron release from TFR-1. After reduction to Fe^{2+}, iron is delivered to the cytosol by divalent metal transporter 1 (DMT1). These iron ions are part of the LIP, being either used for metabolic purposes or stored securely in ferritin. Excess iron can be transported back into the blood via ferroportin (FPN), another divalent-iron transporter, where it again bind to transferrin after oxidation to Fe^{3+} by transferrin itself or by another ferroxidase [5], [6], [12].

Another way to release iron into the blood circle is the secretion of cytosolic ferritin, thereby contributing to the serum ferritin level. In contrast to cytosolic ferritin, serum ferritin molecules consist predominantly of truncated light chain ferritin subunits, which are also found in lysosomal fractions. Cohen et al. hypothesized that the truncated light chain may be a product of lysosomal processing and that processed ferritin is secreted via a non-classical lysosomal secretory pathway [40].

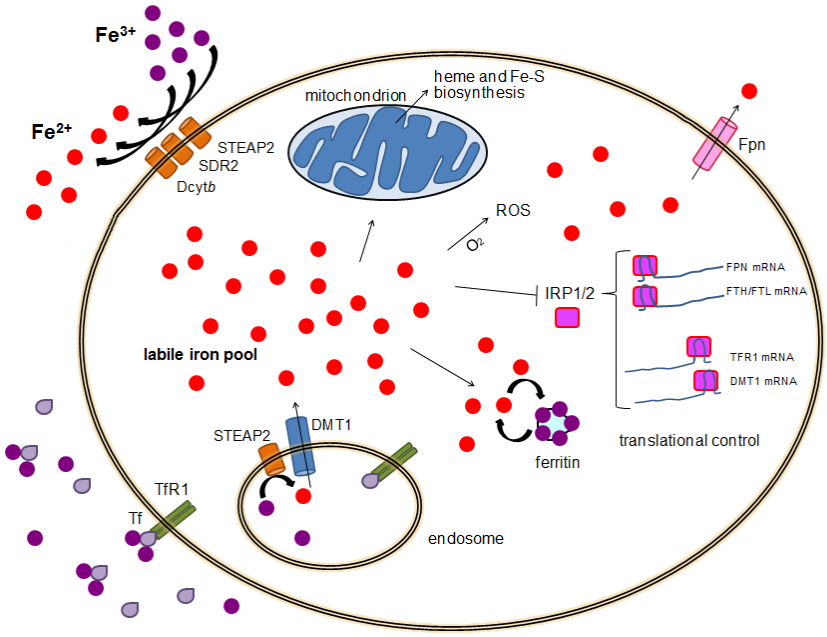

Figure 1. Intracellular iron trafficking: *this picture gives an overview about well-known iron homeostasis pathways (adapted from* [41]*).*

At subcellular level, the expression of TFR-1, FPN, DMT1 and ferritin (Ft) is modulated by the iron response element (IRE)/ iron response protein (IRP)-system, thereby balancing the LIP. The m-RNA of many iron regulating proteins possesses an IRE sequence, which is either located at their 5` untranslated region (5` UTR) in case of ferritin and FPN, or at their 3` untranslated region (3` UTR) for TFR-1 and DMT1. When the IRE at the 5` UTR is bound by one of the iron response proteins, 1 or 2 (IRP-1 or 2), the ribosome

binding sequence is blocked, resulting in the repression of protein-expression. Binding to the 3` UTR renders the m-RNA even more stable against nuclease caused degradation, thus raising the capability for protein translation. Iron deficiency triggers IRP binding to IRE sequences, thereby stimulating TFR-1 and DMT1 expression, which facilitates iron influx, while FPN and Ft production is repressed. The opposite process takes place with excess iron [5], [6], [12].

In addition to iron uptake from the environment, intracellular iron levels can be restored by making use of iron filled ferritin molecules. It is already known, that iron can be released from ferritin molecules via lysosomal degradation of their protein shell [5]. Other mechanisms need to be investigated in further detail. Under in vitro conditions, iron can be easily solubilized from isolated ferritin molecules by treatment with reducing- and/ or chelating agents [42]. However, this process has not been observed in vivo. La et al. showed, that treatment of cells with reducing- and/ or chelating agents do not influence the LIP at all. Hence, they concluded, that lysosomal degradation is the major route for iron release out of ferritin molecules [3].

In case of an iron deficiency, iron filled ferritin molecules can bind to the autophagic cargo receptor NCOA4, which mediates its entry into autophago-lysosomes. Once internalized, the protein shell is degraded by lysosomal proteases and the iron core solubilized by treatment with reducing agents being present in relatively high concentrations. Freed iron ions are transported back to the cytosol via DMT1 [3], [5]. Interestingly, ferritin binding to NCOA4 and DMT1 association with autophago-lysosomes are modulated by the iron-ion concentration in the cytosol and in the lysosome, respectively [3], [43].

Apart from that, it seems that the iron core protects ferritin molecules against proteasomal degradation, as degradation of ferritin in the cytosol does not contribute to the LIP [5].

Although iron is essential for the human metabolism, its excess and deficiency contributes to various pathological states ranging from anemia to toxicity due to reactive oxygen species production via fenton reaction [2], [44]. Novel studies have further demonstrated that iron accumulation in the brain, especially in basal ganglia, could be linked to neurodegenerative diseases and aging [10], [45]. Iron retention in various cell types, such as neurons, is the result of a dysregulated iron homeostasis. This triggers lipid peroxidation and aggregation of proteins, which eventually lead to neuronal cell death via ferroptosis [6]. In addition to that, uncontrolled iron levels can directly induce DNA damage [46], can disable p53 mediated DNA repair [47] and have the potential to alter the epigenome via DNA hypomethylation and mobilization of transposable elements [48], [49]. An overview of these mechanisms is given below.

Membrane lipids are not evenly distributed across the lipid bilayer, but two lipids, cholesterol and sphingomyelin, form ordered microdomains, the so-called lipid rafts. These domains contain a subset of plasma proteins, which are crucial for neurotransmission and iron efflux [6], [50]. Mitochondria associated membranes (MAMs) also house the main actors of Alzheimer disease (AD), Parkinson disease (PD), amyotrophic lateral sclerosis (ALS) and frontotemporal dementia (FTD), such as amyloid precursor protein (APP), tau, alpha synuclein and TAR DNA binding protein 43 (TDP-43) [51]. Since membrane rafts,

endoplasmic reticulum (ER) rafts and MAMs manly consist of lipids, they are vulnerable to lipid peroxidation, leading to membrane distortion and damage and thereby impairing neurotransmission [52], [53]. Another process caused by lipid peroxidation is ferroptosis, which defines a regulated iron dependent cell death being associated with neurodegeneration [6].

Mollet et al. showed in cultured endothelial cells that iron induce direct DNA damage, triggering rapid changes in RNA expression profiles and p53 mediated DNA repair mechanisms [46]. This result highlights the role of p53 in maintaining genome integrity, hence it is called “guardian of the genome”. However, a recent study showed, that p53 possesses an iron binding site, which enables excess iron to inactivate this protein, thereby impairing genome repair [47]. This mechanism is equivalent to what was found in mitochondria, where iron-p53 inactivation promotes iron accumulation, leading to mitochondrial DNA damage, which eventually disrupts these organelles as noted in many neurodegenerative disorders [13], [54]. Apart from inactivating this protein, recent studies documented an iron promoted conformational change of p53 and its association with amyloid aggregates, a process known as p53 amyloidogenesis. This process is possible linked with neurodegeneration [14], [55]

Elevated iron levels are not only capable of damaging DNA, but also of affecting the epigenome by altering DNA methylation [46]. A novel study reported lipid peroxidation to trigger cellular senescence through upregulation of DNA methyltransferase 3A and 3B, thereby altering global and promotor specific methylation [56]. Sturm et al. connected genomic hypomethylation with the mobilization of transposons or transposable elements, a process which is associated with aging, cancer [48] and neurodegeneration [6].

Taking these points under consideration, the accumulation of free iron must be prevented among each cell-type. One possibility to do so, is the storage of free iron in ferritin.

Ferritin has a hollow symmetrical structure made up of 24 subunits, resulting from a self-assembly of heavy- (~ 21 kDa) and light (~ 19 kDa) chain subunits to an ~ 480 kDa oligomer. The protein shell has an outer diameter of ~ 12 nm and an inner diameter of ~ 8 nm. The hollow space can be used for iron mineralization, allowing iron to enter through 8 hydrophilic channels along the 3-fold symmetry axes until reaching a maximum of 4500 - 5000 atoms. Overall the ferritin molecule has a cubic point group symmetry of 432 [16], [18], [57]. The two types of subunits can co-assemble in various ratios, thereby determining how fast and how much iron is incorporated into the protein shell to form the iron core. Carmona and his team demonstrated that there is a preference of certain subunit ratios for certain types of tissue. Tissues that exhibit high metabolic activity (e.g. heart and brain) have ferritin molecules with high proportion of the heavy-chain subunit, while ferritin molecules present in tissues responsible for iron storage (e.g. liver and spleen) have higher proportion of the light-chain subunit. Moreover, ferritin molecules that have up to 90 % light-chain subunits have a low turnover for iron oxidation but can house a relatively high amount of iron (> 1500 iron atoms per protein shell). In contrast, molecules with high heavy-chain proportion show a high iron oxidation turnover, but a low average iron content (< 1000 iron atoms per protein shell) [15].

The heavy-chain subunit has a hydrophilic region, the di-nuclear ferroxidase center, where rapid pairwise oxidation of Fe^{2+} to Fe^{3+} in presence of molecular oxygen occurs [15], [17]. On the other side, the light-chain subunit lacks an enzymatic activity, but has a high number of carboxyl groups on the inner surface, which provide efficient sites for iron nucleation and mineralization [16]. Mehlenbacher et al. provided further evidence, that light-chain ferritin subunit is not only responsible for nucleation and mineralization, but also for facilitating iron oxidation at the heavy- chain ferroxidase center. Hence, a complex interaction between both subunit- types seems necessary for an efficient iron core formation.

The general iron core formation process involves binding of two Fe^{2+}-ions to the ferroxidase center, a μ-1,2-peroxo-diFe(III) intermediate is formed in the presents of molecular oxygen. The evolving of a μ-oxo(hydroxo)-bridged diiron(III) complex and eventually the formation of small iron clusters which finally merge to the iron core itself. The evolving iron core then serves as nucleation site, where incoming Fe^{2+} can be alternatively oxidized and deposited. Commonly the iron core formation is based on the following reactions [15]:

$$2Fe^{2+} + O_2 + H_2O \rightarrow 2Fe(O)OH_{(core)} + H_2O_2 + 4H^+$$

(*ferroxidation reaction*)

$$4Fe^{2+} + O_2 + 6H_2O \rightarrow 4Fe(O)OH_{(core)} + 8H^+$$

(*mineral surface reaction*)

$$2Fe^{2+} + H_2O_2 + 2H_2O \rightarrow 2Fe(O)OH_{(core)} + 4H^+$$

(*detoxification reaction*)

High annular dark field (HAADF) imaging in combination with single particle analysis on isolated ferritin molecules revealed a subunit structure of the iron cores, which were assembled in a cubic array (eight subunits in total). This type of arrangement reflects the eight, three-fold symmetry channels, showing their purpose for iron entry into the protein shell. It was also demonstrated that the iron core subunits are not uniformly crystalline, but are made of crystalline domains surrounded by more disordered material. The disordered fraction is likely to crystallize over time with ongoing iron influx [16]. When the ferritin shells are not fully loaded, an absence of density in the center of the iron core can be expected, as it was observed by the groups of Pan and Jian with the 2D-projection of the iron cores [16], [57].

Since the physiological body temperature of humans is ~ 37 °C, it is unusual for human proteins to have high thermal stability. However, Stefanini et al. showed that equine spleen apo-ferritin (~ 90 % light-chain proportion), is stable up to 93 °C (= T_m, melting temperature), whereas recombinant human heavy-chain apo-ferritin is stable up to 77 °C, both at physiological conditions (pH= 7). Moreover, the denaturation process of ferritin seems to be partly reversible. Destabilization with 2M guanidine-HCl, a chaotropic agent, or acidification to pH= 4, decreased the melting temperature only to 82 or 90 °C for equine spleen ferritin and to 60 or 67 °C for recombinant heavy-chain ferritin. However, there is a considerable difference between heavy- and light-chain rich ferritin molecules [32]. The groups of Stefanini and Santambrogio

hypothesized that a salt bridge inside the four-helix bundle of the light chain subunit confers further stability to light-chain rich ferritin molecules [32], [33]. These initial results indicate not only thermal stability, but also stability against low pH and presence of chaotropic agents. Kim et al. concluded via small angle X-ray spectroscopy (SAXS) that equine spleen apo-ferritin is stable up to pH= 3,4 and noting a partial reassembly properties for denatured ferritin [34]. Interestingly, Listowsky et al. demonstrated that iron filled equine spleen ferritin is less stable in presence of 7M guanidine-HCl, than apo-ferritin with missing iron core, thus iron not only confers stability against proteasomal degradation, but also against treatment with denaturizing agents [37].

By considering these results, it should not be surprising that the relatively high stability of human ferritin (compared to other proteins in the human body) can be utilized for its purification.

2 Principle

This chapter describes the general principles of methods for protein purification and ultrastructural characterization, exploited during this work. When purifying proteins, the purity that needs to be achieved depends on the type of further analyses. Ultrastructural characterization of the ferritin iron load demands no highly pure protein. Nevertheless, high enrichment and purity concerning the monomeric state of ferritin should be aimed for. There is no standard protocol for protein purification, because each cell type, each tissue type, and each protein requires special treatment. Size and cell wall characteristics of cells as well as chemical and physical properties of proteins must be considered, when thinking about the purification strategy [58], [59]. According to Hubert Rehm, it is advisable to use up to four purification steps that meet the following requirements: no step must have a purification factor (enrichment of the protein of interest compared to the impurities) under five, no step must have a yield under 30 % and their overall duration should not exceed 24 h [60].

2.1 Homogenization

Except for extracellular proteins, a homogenization step is indispensable to make proteins accessible. However, two points must be considered concerning homogenization: first, the method/ tool used for the homogenization process, and second, an appropriate lysis buffer for efficient cell disruption and stabilization of the target protein. Both depend on the protein`s location, their physical properties, and the desired yield [58]. As we are interested in the comprehensive isolation of each ferritin species, complete liberation should be aimed for, regardless of organelle integrity. Here a one-step homogenization process was compared with a two-step one. Since physiological conditions get lost through the homogenization process, the lysis buffer should provide the following characteristics [59]:

- Protection from proteases
- Preserving the native state of the protein (pH, ionic strength, …)
- Prevention of aggregation
- No interference with further analysis

2.1.1 Utilizing Turrax Homogenizer

The tool of choice here, for disintegrating cell-cell contacts and subsequently disrupting their membrane structures was the Turrax Homogenizer. This rotor-stator homogenizer works by means of shear forces applied to the sample. A rotor-stator is composed of two parts: an outer stationary tube (stator) and an inner turning shaft (rotor), which is connected to a motor. Shear forces are generated by slots located at the bottom of the rotor-stator on both, the stator and the rotor. Sample components entering these slots are effectively sheared by fast rotor-rotation. The Turrax Homogenizer enables production of uniform sample-suspensions in a short period of time. However, heat generation through the homogenization process must be reduced at least by continuously cooling sample on ice. When working with fibrous

material, connective tissue can be get caught within the shaft assembly, leading to reduced homogenization efficiency, which requires repeated cleaning of the assembly [58].

2.1.2 Sonication

In the two-step homogenization approach, ultrasonic waves are directed at the remaining cell components after initial protein extraction with the Turrax Homogenizer. Here, the disruption process is based on cavitation. Cavitation describes a process where microscopic shock waves are produced through rapid oscillation of piezoelectric crystals being attached to a metal probe. During crystal contraction, small vacuum cavities are formed, which subsequently implode when the crystal expands, generating so-called micro jets that destroy membrane structures. Compared to shear forces, even more heat is released during cavitation. Thus, only short recurring pulses of oscillation should be applied [58], [59].

2.2 Ammonium sulfate precipitation and -fractionation

The utilization of ammonium sulfate in protein purification provides various benefits. It can be used either for protein stabilization, -concentration or -fractionation (in terms of purification) [61], [62]. Protein solubility decreases with higher concentration of a certain salt, showing antichaotropic properties. The so-called “salting out” effect is based on the competing nature of antichaotropic salts for water molecules. Hence, the proteins lose their hydration shell, which results in an increase of hydrophobic interactions, promoting aggregation [59], [62]. The ability of a certain salt to precipitate proteins is described in the Hofmeister series. Wingfield has proposed that the likelihood of precipitation of proteins increases with higher molecular weight. This under consideration, the first step in protein fractionation is usually to precipitate as many impurities as possible, before the protein of interest is precipitated with an even higher salt concentration. Subsequently, the protein of interest can be resolved in the buffer of choice. A relatively high ionic strength remains, which can interfere with further purification steps. Thus an additional desalting step might be necessary [59], [61].

2.3 Size Exclusion Chromatography (SEC)

Size exclusion- or gel filtration chromatography describes a separation method based on the hydrodynamic volume of proteins, which corresponds to their molecular weight. The stationary phase used for separation is made of porous beads. Low-molecular weight proteins can permeate into the pores of the stationary beads, while bigger proteins are excluded and elute in the void volume of the column. Additionally, small proteins that exhibit a high permeation coefficient, spend even more time within the pores than bigger ones. The bigger/ heavier a protein, the lower their permeation coefficient. A major advantage of size exclusion chromatography is the use of a non-binding porous stationary phase, which makes harsh elution conditions expendable. Two different operating types are known: group separation and high-resolution fractionation. In group separation, small molecules are removed from big molecules, thus making this method predestined for desalting or bugger exchange processes. As we aim to purify,

high-resolution fractionation has been the method of choice [61], [63]. Proteins with known molecular mass/ column depended retention time can be used for calibration to estimate the molecular mass of other proteins [50]. Some parameters may be considered to enhance the resolution of separation: sample volumes under 2 % of the column volume are desired (at least 5 %); utilizing a lower flow-rate; avoiding protein concentrations above 70 mg/ mL; a low salt concentration is recommended to eliminate possible electrostatic interactions [61].

2.4 Density Gradient Centrifugation (DGC)

Ultracentrifugation can be used either analytically for sedimentation rate measurements or preparatively for separation of particles. Protein purification via centrifugation is based on size and density depended separation of particles. Three different variations for separation are known: differential-, zonal- and isopycnic centrifugation. Briefly, separation characteristic of differential centrifugation is based on different sedimentation rates of particles only. Zonal- and isopycnic centrifugation both are based on a density gradient that enhances the separation of particles that do not differ sufficiently in sedimentation rates. All particles have the same starting point in contrast to differential centrifugation, as the protein mixture is layered on the top of the gradient [59], [64]. Sedimentation rates of particles in viscous fluids, such as density gradients, can be described by Stokes-`law, where v is the sedimentation rate, g is the relative centrifugal acceleration, d is the particle diameter, ρ_p and ρ_m are the density of particle and medium, respectively, and η is the viscosity of the medium:

$$v = \frac{d^2(\rho_p - \rho_m)g}{18\eta}$$

(Sedimentation rate)

While differential- and zonal centrifugation are suitable for separation of particles that differ in size, equal sized particles with different density are poorly separated. For such a case, isopycnic centrifugation is the technique of choice. Proteins show relatively homogenous density and sedimentation coefficient properties, but differ in size. Here, zonal centrifugation was selected for ferritin purification, as viscosity and density of the medium can be adjusted for selective separation [59].

2.5 Determination of protein concentration

When establishing a method, it is essential to assess each step for effectiveness and efficiency. Advisable points during protein purification, which should be monitored, are yield and relative enrichment of the target protein. One opportunity to meet this recommendation is a reliable and robust protein quantification assay. Here, the Lowry assay was selected, as it tackles the challenges accompanied with tissue extracts [60]. The assay is a modification of the biuret assay. In an alkaline environment, Cu2+ ions become complexed between two molecules presenting at least two peptide bonds giving a purple color, referred to as biuret reaction. The next step involves reduction of the Cu2+ to Cu1+ ions through tyrosine, tryptophan, cysteine, cysteine and histidine residues of the protein to be measured. This supports the

reduction of molybdate, a component of the Folin Ciocalteau phenol reagent. The end result is an intense blue color, whose absorption value corresponds in a linear manner (at 620 nm) to the amount of protein present in the sample. The additional color reaction is responsible for its higher sensitivity compared to the biuret assay [60], [65].

2.6 Electrophoresis

Electrophoresis describes the migration of charged particles exposed to an electric field. As migration characteristics of particles depends on their level of charge, size and structure. Differences, regarding these points can be utilized for separation of protein mixtures into singular zones. Basically, three different variations are available: zone electrophoresis employing a homogenous buffer system, isotachophoresis with a discontinuous buffer system and isoelectric focusing with a pH gradient. Furthermore, a subdivision into SDS-Page and Native-Page exploiting denaturing and native conditions, respectively, is possible [66].

2.6.1 Sodium dodecyl sulfate poly-acrylamide gel electrophoresis (SDS-Page)

SDS-Page belongs to the isotachophoresis techniques and their gel matrix consists of two distinct parts: a stacking gel layered on a resolving gel, which are made with buffers that differ in pH, hence, it is called discontinuous buffer system. Compared to zone electrophoresis, the additional stacking gel is responsible for the so called “stacking effect”. Proteins get ordered according to their net charge or electrophoretic mobility, providing several benefits, such as prevention of protein aggregation and the production of sharper bands [66]. In general, sodium dodecyl sulfate (SDS) is added to the protein mixture and covers the intrinsic charges of each protein with a constant negative charge per mass unit (appr. 1,4 g SDS per g protein). Thus, only their size difference (~ molecular weight) remains for separation. In combination with a reducing agent, such as ß-mercaptoethanol and heat, SDS lead to complete denaturation of each protein. Glycosylated proteins must be considered separately, as they bind much less SDS, slowing down migration through the gel and thus, leading to overestimation of their molecular weight [60], [66].

2.6.2 Blue-Native-Page

Native-Page electrophoresis is based on the same general principle as SDS-Page, except that the native state of the proteins is preserved. Negatively charged proteins are separated according to their net charge and size. The required negative charge can either be produced by pH shift, considering the isoelectric point of the proteins to be separated, or similar to SDS-Page, by a charged dye, that specifically binds to proteins. In case of the Blue-Native-Page, the anionic dye Coomassie Brilliant blue shows a strong binding affinity to hydrophobic areas of proteins. Since the dye binds preferable to hydrophobic areas, cytoplasmic proteins, such as ferritin are almost excluded. Thus, the negative charge per mass unit is not constant throughout the protein mixture. Both, hydrodynamic diameter (~ molecular mass) and charge therefore influence protein migration pattern [60], [66], [67].

2.7 Western Blotting

Western blotting provides a sensitive technique for specifically detecting the target protein among other proteins present and can be used for relative quantification. Thus it is an essential tool to assess the relative enrichment of the target protein [68], [69]. Furthermore, degradation products can be easily visualized, which may emerge due to proteolytic degradation during purification, highlighting inappropriate conditions (e.g. too little protease inhibitor, too high temperatures) or due to autolytic processes within the brain tissue during storage.

2.7.1 Electroblotting

Since the proteins separated by electrophoresis are enclosed in the gel matrix, they are not directly accessible for immunodetection and must be transferred onto a suitable carrier membrane. Nitrocellulose membranes for example exhibit a higher binding affinity for low molecular weight proteins and have a strong retention ability. In contrast, poly-vinylidene fluoride (PVDF) membranes provide better mechanical properties, as nitrocellulose is brittle, and higher binding capacities. However, their background signal is higher, which makes the subsequent blocking and washing steps even more important. The membrane is placed onto the gel, sandwiched between buffer-soaked filter papers and sponges and eventually fixed in a grid cassette, which is inserted vertically into the transfer tank filled with transfer buffer, as depicted in Figure 2. The transfer is proceeded by applying a constant electric field perpendicular to the surface of the gel, causing the negatively charged proteins to be pulled out of the gel matrix and moving towards the anode until they are trapped onto the membrane. The bigger the protein, the longer the transfer takes [60], [66], [68].

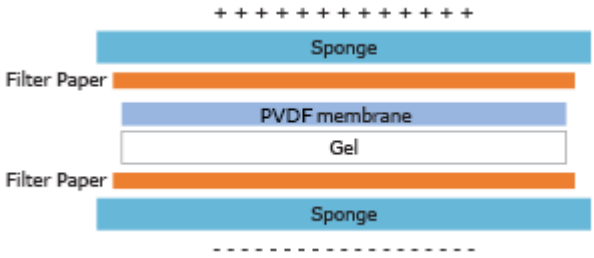

Figure 2. Arrangement of the components for western blot transfer: *separated proteins are forced from the gel onto the membrane after applying an appropriate voltage.*

2.7.2 Blocking, antibody concentration and washing

Ideally, the selected primary antibody should only recognize target protein epitopes. In practice however, unspecific binding properties for impurities and even binding to the membrane itself remain challenging. For the latter it is indispensable to block antigen-free areas with an appropriate blocking solution, like bovine serum albumin (BSA) or non-fat dry milk diluted in Phosphate- or Tris Buffered Saline with Tween (PBST or TBST). The blocking reagent must not interfere with the detection method [68], [69]. Different antibody concentrations should be tested to further reduce unspecific binding while preserving their specific binding affinity, thus optimizing the signal to noise ratio [70]. In addition to that, subsequent

washing steps after each antibody incubation step remove unbound and even unspecific weakly bound antibodies, as the washing buffer contains a nonionic detergent (e.g. Tween) [60], [68]–[70].

2.7.3 Immunodetection

The primary antibodies bound to the target proteins are incubated with so-called secondary antibodies, which exhibit high specificity for the primary antibody. Secondary antibodies are labeled such as the antigen-antibody binding can be visualized through fluorescence-, luminescence-, radioactivity-, chemical- or enzymatic color reactions. The obtained signal indirectly reflects the amount of antigen. An enhanced chemiluminescence system (ECL) has been selected for this project. Briefly, horseradish peroxidase is linked to the secondary antibody and catalyzes the cleavage of a chemiluminescent agent resulting in emitted light. The intensity can be measured with a charge coupled device camera (CCD) [60], [69], [70].

2.8 Transmission Electron Microscopy (TEM)

The use of TEM enables us to analyze even the smallest structures, such as proteins, at near-atomic resolution, which would not be possible with conventional light microcopy. The relatively high wavelength of visible light limits the resolution of conventional light microscopes to ~ 200 nm [50], based on the following equation (defined as the Abbe-limit):

$$d = \frac{\lambda}{2n * sin\alpha}$$

(Abbe-limit)

Here, d denotes the observable distance between two points, which should be as small as possible to obtain an image with high resolution. The resolution is determined by the wavelength of light (or electrons), reflected by λ, by the refractive index of the viewed object, outlined by n, and α denotes half of the aperture angle (beam width) of the object lens. The term n * sinα, known as numeric aperture is in the order of 1 for light microscopy, but only ~0,01 in case of electron microscopy, thus limiting their possible resolution 100-fold. However, owing to the extremely small wavelength of an electron beam, which is approximately 0,0037 nm at 100 keV (= accelerating voltage), the theoretical resolution obtained with TEM is 0,005 nm [71]. Spherical and chromatic aberrations limit the reachable resolution in practice to 0,1 – 0,2 nm, which is nevertheless 1000 – 2000 times higher than with light microscopy [50].

In general, TEM and light microscopes share a similar construction, as can be seen in Figure 3, except that an electron beam is used instead of visible light and magnetic lenses rather than glass lenses serve for focusing purposes. The samples (=object) are placed on copper grids, with meshes of 30 – 100 µm, which are covered with a thin carbon film (5 – 10 nm). Since the carbon coat is hydrophobic, it must be rendered hydrophilic with the aid of ionized gas molecules through glow-discharging. Eventually, the grids can be placed in an object holder and inserted into the microscope, thereby reflecting the object plane. Emitted electrons from a filament (the cathode) are accelerated towards an anode making use of a potential

difference of 100 kV or more. Then the emitted electron beam is focused by the condenser lens into the object plane, where it passes through the object and is further directed towards the image plane with subsequent objective- and projective lenses. The lenses are made of iron-sheathed coils and generating a magnetic field directed towards the inner space, when current is applied. In contrast to a light microscope, the focus length can be adjusted by varying the applied lens current, thus altering the magnification does not require another objective lens [71]. The generated image can be visualized on a fluorescence screen and recorded with special sensor systems (e.g. with a CCD camera). Since the image information relies on the interaction of the electrons with the object, the electron microscope must be operated under vacuum to prevent interaction with gas molecules [50], [71].

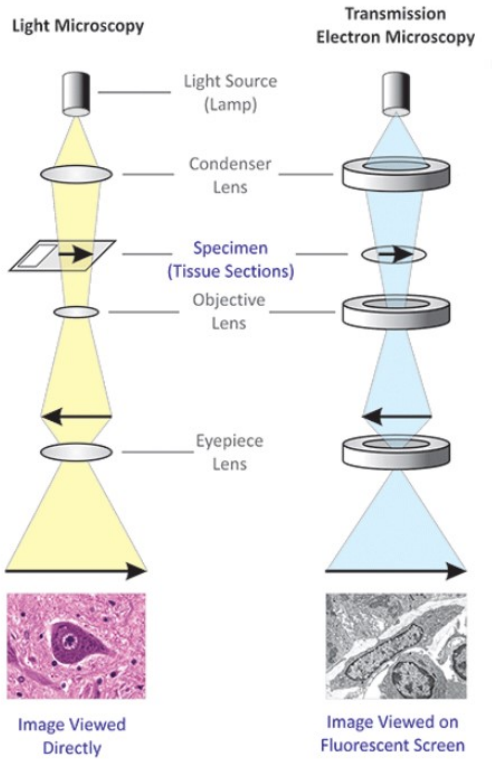

Figure 3. Light microscopy vs. transmission electron microscopy: *In general, light- and transmission electron microscopy share similar construction features. Both have condenser- and objective lenses, and project the image of the object on the opposite of the light- or electron source. In contrast to the light microscope, TEM uses electrons and magnetic lenses instead of visible light and glass lenses. TEM also has a projective lens, which is comparable to the eyepiece lens of the light microscope. Adapted from* [72]**.**

Two different interactions of the electrons with the object are known, elastic- and inelastic scattering. An electrostatic interaction of a beam electron with an object atomic nucleus leads to a deflection of the electron path. Even stronger deflection occurs when the electron passes the nucleus, when the nucleus positive charge is high (with heavy elements) and when the velocity of the electron is low (based on the acceleration voltage). Strongly deflected electrons are blanked out by the objective aperture, thereby enhancing the contrast of the image. Since the energy of the deflected electrons remains constant, this process is called elastic scattering. Inelastic scattering takes place when the accelerated electrons of the beam hit the electrons of the object, thereby losing kinetic energy, which is accompanied with an

increasing wavelength. As the energy loss of the beam electrons correlates with the energy uptake by the object atoms, the scattered electrons contain information of the interacting object. The in-elastically scattered electrons may be analyzed to determine the element composition of the object, as it can be done with electron energy loss spectroscopy (EELS). As no energy can be lost in total, the lost energy of the beam electrons is transferred to the object electrons, thereby increasing their energy level. When the transferred energy is high enough, the electrons get ejected from their corresponding shell, serving information about the object surface, which can be analyzed with scanning electron microscopy (SEM). The removed electrons leave behind a gap, which is eventually filled with an electron of a higher energy level, thereby emitting the energy difference by radiation (= X-rays), that can also be used for element analysis with energy dispersive X-ray spectrometer (= EDX) [71].

2.8.1 Negative Staining

Although the iron core of ferritin can easily be visualized by TEM, uncontrasted proteins are difficult to visualize. Proteins consists mainly of low weight atoms, such as H, C, N and O [50], thus, interaction of the beam electrons with these atoms leads only to a weak deflection, resulting in a weak contrast of these structures. Negative staining with heavy metal salts, such as uranyl acetate, is a simple and quick method to assess the purity of isolated protein samples. A droplet of the protein sample is applied on a glow-discharged, carbon coated grid. After a certain time (15 – 60 sec.), most of the proteins have settled down onto the grid surface and the rest of the suspension is removed with a filter-paper [71]. Subsequently, the sample is stained with 0,5 - 2 % heavy metal salt solution. The heavy metals cover the surface of the grid and fill cavities and depressions of the proteins. When the sample is examined with TEM, actually the heavy metal layer is observed, which gives us indirectly information about the specimen structure itself “negative staining” [71], [73].

3 Methods

The aim of this project was to isolate the iron storage protein ferritin from different human brain regions, so as to analyze the tissue specific iron load distribution with TEM, form apo-ferritin with missing iron core, up to ferritin molecules with highest iron load. First of all, an efficient method had to be established by extracting pig brains for ferritin, while preserving its native state. That included the testing of different purification steps with subsequent evaluation in terms of ferritin enrichment and its overall yield. Ferritin enrichment and its yield were monitored by measuring the iron correlated absorbance value at 315 and 420 nm at different purification steps, by determining its concentration conducting the Lowry assay and by visual evaluation including SDS-Page, Native-Page, corresponding western blotting and bright field imaging via TEM.

Once the purification process was established with pig samples, two different human brain regions (occipital- and frontal cortex) from three deceased patients are assayed for their ferritin iron load distribution (see Table 1 for details).

Table 1. Human brain samples obtained from autopsy: *in-house number includes the date, when the samples were received. Time until storage represents the time between the death of the patient and the start of storage in the freezer.*

in-house number	time until storage (in frozen state) [h]	age of the deceased patient	gender
Fe180323	20	86	male
Fe180326	15,5	74	female
Fe180418	-	-	-

3.1 Sample dissection and storage

Fresh pig brain samples were obtained from a local slaughterhouse and transported in a cooling bag to minimize autolytic processes/ protein degradation within the tissue. All brains were rinsed with water to remove attached blood and stored in plastic bags at -20 °C until further processing.

Human brain regions from three deceased patients were dissected during autopsy at the Department of Pathology of the Medical University of Graz. Samples were transported in physiological saline on ice, transferred into closable tubes and stored at -20 °C until further processing. The protocol was in accordance with the ethics department of the Medical University of Graz vote number 28 - 549 ex15/16.

3.2 Homogenization

3.2.1 Turrax Homogenizer

Brain samples were slightly thawed, cut into small pieces with a ceramic knife and transferred into falcon tubes. Up to 3 - 4 volumes of a buffer consisting of either 0,1 M Tris-HCl (for pig brain samples) or 10 mM Tris-HCl + 150 mM NaCl (for human brain samples) containing protease inhibitor (+ 0,5 mL of the stock solution diluted 1:100) were added to the tissue before homogenization was carried out with a Turrax Homogenizer IKA T-10. Samples were constantly cooled on ice during the homogenization process to avoid uncontrolled heat denaturation of proteins. Afterwards the homogenized samples were centrifuged at 10000 g for 30 - 60 min at 4 °C, retaining the supernatant for further purification.

Some approaches (see Figure 5) included two homogenization steps with the Turrax Homogenizer. The tissue pellet after centrifugation was re-suspended in 10 mL buffer (as used for homogenization), homogenized again to ensure complete breakup of the tissue and cells, and centrifuged again.

3.2.2 Sonication

The samples were homogenized as described above, the pellets re-suspended in 1 volume of buffer and subjected to sonication for 2 min using the Branson Sonifier 250 at power level 6 under constant cooling with ice. Afterwards the homogenized samples were centrifuged at 10000 g for 30 - 60 min at 4 °C retaining the supernatant for further purification.

3.3 Heat precipitation

The supernatant was heated up to 70 - 75 °C for 10 min on a heating plate under constant stirring and afterwards immediately cooled on ice. After heat precipitation the samples were centrifuged at 10000 g for 30 - 60 min at 4 °C and the pellet discarded.

Depending on the approach (see Figure 4), the supernatant was further processed or stored overnight at 4 °C with or without anti-aggregation agents.

One approach included heat precipitation in presence of 40 % [v/v] methanol (see Figure 4). For this, the methanol was added slowly under constant stirring to the supernatant and heated.

3.4 Acidic precipitation

The pH of the supernatant was adjusted with 1 M citric acid to 4,6 under constant stirring by monitoring the pH with a Mettler Toledo SevenMulti pH-Meter and incubated for 1 h at 4 °C. The acidic precipitated sample was centrifuged at 10000 g for 30 - 60 min at 4 °C.

3.5 Ammonium sulfate precipitation

The proteins in the supernatant were precipitated with 75 % saturated ammonium sulfate. The required amount of ammonium sulfate was calculated by using the online calculator from EnCor [74]. Solid ammonium sulfate was slowly added under constant stirring at 4 °C and precipitation performed overnight at 4 °C. The precipitated proteins were collected by centrifugation at 10000 g for 60 min at 4 °C and the supernatant discarded.

In one approach, fractionated precipitation was tested (see Figure 4), by precipitating at first with 50 % saturated ammonium sulfate, collecting the pellet and then increasing the saturation to 75 %.

3.6 Concentration and desalting of the protein sample via ultra-filtration

3.6.1 Concentration

Vivaspin® concentrators with a molecular weight cut-off of 100 kDa were used for concentrating protein samples prior application on SEC or density gradient centrifugation. Membranes fitted to Vivaspin® concentrators were pre-rinsed with the same buffer as used for the samples to remove glycerin and sodium azide. Subsequently, the concentrators were filled with the protein sample up to their maximum volume according to the manufacturer`s instruction. Concentration was carried out with maximum g-force considering rotor-type and molecular weight cut-off. Centrifugation was stopped from time to time for mixing the sample to avoid a concentration gradient and/ or precipitation of proteins.

3.6.2 Desalting

Ultra-filtration devices can be also used for desalting purposes. Therefore, the protein sample is concentrated to a desired level, refilled with buffer and concentrated again until contaminating solutes are sufficiently reduced. Usually, two wash cycles were appropriate for our requirements.

3.7 Size Exclusion Chromatography (SEC)

A pre-packed Sepharose CL-6B column was equilibrated with 50 mM $NaPO_4$ buffer. Afterwards, the column was loaded with the protein sample, used with the settings listed in Table 2 and fractions were collected according to the monitored chromatogram at 280 nm, which reflects the protein content. Afterwards, the column was either rinsed with buffer, preparing the column for the next run or with ethanol for storage purpose.

Table 2. Size Exclusion Chromatography parameters: *the setting listed below was used for brain 1, 3 and 5, with variation in attached protein amount.*

	Parameter
buffer	50 mM NaPO4 (pH= 7,4)
resin material	Sepharose CL-6B
column dimension	1,5 * 32 cm
flow-rate	0,33 mL/min
volume per fraction	1 mL
monitored wavelength	280 nm

Different amounts of protein samples were tested for estimating the upper capacity limit of the column (see Table 3):

Table 3. Attached protein amount concerning size exclusion chromatography

	V(sample) [µL]	m(protein) [mg]
1. brain	2700	48,15
3. brain (1. approach)	100	4,62
3. brain (2. approach)	400	18,50
5. brain	710	10,86

3.8 Density Gradient Centrifugation

Initially, a 4-step gradient was prepared. This was done by pipetting 2,5 mL of a 60 % glycerin solution onto the bottom of the centrifugation tube. Before the next glycerin solution (45 %) could be layered on top, the gradient had to be frozen at -80 °C for 1 h. Afterwards, it could be proceeded the same way with the remaining glycerin solutions (30 and 15 %). Glycerin solutions were either prepared in 50 mM Sodium Phosphate buffer or in 10 mM Tris-HCl + 150 mM NaCl, both at physiological pH. Creation of a linear gradient was achieved by thawing the 4-step gradient in the cooling room at 4 °C. Eventually, concentrated protein samples were carefully layered on top of the gradients and subjected to ultracentrifugation for 16 h at 34000 rpm at 4 °C.

Table 4. Conditions tested for density gradient centrifugation: *the whole sample volume, retrieved after ferritin enrichment, was layered on top of the linear gradients*

	buffer	sample	M(DTT) [mmol/L]
1. Condition	50 mM NaPO4	10/F	-
2. Condition	50 mM NaPO4	10/11	5
3. Condition	50 mM NaPO4	10/D	10
4. Condition	10 mM TBS	10/CS	-
5. Condition	10 mM TBS	10/ES	5
6. Condition	10 mM TBS	10/AS	10

Fraction collection was performed as follows:

A needle was inserted on the bottom of each centrifugation tube to create a connection between gradient and detector. Fresh buffer was applied continuously on top and forcing the gradient through the needle towards the detector. Protein containing fractions were selected by monitoring UV absorption at 280 or 290 nm (due to problems with 280 nm detection) and collected in a 96-well deep well plates. Ferritin fractions could be distinguished from other proteins due to their iron core related absorption characteristic at 315 nm.

3.9 Measuring absorbance values of samples via NanoDrop®

The NanoDrop® ND-1000 spectrophotometer was chosen for our needs as only 2 µL of sample are required for one measurement and it enabled us to estimate ferritin concentration. Blank measurements based on sample buffer are essential as absorbance spectra of buffer components could overlap with the sample. All measurements were done in duplicate. The ferritin concentration within the samples could be estimated, by interpolating the iron related absorbance values at 315 and 420 nm with a calibration that was created with equine spleen and human liver ferritin in known concentrations. Table 5 highlights that high concentrations of non-iron containing proteins also absorb light in the range usually used for estimating the ferritin content.

Table 5. BSA related absorbance values measured with NanoDrop®

	Absorbance		
ß(BSA) [mg/ml]	280 nm	315 nm	420 nm
50	1,988	0,077	0,018
20	1,050	0,038	0,011
10	0,557	0,021	0,007
5	0,275	0,015	0,007
2	0,107	0,010	0,006
1	0,054	0,006	0,004

0,5	0,037	0,009	0,005
0,1	0,013	0,006	0,005

3.10 Protein determination via Lowry-Assay

Since it resembles the globular structure of ferritin, Bovine Serum Albumin (BSA) was used as reference ranging from 0,16 - 10 mg/mL representing the calibration series. The working solution consists of 100 parts solution A, 1 part solution B and 1 part solution C mixed together (see Table 19 for details on components). Afterwards, 3 µL of sample, reference or blank were mixed with 375 µL working solution and incubated for 10 min at room temperature. In the meantime, Folin Ciocalteus Phenol Reagent was mixed in equal amount with double distilled water, 37,5 µL added to each specimen, vortexed and incubated for 30 min. Absorbance measurements were performed in duplicate in 96-well plates pipetting 190 µL of each prepared specimen. Absorbance values were measured with the Anthos 2010 microplate reader at 620 nm.

3.11 SDS-Page

3.11.1 Sample preparation and separation

Samples were diluted with bidest. water, 4x NuPage® LDS Sample Buffer and 10x NuPage® Sample Reducing Agent (final concentration 1x, respectively) to a final protein amount of 50 µg and heated at 95 °C for 5 min. In case the protein concentration was too low, samples were precipitated in presence of 10 % Trichloroacetic acid (TCA) on ice for 30 min and the pellets collected by centrifugation at 10000 g for 15 min. The protein pellets were re-suspended in appropriate amount of 1 M Tris (base), 4x NuPage® LDS Sample Buffer and 10x NuPage® Sample Reducing Agent (final concentration 1x, respectively) and treated as described above.

Electrophoresis was performed with NuPageTM Bis-Tris gels (acrylamide concentration mentioned in figure description where needed) and 1x NuPage® MES SDS Running Buffer (stock: 20x, diluted with bidest. water). Per gel, 5 µL of PageRuler™ Plus Prestained Protein Ladder was loaded into one pocket, used as molecular weight reference and the prepared samples into the left pockets. Electrophoretic separation was carried out with the PowerStation 200 at 140 V for 60 - 70 min.

3.11.2 Coomassie Blue Staining

The running buffer was discarded, the retained gel was washed 3 times for 5 min with bidest. water and stained with Simply Blue Dye for 1 h. Then, the dye was discarded and the background lowered by washing 1 h with double distilled water.

3.12 Blue-Native-Page

3.12.1 Sample preparation and separation

All performed steps were done on ice or in the cooling room. Samples were diluted with double distilled water and 4x NativePageTM Sample Buffer (final concentration 1x) to a final protein amount of 50 µg. Electrophoresis was carried out with NativePageTM 3 - 12 % Bis-Tris gels, 1x NativePageTM Anode Buffer (stock: 20x NativePageTM Running Buffer, diluted with double distilled water) in the upper chamber and 1x NativePageTM Light Blue Cathode Buffer (1x NativePageTM Anode Buffer + 0,1x NativePageTM Cathode Additive, diluted with double distilled water from 20x stock) in the lower chamber. Samples were applied as described above for the SDS-Page run, with exception that 5 µL NativeMarkTM Unstained Protein Standard was used as molecular weight reference. Subsequently, electrophoretic separation was performed with the PowerStation at 150 V for 60 min and then adjusted to 250 V for 30 - 45 min.

3.12.2 Coomassie Blue Staining

After separation of proteins, the retained gel was immediately stained with Simply Blue Dye for 1 h and the background lowered by washing 1 h with double distilled water.

3.12.3 Prussian Blue Staining with DAB enhancement

The gel was washed 3 times for 5 min with double distilled water prior staining. Afterwards, the gel was pre-incubated in 10 % $K_4(Fe(CN)_6)$ solution for 5 min, stained with Prussian blue solution containing 1 % $K_4(Fe(CN)_6)$ and 2 % HCl for 15 min, and the iron-related staining was enhanced by incubation in diaminobenzidine (DAB) solution containing 0,05 % DAB and 0,033 % H_2O_2 in 0,1 M PBS until intensive brown bands appeared. Eventually, the stained gel was washed with double distilled water for 30 min.

3.13 Western Blotting

3.13.1 Concerning SDS-Page

The separated protein bands were transferred onto a nitrocellulose membrane, using 1x NuPage® Transfer Buffer (stock: 20x) with 20 % (v/v) methanol and the Nitrocellulose Blotting Membrane. The Nitrocellulose Membrane needs activation in double distilled water. The components for the transfer were placed in a blotting module as depicted in Figure 2 and transferred into the transfer chamber that had been filled with transfer buffer. After providing sufficient cooling, by placing the transfer chamber in an ice box, protein blotting was proceeded at fixed 160 V for 1,5 h in the cooling room.

Whether sufficient protein had been transferred was checked with Ponceau Red staining of the membrane for approximately 5 min, washing away staining solution bound on background with double distilled water. This stains the proteins and fixes them on the membrane, since Ponceau Red contains methanol. After

protein fixation, any spaces providing unspecific binding properties were blocked with 5 % non-fat dry milk diluted in TBST.

The target protein was marked with the corresponding primary antibody diluted in blocking solution by incubation at 4 °C overnight. Selected antibodies, their dilution, and the target protein subunit are listed in Table 6.

Table 6. Characteristics of the used primary antibodies

antibody	company	target protein	dilution	expected molecular weight [kDa]
ab81444	Abcam	ferritin heavy-chain	1:500	21
bs-5907R	Bioss	ferritin heavy-chain	1:500	21

After washing the membrane 3 times for 5 - 10 min with TBST to remove excess and unspecific bound primary antibody, the membrane was incubated with Goat Anti Rabbit antibody diluted 1:3000 in TBST targeted against the primary antibody for 2 h at room temperature.

The membrane was washed again 3 times with TBST and gently with TBS to remove residual Tween. Afterwards, the membrane was layered with WesternBright™ ECL HRP substrates (ECL luminol/enhancer & peroxide chemiluminescent solution) mixed 1:1 for chemiluminescence development. The emitted light, reflecting the amount of target protein, was detected using the FluorChem® Q System and the signal analyzed with Image Studio Lite (Version 5.2).

3.13.2 Concerning Blue-Native-Page

In general, the procedure as described above for SDS-Page was also used for native protein transfer, with the following exceptions:

PVDF/ Filter Paper was used as blotting membrane instead of nitrocellulose, as the latter tightly binds Coomassie Blue present in the running buffer [75]; methanol was omitted from the transfer buffer; the PVDF membrane was initially pre-wet in methanol for 30 sec. and briefly rinsed with double distilled water before placing it in transfer buffer; staining with Ponceau Red was omitted, as protein bands were transferred with adherent Coomassie Blue; native proteins were fixed on the membrane by incubation in 8 % acetic acid for 15 min and washed afterwards with double distilled water.

3.13.3 Antibody stripping

For probing the same membrane with a second antibody, primary-/ secondary antibody complexes from the previous run were removed by incubating the membrane in Restore™ Western Blot Stripping Buffer

for 5 - 15 min (depending on the level of signal), then washed gently with TBS and the labeling started again as described above with the primary antibody incubation.

3.14 Analyzing ferritin with TEM, CellProfiler™ and SPSS®

Ferritin molecules and their iron cores were viewed using a FEI Tecnai G2 20 at 120 kV with a LaB_6 cathode. All images were acquired at 50 kx magnification by means of a Gatan Ultrascan 1000 camera and exposure time was set automatically (between 1,5 - 2,5 sec.).

3.14.1 Bright field imaging

In order to provide a hydrophilic surface, the 400-mesh carbon coated copper grids were glow discharged prior sample application. A two-sided sticky tape was placed onto a glass-bar in such a way as to allow an appr. 2 mm overhang. The glow-discharged grid was attached onto the overhang, just with its outside and with the carbon coating being on top. Subsequently, 5 µL of the protein samples were carefully applied to avoid air bubbles and being allowed to settle for 1 min. Excess solution was drawn carefully with a filter paper. Eventually, the grid was placed into the grid holder and inserted into the transmission electron microscope for image acquisition.

3.14.2 Negative staining

For negative staining, the same steps as described above were carried out, with the following additions. High contrast was provided by application of 5 µL uranyl acetate (1 %) onto the sample loaded grid. After 30 sec. excess solution was drawn with a filter paper. These steps were repeated once and afterwards analyzed as described above.

3.14.3 Identifying iron cores with the CellProfiler™ program & statistical evaluation

Images were analyzed with the CellProfiler™ program (version 3.1.5). Image analysis concerned the untreated sample grids, since we wanted to measure the iron cores, where additional contrasting with heavy metals would have been disadvantageous. Negative stained sample grids were used for assessment of purity. First of all, the images had to be smoothed using a Gaussian filter with a defined artifact diameter of 8 pixels. This smoothing step was necessary, as the image appeared grainy due to limited resolution. In addition to that, a further smoothing step was applied to the background (artifact diameter of 64 pixels) and subtracted from the original image to compensate for irregular grey-values present in the background. Since, the software algorithm works better with high white values, the images had to be inverted for facilitating the identification process of electron dense iron cores (appeared as dark irregular-shaped spots). Although the purified samples were extensively washed by ultra-filtration after the density gradient centrifugation, the samples still contained a noticeable amount of glycerin leading to the formation of lipid droplets on the grid (see Figure 27 for an example). These lipid droplets were tried for being identified and removed to ensure unhindered detection of the iron cores. Applied parameters for identification and

masking of ferritin iron cores and lipid droplets are outlined in Table 7. Eventually, identified iron cores were counted and measured for their minimum- and maximum diameter.

Table 7. Parameters for identifying ferritin iron cores and for masking lipid droplets: *1 nm are equal to 4,95 pixels. Form factor is calculated as $4*\pi*area/perimeter^2$ (equals 1 for a perfect circular object). Lower- and upper bound of greyscale represent intensity range.*

	Ferritin iron cores	lipid droplets
typical diameter of objects [pixels]	10 - 45	50 - 400
mean radius		10 - 100
form factor (minimum value)		0,4
max. radius (minimum value) [pixels]	10	
max. radius (maximum value) [pixels]	45	
lower bound of greyscale	0,1	0
upper bound of greyscale	1	1

The various iron core morphologies were classified by their 2D projection according to the definition of Jian et at., which was as follows: “small circle”, “dumbbell”, “crescent”, “doughnut” and “full-raft”. The full-raft shape represents full iron loaded ferritin molecules (in context of the 2D projection). Small circles differ from full-rafts, as they are characterized by smaller maximum diameters (< 4 nm). The dumbbell shape has an iron core with aspect ratio larger than 1,5. The crescent shape is characterized by a low intensity at their center and an imperfect outer shell, compared to doughnut like iron cores, which have complete outer shells.

Further statistical analysis of the iron load distribution of ferritin molecules was performed using the SPSS® software (version 23). Here, two histograms were generated, based on the measured minimum- and maximum diameters of the iron cores, and compared with the literature.

4 Experimental

It is a prerequisite to evaluate each step of the purification procedure in terms of duration, heat evolvement, protein enrichment and yield, as elaborated in the chapter Principle [60]. Physiological and chemical reactions, which include protein degradation by proteases, run 2 - 4 times as fast when temperature rises by 10 degrees [76]. Hence, it is necessary to handle the protein sample in a minimum time and temperature. The latter is achieved by performing each step on ice or in the cooling room, while time can be saved by eliminating expandable purification steps.

4.1 Method development

Several approaches, pointed out below (see Figure 4 for an overview) have been extensively tested for level of ferritin enrichment and yield. Appropriate methods for carrying out such an evaluation are the Lowry Assay, absorbance value determination via NanoDrop® spectrophotometer, SDS-Page with corresponding western blotting and especially Native-Page electrophoresis, where specific staining of the ferritins` iron core is possible. The final test of sample purity was performed by negative staining ferritin samples and their evaluation via bright field imaging under TEM. For better comparability, purification steps beyond protein precipitation were not evaluated here. The approach number below corresponds to the brain number, e.g. the first approach is designated as brain 1. The purification procedure was varied as follows:

- In a first approach, brain tissue was homogenized in one step with the Turrax Homogenizer, the supernatant heat precipitated and subsequently ammonium sulfate fractionated in 50 and 75 % saturated solution.
- In order to shorten the procedure, the heat precipitation step was omitted in the second approach.
- The third approach included one homogenization step with Turrax Homogenizer, heat precipitation, acidic precipitation and ammonium sulfate precipitation in 75 % saturated solution.
- To increase the yield of ferritin, a two-step homogenization was tested in a fourth approach with subsequent heat- and ammonium sulfate precipitation. The tissue-pellet obtained after the initial homogenization was re-suspended and subjected to sonication.
- The fifth approach was crucial for the project, as the amount of pig brain tissue was reduced from former ~ 80 g to ~ 10 g (was kept at this amount for further approaches). The reason for this effort is grounded in a limited supply of human brain tissue. Hence, the major focus was set to the verification, if the obtained protein amount is sufficient for further processing, especially in terms of ferritin. Here the tissue was subjected to two-step homogenization and subsequent heat precipitation. Ammonium sulfate precipitation was skipped, as a high ionic strength interferes with the Native-Page run [75].

Method development:

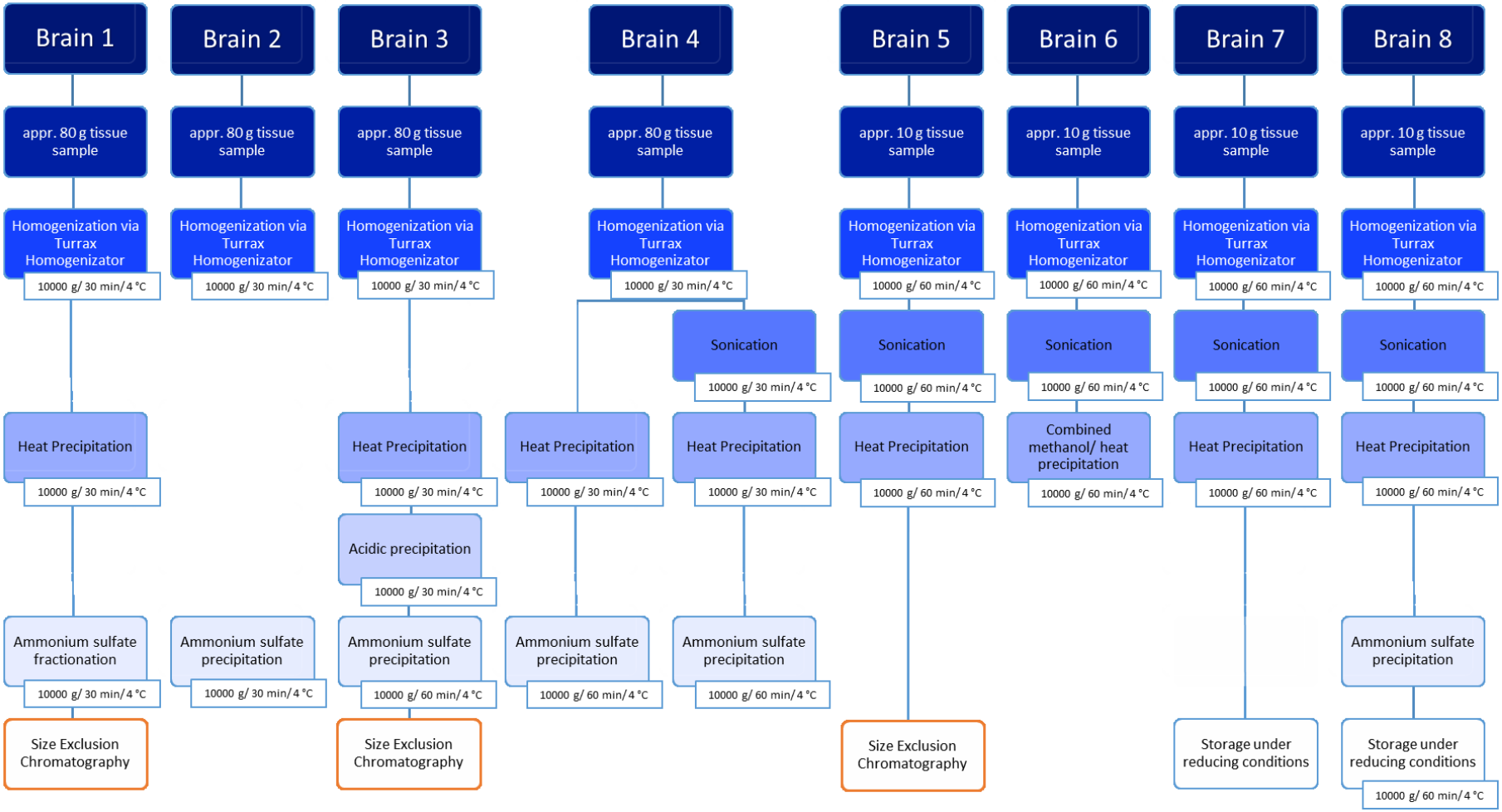

Figure 4. Overview about the method development: *subsequent to the last centrifugation, the protein samples related to brain 1, 3 and 5 were purified with size exclusion chromatography (see orange framed blocks). Eventually, each protein sample was concentrated by ultra-filtration and analyzed for ferritin amount and -yield.*

Statistical evaluation:

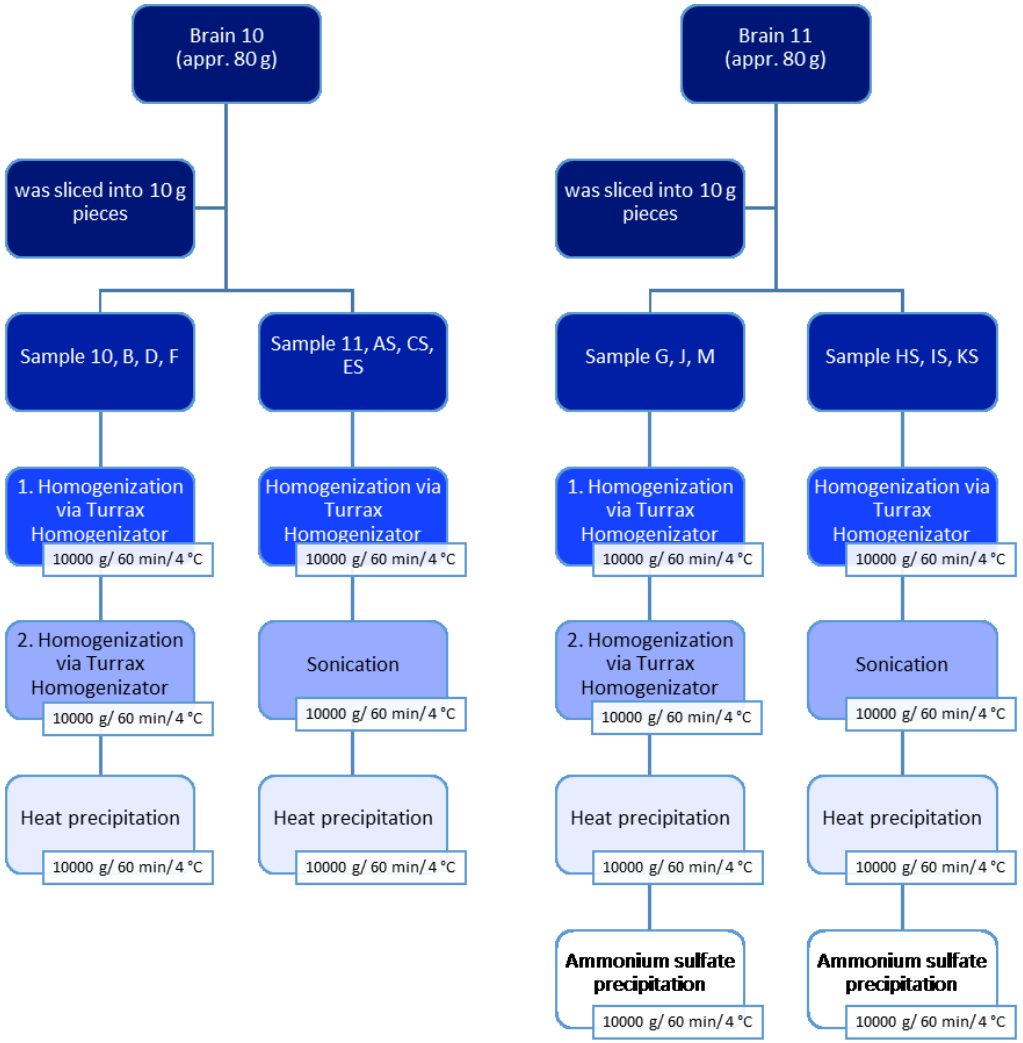

Figure 5. Overview about the statistical evaluation procedure: *two pig brains were cut randomly into 10 g pieces, each representing a separate sample. Each protein sample was concentrated by ultra-filtration and analyzed for ferritin amount and -yield. Eventually, the results were statistically evaluated to find possible differences between the varied steps.*

- The sixth approach concerned the enhancement of ferritin enrichment by performing the two-step homogenization procedure and a combined methanol/ heat precipitation.
- The seventh and eight approach are based on the fifth approach with the addition of providing 1 mM 2-mercaptoethanol in the supernatant after heat precipitation in order to prevent protein aggregation, which may interferes with the Native-Page run and lowers the separation performance. The eight approach included the ammonium sulfate precipitation to check the effect of reducing agents for both storing conditions.

4.2 Statistical evaluation of critical steps

The following steps appeared to be critical, as one of them may have the potential to alter the protein solution towards protein aggregation whereas the other was expected to interfere with Native-Page electrophoresis. Therefore, we did a statistical evaluation of these two steps in order to verify, if they are really necessary for reaching our goal. An overview of the experimental setup is given in Figure 5.

4.2.1 Sonication

An additional sonication process in the homogenization procedure consumes time, produces a heat-gradient and may contribute to protein damage leading to aggregate formation [77]. All these three points should be avoided. We performed a statistical evaluation of its effectiveness compared to homogenization with the Turrax Homogenizer alone by analyzing seven randomly selected tissue samples, respectively. The evaluation is based on yield and level of protein aggregation, tested with the Lowry Assay, NanoDrop® and Native-Page.

4.2.2 Ammonium sulfate precipitation

Ammonium sulfate precipitation leads to high ionic strength within the sample, especially when a dialyzing step is omitted (desalting with ultra-filtration was not sufficient, see Figure 20), resulting in interferences with the Native-Page [75]. In addition to that, it cannot be ensured that all proteins get precipitated, which would reduce the yield of ferritin. On the other hand, ammonium sulfate precipitation may significantly contribute to the stabilization of ferritin during storage, preventing loss of protein through degradation or lowering the risk for protein aggregation. Hence, it is interesting to know, if the benefits overweight the disadvantages. Here, six randomly selected tissue samples were purified without ammonium sulfate precipitation, whereas an equal number was treated with an additional ammonium sulfate precipitation step. Evaluation was done as described above.

4.3 Testing ferritin purity with SDS-/ Native-Page and western blotting

During this project, SDS-Page, Native-Page and western blotting were used to assess the relative enrichment, or the purity of ferritin after various steps of purification. Coomassie Blue unspecific stains all proteins present in the gel matrix. Therefore, ferritin standards, human liver- and equine spleen ferritin

were used as reference for comparative purposes. Concerning Native-Page, we tested the ability, to specifically stain ferritin or rather its iron core with Prussian Blue staining and subsequent DAB enhancement. Western blotting was chosen as gold standard to confirm that selected "ferritin-" bands are ferritin and not just another protein possessing a similar molecular weight. Moreover, western blotting was used to check which fractions still contain ferritin, with reference to size exclusion chromatography and density gradient centrifugation.

4.4 Aiming band smearing and protein aggregation

Since we were confronted with troubles related to Native-Page electrophoresis, characterized by smearing of the ferritin band, the troubleshooting part of the manufacturer's manual was consulted for further steps. Possible sources of error are sample overload, high ionic strength, protein degradation, particulate material or DNA complexes within the sample. Solid particles could be neglected, as samples were centrifuged at 10000 g for 15 min prior to electrophoresis. Protease inhibitors were added to the sample solution prior to homogenization to avoid protein degradation. Various efforts were made to aim the other points:

- Two different protein amounts, 25 and 50 µg, were applied in the gel pockets
- The samples were desalted by ultra-filtration as described above
- In order to remove possible DNA-complexes, the samples were incubated with DNase I and Benzonase® as recommended in the manufacturer`s material (see Table 8 for details) [75], [78]

Table 8. Incubation conditions at varied DNase Kunitz units: *1. and 5. approach were carried out according to the manufacturer`s recommendation* [75], [78]*. DNA digestion was performed prior separation via Native-Page*

	enzyme	ß(enzyme) [µg/mL]	activity [U]	M(MgCl2) [mmol/L]	incubation conditions
1. approach	Dnase I	50	4,15	10	37 °C/ 60 min
2. approach	Dnase I	100	8,3	10	37 °C/ 60 min
3. approach	Dnase I	200	16,6	10	37 °C/ 60 min
4. approach	Dnase I	500	41,5	10	37 °C/ 60 min
5. approach	Benzonase®		60	2	25 °C/ 60 min

Although not mentioned in the troubleshooting part of the manual, the purification procedure was also improved concerning protein aggregation:

- In a first approach, the samples were treated with detergents (1 % concentration), specifically 4,4`-diaminodiphenylmethane (DDM) and digitonin, respectively to prevent hydrophobic interactions
- 1 mM 2-mercaptoethanol was added to the supernatant after heat precipitation to preserve a reductive environment

- Various amounts of dithiothreitol (DTT) in a range of 1 - 5 mM were tested for reducing the proportion of aggregated proteins and added immediately prior to Native-Page electrophoresis

Since the used agents against protein aggregation might have the ability to solubilize the iron cores, their harmlessness for utilization in the purification procedure had to be proven. Therefore, untreated and equine spleen ferritin with added 1 mM EDTA (used in the final purification procedure) and 5 mM DTT were visually compared by aids of TEM.

4.5 SEC vs DGC

During this project, size exclusion chromatography and density gradient centrifugation appeared to be decisive purification steps. As only one of both technique will be included in the final procedure, we compared their effectiveness for separation of ferritin from impurities. The following parameters were optimized before comparison was done:

Size exclusion chromatography

- Varied amounts of protein and sample volumes were attached on the column to test their maximum capacity, see Table 3

Density gradient centrifugation

- 2 different gradient- and 3 different sample conditions were tested, respectively to find the best one for our purpose, see Table 4 for detail

Visual comparison was based on obtained chromatograms, monitored during (for SEC) or after the separating process (for DGC). In case of size exclusion chromatography, only the total protein amount could be monitored at 280 nm (detector limitation), while for the density gradient centrifugation, it was possible to measure also ferritin amount using both wavelengths, 280 and 315 nm. SDS- and Native-Page were carried out for assessment of separation performance. Apart from that, the capability of ultra-filtration equipped with a 300 kDa cut-off filter for ferritin isolation, was also tested here. Therefore, the fractions containing mainly impurities were pooled (= pool 2) and forced through the filter. Remaining ferritin molecules should be held back (= new pool 2), while smaller proteins have the ability for passing the filter (= flow-through).

4.6 Evaluation of the final procedure & analysis of the ferritin iron load

Only minor optimizations were made for extraction of ferritin out of human brain tissue. The final procedure was carried out as follows:

- Lysis buffer concentration was reduced from 100 to 10 mM Tris-HCl to reduce its buffer related pH characteristic, as pH decreases 0,03 units per °C (with 100 mM Tris) during heat precipitation [79]. In addition to that 150 mM NaCl was added to provide physiological conditions
- Homogenization was performed in presence of protease inhibitor mix (0,5 mL of stock solution diluted 1:100) with Turrax Homogenizer 2 times
- Supernatant was subjected to heat precipitation at 70 - 75 °C for 10 min
- 1 mM EDTA and 5 mM 2-mercaptoethanol were added to the supernatant after heat precipitation
- 1 mM EDTA and 5 mM DTT were added after ultra-filtration (as residual EDTA and 2-mercaptoethanol are removed during the washing step)
- Concentrated protein samples were separated via density gradient centrifugation in 50 mM sodium phosphate buffer/ glycerin gradients
- Fractions with pure ferritin were pooled and concentrated according to the chromatograms and SDS-Page results

Here, the resulted ferritin samples were assessed for purity with SDS-/ Native-Page and with bright field imaging using negative stained samples. The visualization of the iron load distribution in ferritin molecules was performed with native samples, again with bright field imaging. In order to ensure a representative evaluation of the samples, 5 areas on each grid were randomly selected for image acquisition. These images were analyzed with the CellProfiler™ program for identification, count and morphological measurements of ferritin iron cores. The subsequent statistical analysis was done with the SPSS® software.

5 Results

A method was established for native isolation of ferritin out of brain tissue. The method development was performed with pig brains, testing various purification steps with subsequent evaluation of their effectiveness. In order to find the best purification procedure, the following steps/ parameters were tested: comparison of homogenization techniques (one- or two-step); heat precipitation alone or in combination with methanol; acidic precipitation; ammonium sulfate precipitation or -fractionation; size exclusion chromatography with different protein amounts and density gradient centrifugation with different buffer compositions and reducing agent concentrations. In addition to that, much effort was done towards prevention of protein aggregation. The results of the method development and the current purification procedure are presented here.

5.1 Assessment of all varied parameters

5.1.1 Overview about all approaches

The main goal of the method development was to enhance the enrichment for ferritin, while providing as much yield as possible. Table 9 shows an overview about the reached ferritin yield and enrichment. It became obvious, that with exception of the sixth approach (brain 6), the amount of obtained ferritin remained quite stable throughout all approaches. Interestingly, the proportion of ferritin within the enriched sample seems to decline from the first to the fifth approach, remaining stable for the latter ones. Since, no brain sample was equal in terms of weight and protein expression, both parameters have an impact on the amount of present ferritin, the results are presented in detail in the further sub-chapters.

Table 9. Ferritin content and -yield after performing the listed approaches: *brain number corresponds to approach number. Listed values resulted from: 1) the sum of the retrieved protein samples after precipitation in 50 and 75 % saturated ammonium sulfate solution, respectively; 2) the sum of the concentrated protein sample and their corresponding flow-through (retained after ultra-filtration, as a filter with 300 kDa cutoff was used → some of the ferritin passed the filter); 3) the sum of the retrieved protein samples and flow-throughs after ultra-filtration (a filter with 300 kDa cutoff was used; sample was split after homogenization via Turrax Homogenizer and one of them subjected to sonication). Protein amounts are based on the Lowry-Assay. Ferritin amounts were interpolated by comparing the iron related absorption values of the samples, measured via NanoDrop® at 315 and 420 nm, with calibration series based on ferritin standards from human liver and equine spleen.*

	m(Brain) [g]	*V(Sample) [µL]*	*w(Protein/ tissue) [µg/g]*	*w(Ferritin/ tissue) [µg/g]*	*Ferritin content*
Brain 1 (sum.)[1]	82,47	25000	714,5	61,8	8,7 %
Brain 3 (sum.)[2]	80,82	18950	690,8	42,5	6,1 %
Brain 4 (sum.)[3]	84,64	33470	895,8	55,7	6,2 %
Brain 5	9,74	710	1114,8	49,6	4,5 %
Brain 6	9,85	785	58,2	8,0	13,7 %
Brain 7	9,78	600	1202,1	53,6	4,5 %
Brain 8	9,93	580	1371,9	65,7	4,8 %

5.1.2 Adding sonication for enhancing ferritin yield

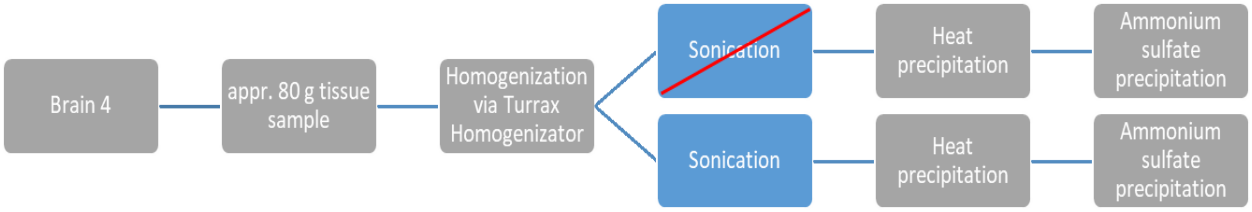

Figure 6. Workflow of the fourth approach: *the step that has to be evaluated is highlighted in blue.*

In this approach we tried to release as much ferritin as possible from the homogenized tissue, by addition of a sonication step after conventional homogenization. Therefore, the tissue pellet obtained after homogenization with the tissue homogenizer was re-suspended in fresh 50 mM $NaPO_4$ buffer, subjected to sonication and treated as a separate sample.

Using sonication seemed to be satisfying, as the yield of ferritin could be increased by about 50 %. Although the amount of impurity was also increased through this process, even more ferritin could be set free, see Figure 7 for ferritin heavy-chain (red frame).

Table 10. Enhancing ferritin yield with sonication: *calculated gain is based on the non-sonicated sample obtained after ultra-filtration (concentrate + flow-through). Protein amounts are based on the Lowry-Assay. Ferritin amounts were interpolated by comparing the iron related absorption values of the samples, measured via NanoDrop® at 315 and 420 nm, with calibration series based on ferritin standards from human liver and equine spleen. The suffix "S" reflects the sonicated sample.*

	m(Brain) [g]	*V(Sample) [µL]*	*w(Protein/ tissue) [µg/g]*	*Gain*	*w(Ferritin/ tissue) [µg/g]*	*Gain*
Brain 4	84,64	21700	646,1		36,6	
Brain 4S		11770	249,7	+ 39 %	19,2	+ 52 %

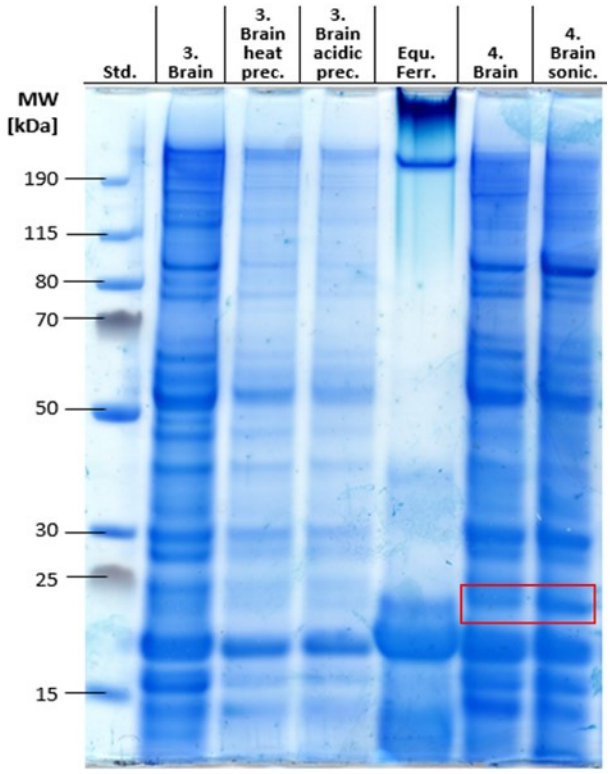

Figure 7. Effect of heat-, acidic precipitation and sonication treatment on ferritin content and -yield: *Lanes designated with "brain" only contain protein samples, which ran through the whole purification procedure (except SEC). Heat- and acidic precipitation samples were taken from the supernatant after respective treatment. Lane designated with "brain sonic." reflects the sonicated sample: the tissue pellet (obtained after homogenization with Turrax Homogenizator) was re-suspended in buffer, subjected to sonication, heat- and ammonium sulfate precipitation. All sample lanes were loaded with 50 µg protein, except heat- and acidic precipitated sample (too low concentration; were loaded with as much protein as possible). Acidic precipitation had no impact on impurities. Treatment with sonication resulted in enrichment of ferritin heavy-chain subunit (~ 21 kDa), see red-marked area.*

5.1.3 Skipping the heat precipitation step

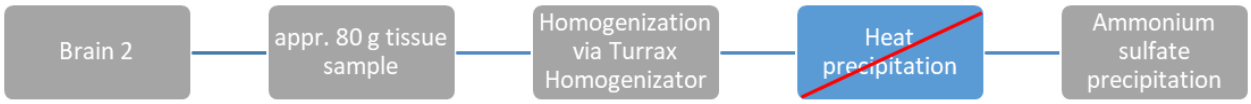

Figure 8. Workflow of the second approach: *the step that has to be evaluated is highlighted in blue.*

Heat precipitation was omitted for one out of eight approaches in order to evaluate if it is critical for the purification procedure. Nevertheless, further processing of the supernatant after homogenization without subsequent heat precipitation appeared to be critical, as solid particles were still present, resulting in a turbid solution. These particles could not be removed by extending the centrifugation run. However, the supernatant was saturated with ammonium sulfate to 75 %. Visual evaluation of the evolving precipitate revealed much more protein compared to approaches with preceding heat precipitation.

5.1.4 Heat precipitation in combination with 40 % methanol

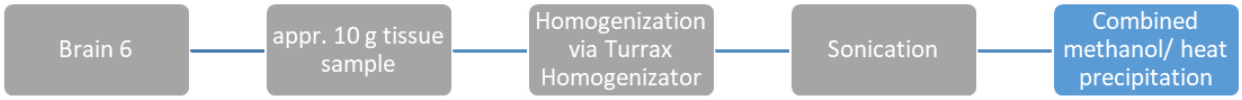

Figure 9. Workflow of the sixth approach: *the step that has to be evaluated is highlighted in blue.*

By combining the heat precipitation with a treatment with 40 % methanol, we tried to increase the ferritin proportion in the protein sample, while not influencing its yield. Although the initial goal, increasing the ferritin content, seems to be achieved when compared with the other approaches, a significant amount of ferritin was lost during the combined heat-/ methanol precipitation. The remaining ferritin amount was about 5 - 7 times lower than generally obtained.

Table 11. Increasing ferritin content by performing a combined methanol-/ heat precipitation: *protein amounts are based on the Lowry-Assay. Ferritin amounts were interpolated by comparing the iron related absorption values of the samples, measured via NanoDrop® at 315 and 420 nm, with calibration series based on ferritin standards from human liver and equine spleen.*

	m(Brain) [g]	*V(Sample) [µL]*	*w(Protein/ tissue) [µg/g]*	*w(Ferritin/ tissue) [µg/g]*	*Ferritin content*
Brain 6	9,85	785	58,2	8,0	13,7%

5.1.5 Adding acidic precipitation for removal of impurities

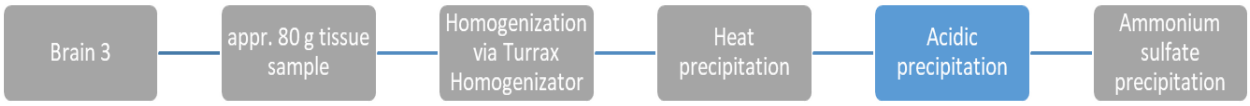

Figure 10. Workflow of the third approach: *the step that has to be evaluated is highlighted in blue.*

Since ferritin possesses a relatively high stability against low pH (see introduction), we tried to acidify the sample for removing as much impurities as possible. In this approach, 500 µL aliquots of the supernatants after heat- and acidic precipitation were taken, respectively, to be able for determination of loss of impurities.

Interestingly, lowering the pH of the heat-treated supernatant to 4,6 was not sufficient to reach a minimum purification factor of 5. The proportions of impurities in the sample remained at almost the same level. Another indicator is Figure 7, it is apparent that no enrichment of ferritin could be achieved.

Table 12. Removing impurities by lowering pH of the protein sample: *the basis for the calculated loss is the sample after heat precipitation. Protein amounts are based on the Lowry-Assay.*

	m(Brain) [g]	*V(Sample) [µL]*	*w(Protein/ tissue) [mg/g]*	*Loss*
Brain 3 (H.P.)	80,82	160000	2,64	
Brain 3 (A.P.)		162000	2,43	
Brain 3 (sub.)			0,21	- 7,9 %

5.1.6 Determining the necessary amount of ammonium sulfate

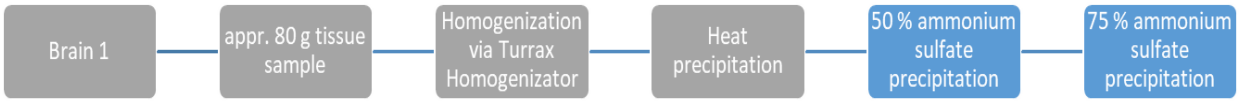

Figure 11. Workflow of the first approach: *the step that has to be evaluated is highlighted in blue.*

Ferritin has a relatively high molecular weight of 480 kDa. As the precipitation likelihood increases with size (~ molecular weight) [62], it should be possible to separate ferritin from lighter proteins. Therefore, we tried to precipitate the whole ferritin fraction with 50 % saturated ammonium sulfate solution, excluding most of the impurities. However, by increasing the ammonium sulfate saturation in the remaining supernatant from 50 to 75 %, the yield of total protein and ferritin could be enhanced by 22 and 26 %, respectively.

Table 13. Gain in protein- and ferritin content after increasing the ammonium sulfate saturation: *the basis for the calculated gain is the sample obtained after precipitation in 50 % saturated ammonium sulfate solution. Protein amounts are based on the Lowry-Assay. Ferritin amounts were interpolated by comparing the iron related absorption values of the samples, measured via NanoDrop® at 315 and 420 nm, with calibration series based on ferritin standards from human liver and equine spleen.*

	m(Brain) [g]	*V(Sample) [µL]*	*w(Protein/ tissue) [µg/g]*	*Gain*	*w(Ferritin/ tissue) [µg/g]*	*Gain*
Brain 1 (50 %)	82,47	15000	584,5		49,1	
Brain 1 (75 %)		10000	130,1	+ 22 %	12,7	+ 26 %

5.1.7 Reducing the amount of brain and skipping ammonium sulfate precipitation

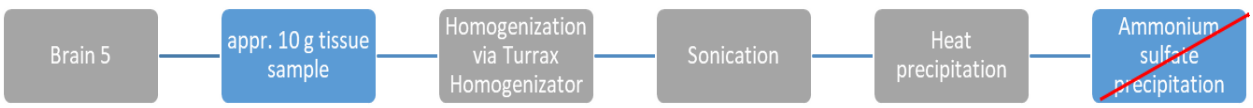

Figure 12. Workflow of the fifth approach: *the step that has to be evaluated is highlighted in blue.*

The aim of this approach was to test if enough protein/ ferritin can be obtained by reducing the initial amount of brain tissue 8 fold. Furthermore, to avoid sample loss, due to an incomplete precipitation, the ammonium sulfate precipitation step was skipped. After all purification steps, a final volume of 710 µL

containing 0,68 mg/mL ferritin and 15,29 mg/mL protein in total was obtained. This was enough for determining ferritin enrichment and its yield, which was comparable with preceding approaches.

Table 14. Protein and ferritin content after reduction of brain amount and cancelled ammonium sulfate precipitation: *protein amounts are based on the Lowry-Assay. Ferritin amounts were interpolated by comparing the iron related absorption values of the samples, measured via NanoDrop® at 315 and 420 nm, with calibration series based on ferritin standards from human liver and equine spleen.*

	m(Brain) [g]	*V(Sample) [µL]*	*w(Protein/ tissue) [µg/g]*	*w(Ferritin/ tissue) [µg/g]*	*Ferritin content*
Brain 5	9,74	710	1114,8	49,6	4,5 %

5.1.8 Storage under reducing conditions

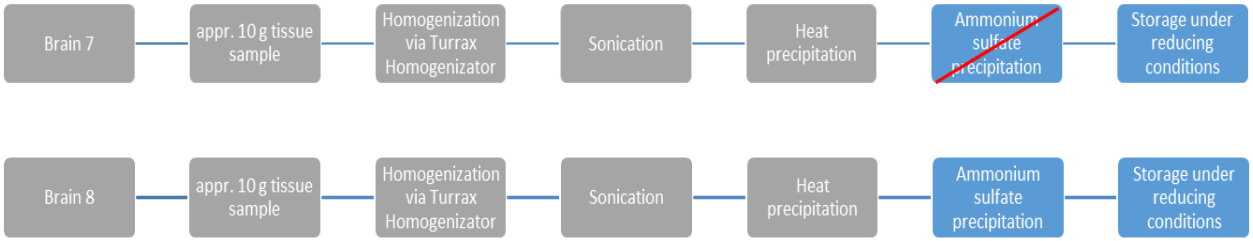

Figure 13. Workflow of the seventh and eight approach: *the step that has to be evaluated is highlighted in blue.*

With the addition of reducing agents, we wanted to aim the problem of smeary bands (only with Native-Page) and moreover we aimed to prevent the formation of protein aggregates. At first glance, the results listed in table x are similar to preceding approaches, especially the fifth one. However, the corresponding Native-Page revealed a substantial difference compared to previous runs (see Figure 14 for an example), at least for the seventh brain with missing ammonium sulfate precipitation. The iron stained ferritin molecules merged in one common band (see red frame), as expected under right conditions, whereas ammonium sulfate precipitated samples appeared smeary.

Table 15. Optimization of storage conditions by preserving a reduced state: *ammonium sulfate precipitation was skipped for brain 7. Protein amounts are based on the Lowry-Assay. Ferritin amounts were interpolated by comparing the iron related absorption values of the samples, measured via NanoDrop® at 315 and 420 nm, with calibration series based on ferritin standards from human liver and equine spleen.*

	m(Brain) [g]	*V(Sample) [µL]*	*w(Protein/tissue) [µg/g]*	*w(Ferritin/tissue) [µg/g]*	*Ferritin content*
Brain 7	9,78	600	1202,1	53,6	4,5%
Brain 8	9,93	580	1371,9	65,7	4,8%

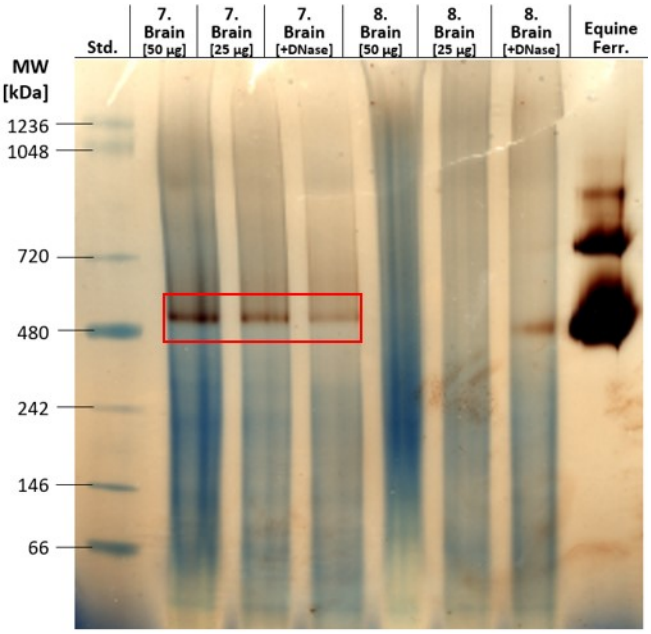

Figure 14. Effect of reduced protein amount and DNA digestion on Native-Page run: *gel was stained with Prussian Blue solution and the sensitivity for iron was enhanced with DAB. All samples ran through the whole purification procedure (except SEC) and a reduced state was preserved during storage (+ 1 mM 2-mercaptoethanol). Lanes designated with "+DNase" were loaded with 25 µg protein being treated with 100 µg/mL DNase I. Reduction of protein amount had no visible impact on protein separation, at least for the 7. Brain. The same was the case for DNase I treated samples. Storage under reduced condition resulted in a sharp ferritin band (~ 480 kDa), see marked area. Further dilution due to reduced protein amount resulted in improvement for ammonium sulfate treated samples (8. Brain), concerning band streaking. However, the ionic strength was still too high, as the ferritin band appeared smeary, see marked area.*

5.2 Testing ferritin purity with SDS-/ Native-Page and western blotting

By using SDS-/ Native-Page gel electrophoresis and western blotting, we aimed to test the ability of certain electrophoretic techniques for a visual based, semi-quantitative determination of the ferritin proportion within the protein sample.

5.2.1 SDS-Page

Separated protein bands could not be certainly assigned to ferritin light- and heavy-chain, as other protein (-subunits) overlap with them (see red frame, SDS-Page). In contrast to that, its use for evaluation of purity was promising, since impurities can be visualized in easy and fast manner. Western blotting of the SDS-Page separated proteins revealed ferritin corresponding heavy-chain subunit at expected height (~ 21 kDa). Interestingly, even more protein bands appeared during signal capturing. Several reasons might be possible: bands lower than expected may reflect degradation products of the ferritin subunits; bands possessing higher molecular weight may represent various oligomeric states of subunits (both, degraded or not), but unspecific binding of the primary antibody must also be considered.

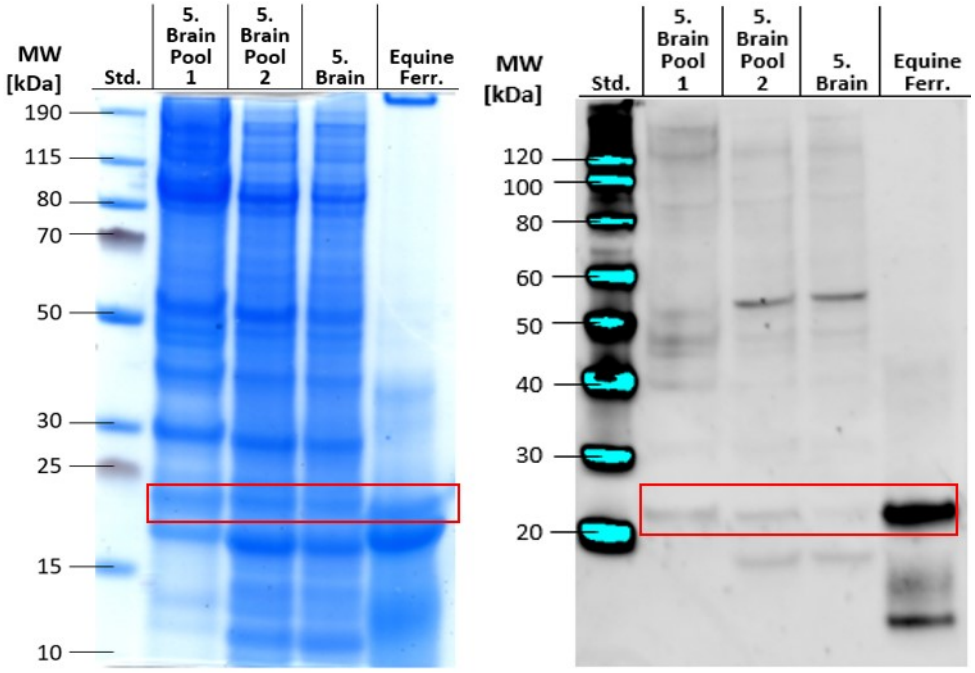

Figure 15. Usability of SDS-Page and corresponding western blotting for estimation of ferritin content and -purity: *all samples ran through the whole purification procedure. Samples present in lanes designated with "pool 1 or 2" were further separated via size exclusion chromatography (pool 1 represents pooled fractions with high amount of iron, whereas pool 2 consisted of the remaining protein fractions). All lanes were loaded with 50 µg protein.* ***Left picture:*** *ferritin enrichment in pool 1 could not be verified, as other proteins overlapped with its heavy-chain subunit band (~ 21 kDa).* ***Right picture:*** *the Abcam rabbit anti H-ferritin antibody (1:500) was used for marking ferritin heavy-chain. The signal for the ferritin heavy-chain was stronger in pool 1, than for the other samples. However, even more protein bands appeared, which could not reliable assigned to ferritin.*

5.2.2 Blue-Native-Page

The same assignment uncertainty, as with SDS-Page, comes along with Coomassie Blue stained Native-Page, though not to such a big extent. However, in contrast to SDS-Page, the ferritin iron core could be specifically stained, which greatly helped us to detect ferritin bands in easy and fast manner. The specificity of this Prussian Blue staining method could be verified with western blotting, see Figure 16, red framed areas. Even the smallest amounts of ferritin could be detected by enhancing the staining intensity with DAB, resulting in a dark brown color.

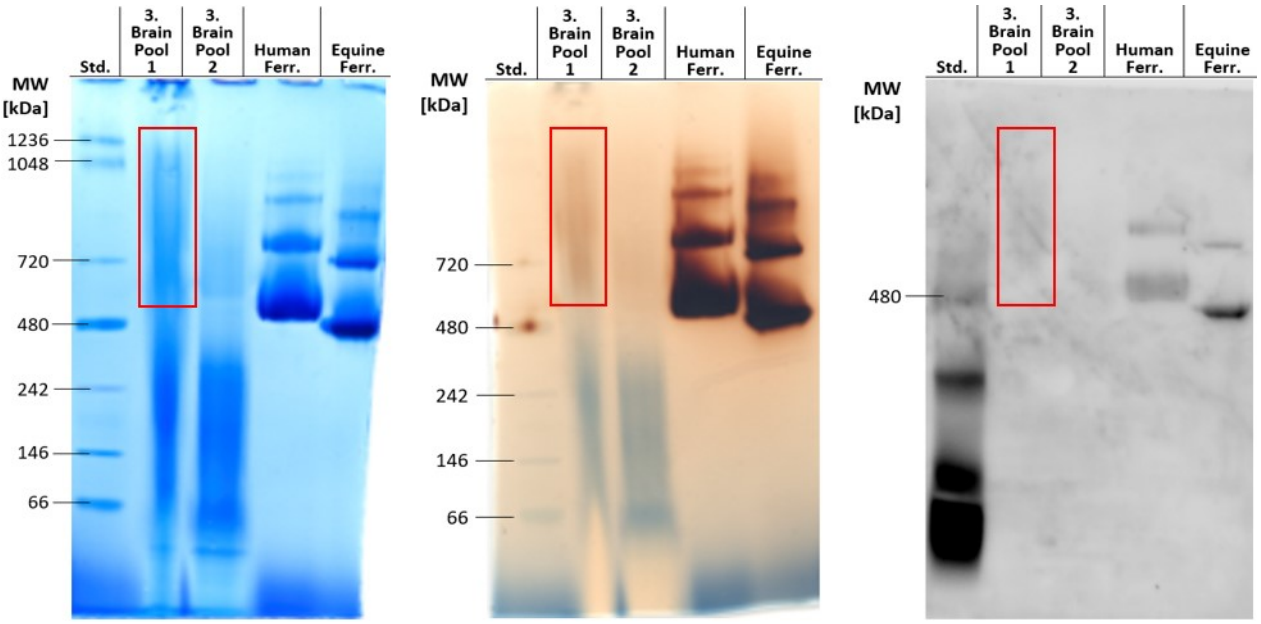

Figure 16. Usability of Native-Page and corresponding western blotting for estimation of ferritin content and -purity: *the first gel was stained with Coomassie Blue, the middle gel was stained with Prussian Blue solution (+ DAB enhancement) and the right picture represents the corresponding western blot. All samples ran through the whole purification procedure. Proteins bands appeared smeary due to high ionic strength within the samples. Samples present in lanes designated with "pool 1 or 2" were further separated via size exclusion chromatography (pool 1 represents pooled fractions with high amount of iron, whereas pool 2 consisted of the remaining protein fractions). All lanes were loaded with 50 µg protein.* ***Left picture:*** *the smeary band (~ 480 kDa, appeared bigger) of pool 1 and 2 could not be reliable assigned to ferritin, as other proteins may have overlapped with it.* ***Middle picture:*** *reliable assignment of the ferritin band became possible with Prussian Blue staining and subsequent DAB enhancement, as ferritin specific iron loading appeared in brown color. Protein pool 1 contained more iron than the second pool, showing a more intense brown color.* ***Right picture:*** *the Abcam rabbit anti H-ferritin antibody (1:500) was used for marking native ferritin. Thereby, the intensive brown stained band of pool 1 in the middle picture could be verified for being ferritin.*

5.3 Aiming band smearing & protein aggregation

During the method development we were faced with ongoing troubles, which may have been related to protein association/ aggregation. Therefore, we tested several approaches in order to reduce and/ or prevent the formation of aggregates. As the problem became most obvious with Native-Page electrophoresis, it was a promising tool for assessment of the results/ effects described below.

5.3.1 Removal of DNA complexes

Prior to electrophoresis, samples were treated with different DNases (DNase I and Benzonase®), in order to break up complex DNA structures. Regarding the Native-Page run shown in Figure 17, it seemed that treatment with 50 µg/mL DNase I had a noticeable effect against band smearing, at least for ferritin located in the range of 480 - 720 kDa. The impact of Benzonase® treatment was weaker. In order to find the minimal concentration for the most satisfying result, DNase I was added in concentrations of 50, 200 and 500 µg/mL. Interestingly, DNase I treatment showed no effect in these experiments, even at the highest concentration, which is in contrast with the first result. Thus, the approach was repeated with 100 µg/mL DNase I, see Figure 14. However, the effect of DNase could not be repeated in further experiments. As

modification to the previous approaches, the heat stable supernatant was stored overnight in presence of 1 mM 2-mercaptoethanol. Again, no effect could be observed compared to samples without DNase treatment.

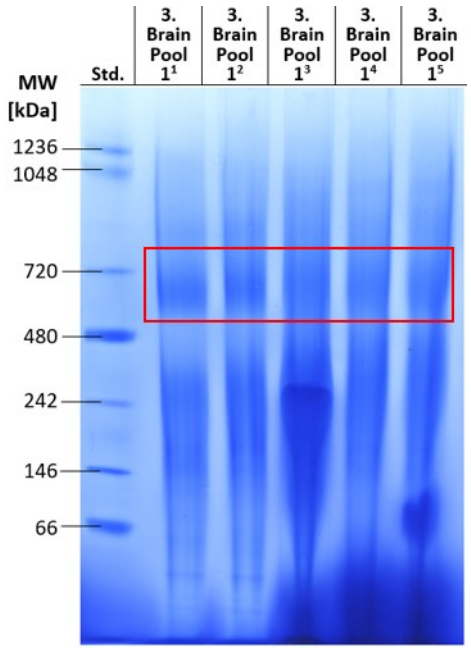

Figure 17. Evaluating the impact of DNase- and detergent treatment on protein separation: *the gel was stained with Coomassie blue and each lane were loaded with 50 µg protein. The samples ran through the whole purification procedure and were further separated via size exclusion chromatography. Fractions with high amount of iron (measured with UV absorption) were pooled. 1) treatment with 50 µg/mL (= 4,15 U) DNase I. 2) treatment with 60 U Benzonase®. 3) treatment with 1 % DDM. 4) treatment with < 1 % digitonin. 5) treatment with 1 % digitonin. DNase I treatment seemed to have a noticeable effect on protein separation and band smearing, at least for ferritin (~ 480 kDa, appeared bigger). The effect of Benzonase® was weaker, whereas treatment with detergents showed no effect at all.*

5.3.2 Prevention of protein aggregation

The formation of protein aggregates might be a reason for the “smeary band effect”. Thus two approaches were carried out aiming to minimize protein aggregation.

Use of detergents

The intention behind using detergents was to prevent hydrophobic interactions that may have led to aggregation, even though rather unlikely, since ferritin molecules are located in a hydrophilic environment [29]. The results are shown in Figure 17. As expected, sample treatment with detergents had no effect on protein smearing at all.

Use of reducing agents

In this case, reducing agents were added to the sample after heat precipitation (2-mercaptoethanol) and/or prior electrophoresis (DTT). Reducing agents antagonizes the effect of an oxidative environment, preventing the formation of intermolecular disulfide bridges and oxidation of Fe^{2+} ions to Fe^{3+}. Referring to figure x, the use of reducing agents had a considerable influence on the separation process, especially on ferritin molecules, as they are merging in a sharp band. The next Native-Page was not carried out with fresh samples, but with one month old ones. The result indicates, that the effect of reducing agents is limited in time, as ferritin molecules were aggregated (> 720 kDa). The higher the added DTT concentration was, the more ferritin molecules could be liberated from aggregated state merging in a sharp band as monomers (see Figure 18, red frame).

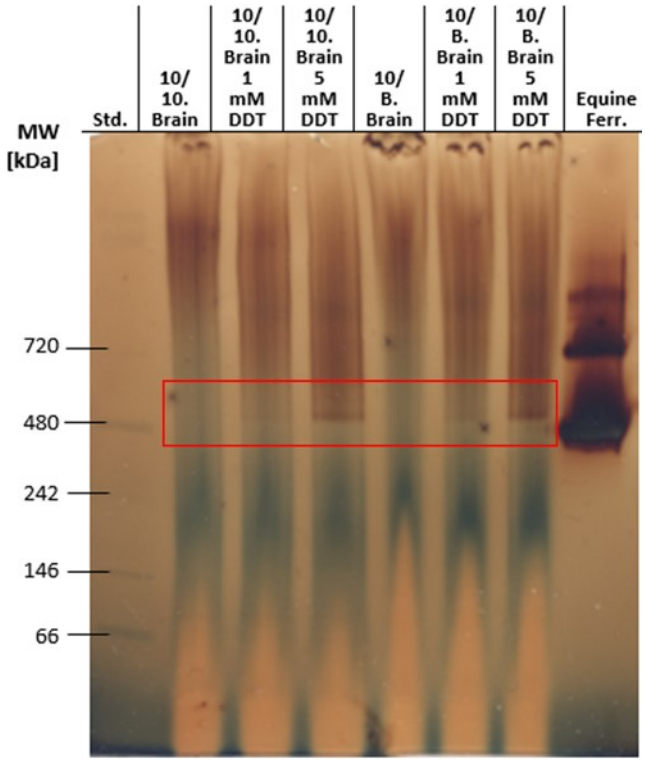

Figure 18. Further testing the impact of reducing agents on protein separation and ferritin aggregation: *gel was stained with Prussian Blue solution and the sensitivity for iron was enhanced with DAB. All samples ran through the whole purification procedure (except density gradient centrifugation) and lanes were loaded with 50 µg protein. It seemed that the effect of reducing agents is limited in time, as one month old samples were used here stored under reduced conditions. The higher the added DTT concentration, the more ferritin molecules merged into one sharp band (~ 480 kDa).*

5.4 Statistical evaluation of critical steps

Since sonication may contribute to the formation of protein aggregates [77] and the use of ammonium sulfate precipitation prevents a clear evaluation with Native-Page (smeary bands), we tested their

necessity for reaching our aim by doing a statistical evaluation. As can be seen in Table 16 and Table 17, there is no noticeable difference ($p \sim 1$), in terms of obtained protein amount, when comparing different storage conditions (ammonium precipitated state, or not). The addition of a sonication step to the homogenization procedure resulted in obtaining slightly more protein in total ($p > 0,05$) and significantly more ferritin ($p < 0,05$). The Native-Page runs referring to both storage conditions were comparable to the results in Table 15, again the high ionic strength coming along with ammonium sulfate precipitation resulted in smeary bands (see green frame). However, the significant effect of sonication on the ferritin yield could not be verified visually by Native-Page (see red frame).

Table 16. Effect of sonication and ammonium sulfate precipitation on yield with respect to total protein: *n= 6 for statistical evaluation of ammonium sulfate precipitation and n= 7 regarding sonication. Protein amounts are based on the Lowry-Assay. Results with a p-value < 0,05 were considered as significantly different.*

total protein	*Mean value [µg/g]*	*SD [µg/g]*	*p-value*
without ammonium sulfate	1040,8	406,1	
with ammonium sulfate	1033,9	55,4	0,9688
without sonication	893,0	254,4	
with sonication	1084,9	294,4	0,2162

Table 17. Effect of sonication and ammonium sulfate precipitation on yield with respect to ferritin: *n= 6 for statistical evaluation of ammonium sulfate precipitation and n= 7 regarding sonication. Ferritin amounts were interpolated by comparing the iron related absorption values of the samples, measured via NanoDrop® at 315 and 420 nm, with calibration series based on ferritin standards from human liver and equine spleen. Results with a p-value < 0,05 were considered as significantly different.*

ferritin	*Mean value [µg/g]*	*SD [µg/g]*	*p-value*
without ammonium sulfate	48,0	17,6	
with ammonium sulfate	45,2	16,8	0,7849
without sonication	34,5	9,4	
with sonication	55,0	14,7	0,0110

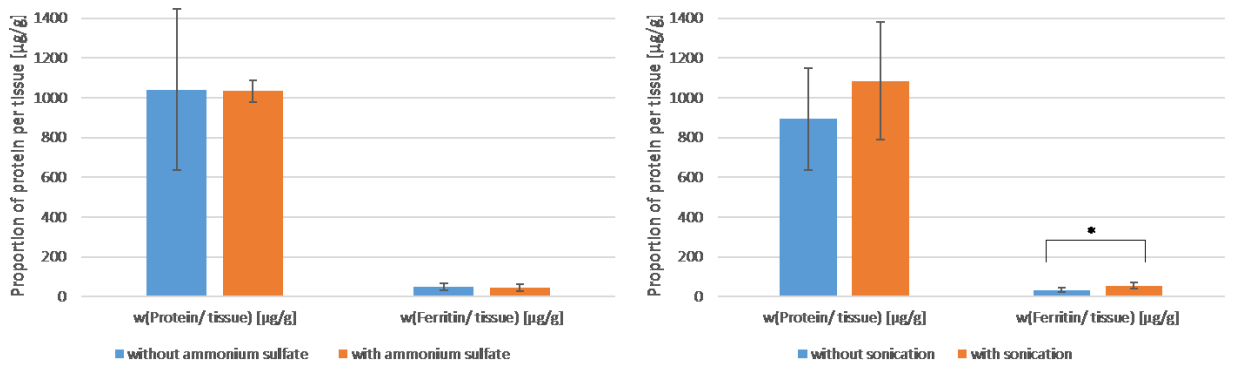

Figure 19. Evaluating the impact of ammonium sulfate precipitation and sonication on protein-/ ferritin yield. *One pig brain (m~ 80 g) per diagram was cut up randomly into smaller pieces, representing individual samples. Protein amounts are based on the Lowry-Assay. Ferritin amounts were interpolated by comparing the iron related absorption values of the samples, measured via NanoDrop® at 315 and 420 nm, with calibration series based on ferritin standards from human liver and equine spleen.* ***Left diagram:*** *further stabilization of proteins due to ammonium precipitated state had no significant effect on protein-/ ferritin yield (n= 6, p~ 1).* ***Right diagram:*** *additional homogenization of the tissue sample with sonication seemed to increase the total protein yield, but not in significant manner (p > 0,05). A stronger effect could be seen on ferritin yield, which raised significantly (p < 0,05), n= 7.*

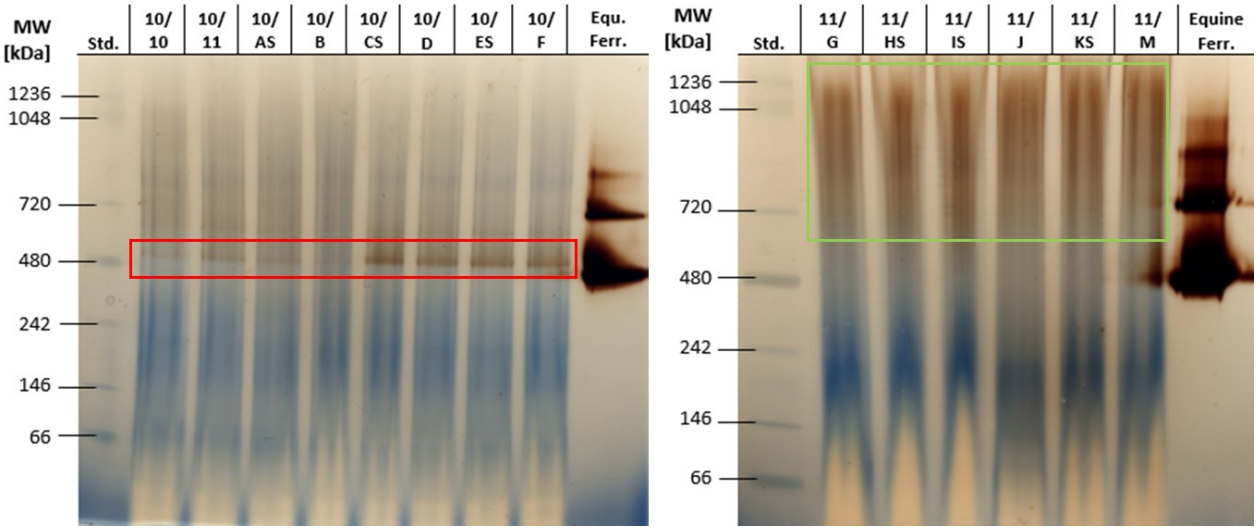

Figure 20. Visual evaluation of the impact of ammonium sulfate precipitation and sonication on protein-/ ferritin yield via Native-Page. *One pig brain (10. and 11. brain, m~ 80 g) per gel was cut up randomly into smaller pieces, representing individual samples (upper number corresponds to common pig brain; lower designation represents individual sample). Both gels were stained with Prussian Blue solution and the sensitivity for iron was enhanced with DAB. All samples ran through the whole purification procedure (except density gradient centrifugation) and a reduced state was preserved during storage (+ 1 mM 2-mercaptoethanol). The suffix "S" reflects sonicated samples including sample 10/11. All lanes were loaded with 50 µg protein.* ***Left picture****: No visible effect of sonication treatment on the ferritin band could be observed. Ferritin molecules merged into one sharp band (~ 480 kDa), even stronger for fresh samples as for 10/CS - 10/F.* ***Right picture:*** *Also here, no significant effect of sonication could be seen visually. However, high ionic strength due to ammonium sulfate precipitation resulted in smeary ferritin bands and overall band streaking (green frame).*

5.5 SEC vs DGC

Size exclusion chromatography and density gradient centrifugation appeared to be decisive techniques for ferritin purification. Since it is not recommended to use both techniques in one trial run to avoid time consumption and sample loss, we compared their effectiveness in terms of protein separation.

5.5.1 Size Exclusion Chromatography

When size exclusion was applied, the chromatogram monitored at 280 nm, see Figure 21 (upper picture), showed no optimal separation of proteins. Two peaks appeared, overlapping each other to a big proportion. Reducing the amount of the attached protein sample did not lead to better separation. In addition to that, the peak of equine spleen ferritin used as reference, overlapped almost completely with both sample peaks, thus each fraction presumably contains ferritin. Poor ferritin isolation could also be detected by looking at each collected fraction from the first peak in detail (separated through a red line), as each fraction still contained impurities, see Figure 22 left picture. However, the fractions showing the highest iron related absorption at 315 and 420 nm, were pooled and concentrated to be further analyzed by Native-Page. As expected, a big proportion of impurity was still present in the polled sample, possessing a smaller molecular weight than 480 kDa. Since the improvements concerning protein aggregation were not yet included in this trial, the ferritin band appeared smeary.

5.5.2 Density Gradient Centrifugation

In contrast to the size exclusion results, protein separation through density gradient centrifugation was more promising. As can be seen in the chromatogram, based on measured absorbance at 280 (blue line) and 315 nm (orange line), two well separated peaks could be monitored, overlapping each other only to a small extent. Monitoring of the iron related absorption at 315 nm revealed that the main fraction of ferritin is present in the first peak. The second peak, containing particularly impurities, showed a slight elevation at exactly the same area, where the measured absorbance at 280 nm reached a maximum. That is most likely due to high concentrated non-iron containing proteins absorb also UV-light at 315 nm, even to a smaller extent, see Table 5 as example. However, the fractions representing the first peak (indicated by a red line) were further analyzed via SDS-Page for impurities, see Figure 22 right picture. All fractions until A12 contained purely ferritin, which could be verified via Native-Page concerning the pooled sample (= pool 1). The capability of ultra-filtration with a 300 kDa cut-off for ferritin isolation was also tested here. This approach seemed to be promising, as impurities could be removed from the second pool, which initially consisted of the remaining fractions (primarily representing the second peak of the chromatogram). However, also ferritin molecules were small enough for passing the selected filter, as can be demonstrated by iron staining of the flow-through, see Figure 23 right picture.

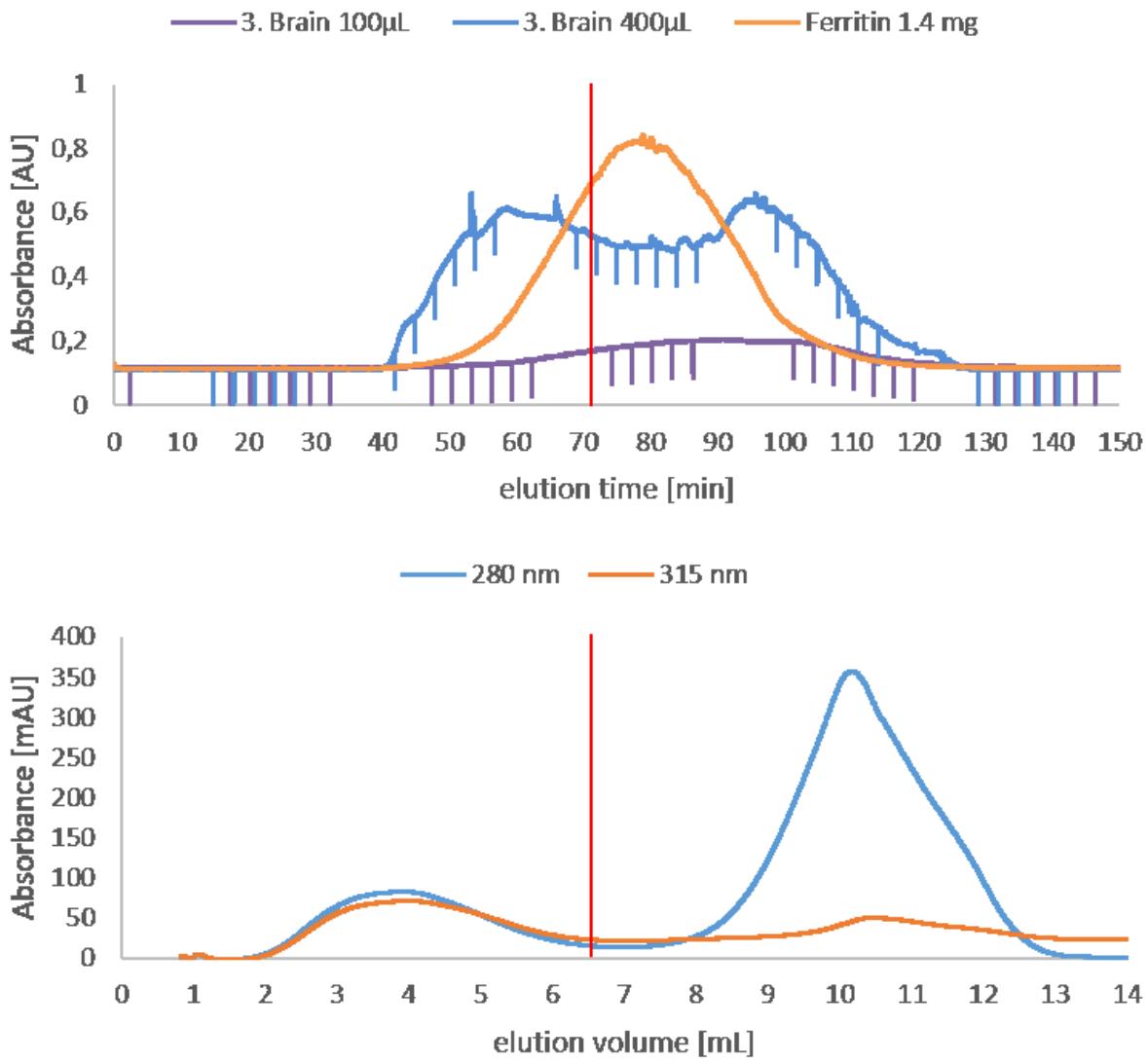

Figure 21. Comparison of SEC with DGC based on protein separation. Upper chromatogram: *the sample was applied in varied amounts on the column. Only protein related absorption at 280 nm was monitored (detector limitation). Protein sample separated into two peaks overlapping each other to a big proportion. Each fraction presumable contained ferritin, as the reference peak (equine ferritin) overlapped almost completely with the sample peaks. Reduction of applied protein amount showed no effect on protein separation.* ***Lower chromatogram:*** *the sample (brain 10/11) was completely layered on the gradient. Protein and ferritin iron core related absorption was monitored at 280 and 315 nm, respectively. Two well separated peaks appeared. The main fraction of ferritin was present in the first peak (based on 315 nm absorption). The second peak reflected the amount of impurities.*

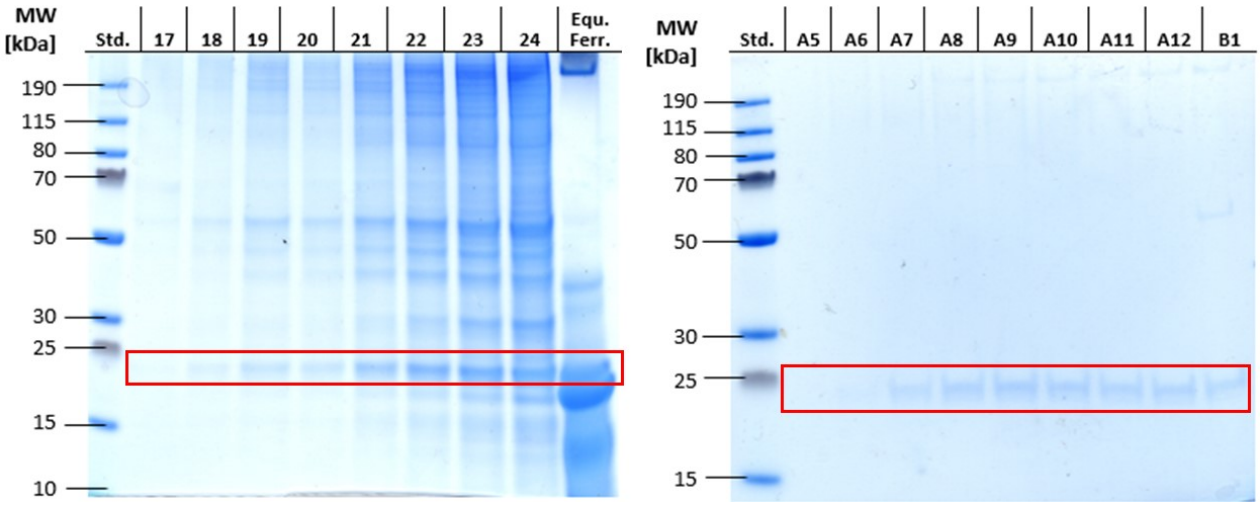

Figure 22. Evaluating the purity of ferritin enriched fractions from SEC and DGC via SDS-Page: *both gels were stained with Coomassie Blue. The maximum possible volume of collected fractions from figure 9 (see mark) was applied in the lanes.* ***Left picture: (based on SEC):*** *each fraction still contained a high proportion of impurities.* ***Right picture (based on DGC):*** *all fraction until A12 contained purely ferritin heavy- and light-chain (~ 21 and 19 kDa).*

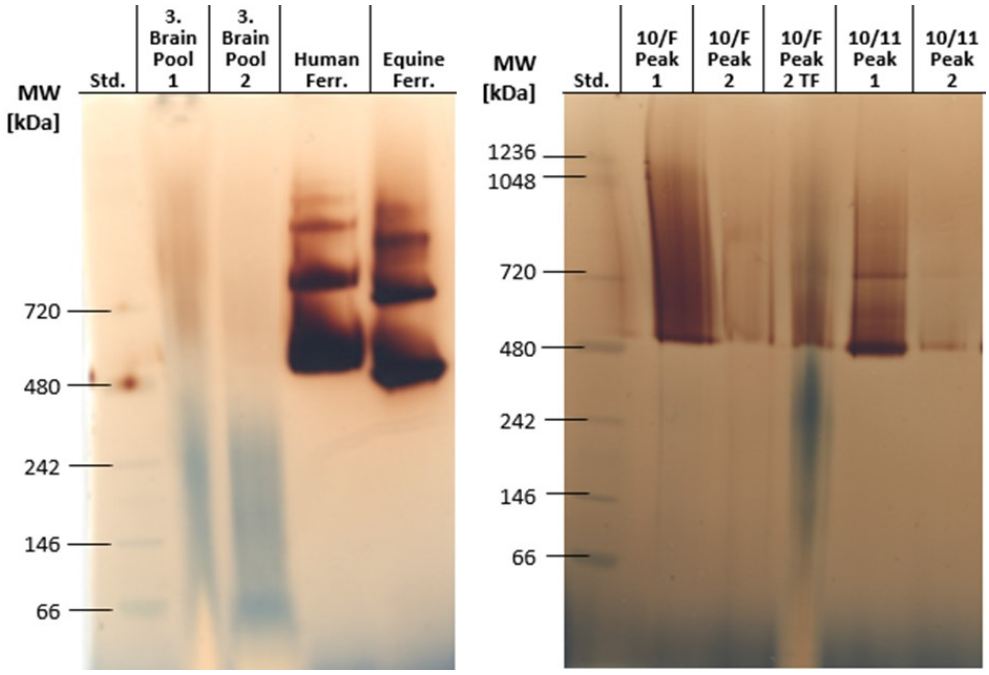

Figure 23. Evaluating the purity of ferritin pooled fractions after SEC and DGC via Native-Page: *both gels were stained with Prussian Blue solution and the sensitivity for iron was enhanced with DAB. Samples designated with "pool 1 or peak 1" represented pooled fractions with highest amount of iron (based on UV absorption). "Pool 2 or peak 2" consisted of the remaining protein containing fractions. "Peak 2 TF" represented the flow through after ultra-filtration (a 300 kDa cut-off was selected for the second peak in contrast to 100 kDa for the other samples).* ***Left picture (based on SEC):*** *the ferritin enriched sample pool 1 still contained a big amount of impurities (stained blue). Ferritin was also detectable in pool 2, at least the iron loaded fraction (apo-ferritin could not be stained by this approach).* ***Right picture (based on DGC):*** *impurities could almost be completely removed by aids of density gradient centrifugation (peak 1) or ultra-filtration with 300 kDa cut-off (peak 2). The flow-through still contained a high proportion of iron loaded ferritin, thus ferritin molecules could also pass the 300 kDa cut-off filter.*

5.6 Evaluation of the final procedure & analysis of the ferritin iron load

All the results obtained and experience made with pig brains helped us finally modify the purification procedure for human brain tissue (see experimental section 4.6 for further detail). Here the results were compared with those obtained with pig brains and even further assessed via electron microscopy.

5.6.1 Assessment of the results using electrophoretic techniques

In terms of protein separation, the results of the final procedure used for human brain tissue resembled those for pig brain samples when the density gradient centrifugation was used. Apparently, the last minor modifications of the procedure went into the right direction, as much more ferritin could be isolated than for pig brains. This is visible in Figure 24, where a 10 times higher maximum absorbance value was monitored for the first peak of the chromatogram corresponding to iron related absorption at 315 nm (chromatograms of the other samples showed similar results). The SDS-Page result, showing fractions from the first peak, confirmed this initial finding, as bands related to the ferritin subunits (light-chain= 19 kDa; heavy-chain= 21 kDa) were stained more intensely blue compared to pig brain samples (see Figure 22 and Figure 24 for comparison). Interestingly, an unknown band, exceeding the molecular weight range of the reference, accompanied the ferritin subunits in designated pure fractions.

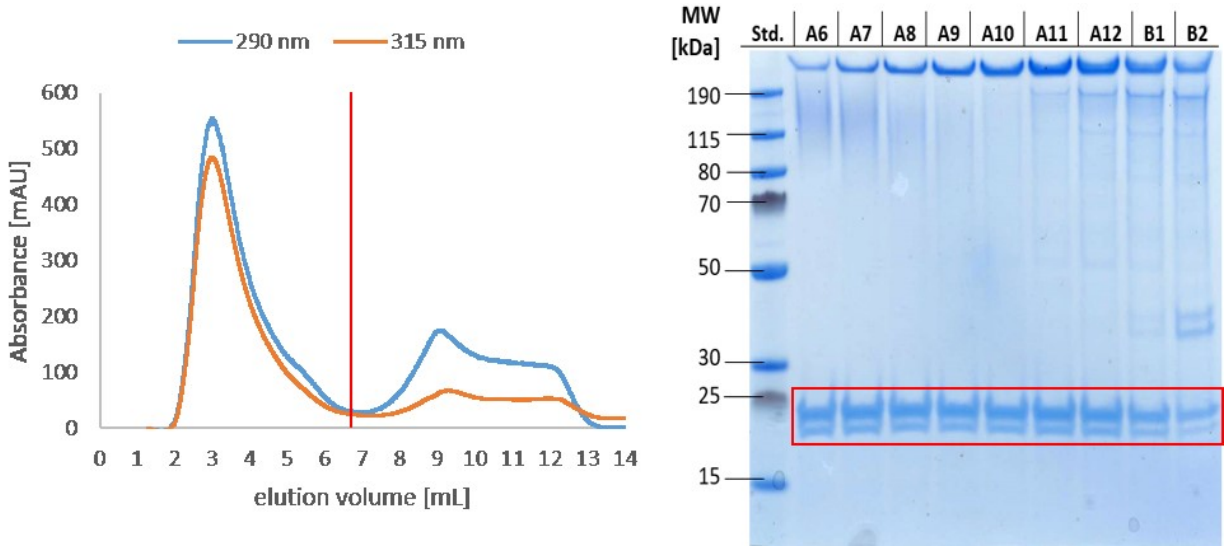

Figure 24. Evaluating the separation performance of DGC concerning human brain tissue samples: *the whole sample was layered on the gradient after ferritin enrichment.* ***Left chromatogram:*** *Protein and ferritin iron core related absorption was monitored at 280 and 315 nm, respectively. Two well separated peaks appeared. The main fraction of ferritin was present in the first peak (based on 315 nm absorption, separated from the second peak by a red line). The second peak reflected the amount of impurities.* ***Right picture:*** *gel was stained with Coomassie Blue. Fractions reflecting the first peak of the DGC run were applied in maximum amount on SDS-Page. Each fraction until A11 contained purely ferritin heavy- and light-chain (~ 21 and 19 kDa). An unknown third band appeared, which exceeded the molecular weight range of the reference.*

Further analysis of the second peak (see red line in the chromatogram) by western blotting revealed that ferritin molecules are present only in the first selected fraction, accompanied by minor impurity. Thus, ferritin could be separated almost completely from other proteins.

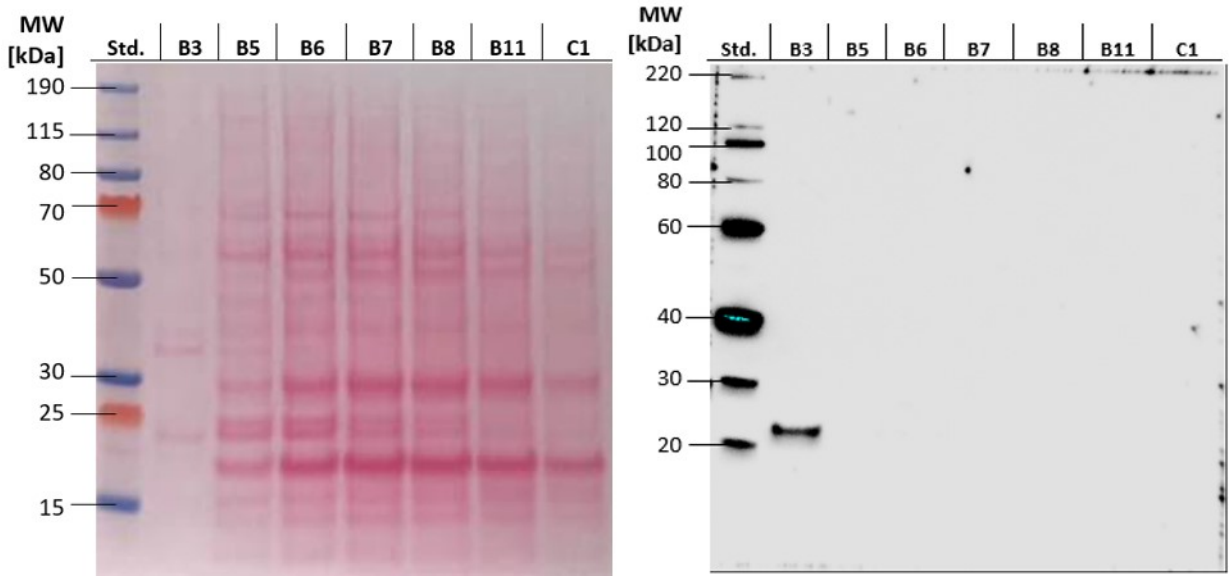

Figure 25. Taking a deeper look at the second peak from the DGC run for ferritin molecules. Left picture: *the picture shows the Ponceau S stained membrane. Fractions reflecting the second peak were randomly selected in order to cover its distribution as much as possible and were applied in maximum amount. Compared to the first peak (see Figure 24), the second peak contained mostly impurities.* ***Right picture:*** *ferritin heavy-chain was marked with the Abcam rabbit anti H-ferritin antibody (1:500). Only fraction B3, reflecting the beginning of the second peak, contained detectable amount of ferritin (~ 21 kDa).*

However, only pure fractions ranging from A4 - A11(12) were pooled, concentrated and evaluated via Native-Page, see right picture of Figure 26. Impurities being smaller than 480 kDa could be completely removed see left picture of Figure 26 for a reflection of the samples before being separated via density gradient centrifugation. Apart from the expected bands for ferritin located at 480 kDa (=monomer) and about 720 kDa (=dimer), one further “smeary”-band could be observed. The location of this additional band (1048 - 1236 kDa for samples from March and > 1236 kDa for samples from April) obviously depended on the duration of storage of the tested tissue samples. Nevertheless, about 50 µg ferritin per g brain could be yielded in the pure sample.

Table 18. Overview about measured ferritin amounts: *here ferritin amount was determined with the Lowry-Assay, as sample was judged to contain purely ferritin.*

	m(brain) [g]	*V(sample) [µL]*	*w(ferritin/ brain) [µg/g]*
Occipital cortex Fe260318	15,80	105	51,7
Occipital cortex Fe180418	11,22	45	37,5
Frontal cortex Fe230318	15,35	80	43,7
Frontal cortex Fe180418	9,25	70	57,5

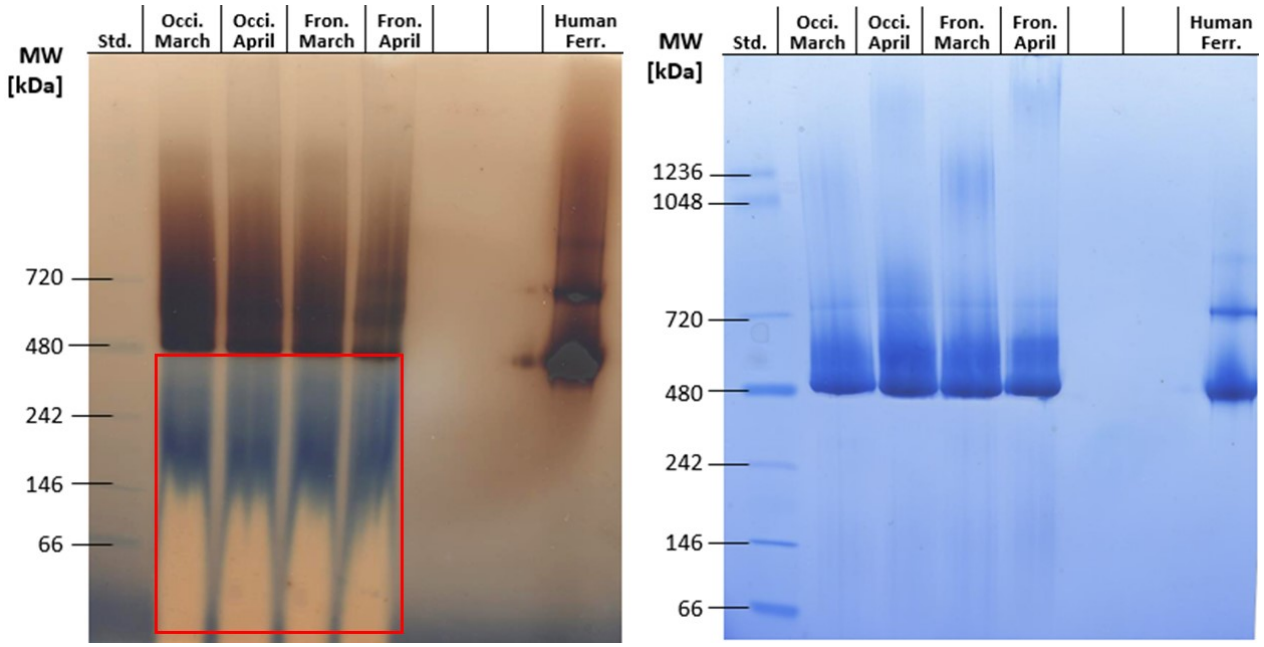

Figure 26. Comparison of purified ferritin samples before and after DGC: *each lane was loaded with 50 µg protein. The left gel was stained for iron with Prussian Blue solution (+ DAB enhancement), whereas the right gel was stained with Coomassie Blue.* ***Left picture:*** *each sample still contained a big proportion of impurities being smaller than 480 kDa, appearing in blue color. Brown coloured ferritin molecules merged into a sharp band at 480 kDa dragging a brown veil behind.* ***Right picture:*** *Impurities being smaller than 480 kDa could be completely removed by DGC. Also, a light stained band representing the ferritin dimer appeared at appr. 720 kDa. An additional smeary band could be observed for all samples but in different location, which obviously depended on duration of storage (1048 - 1236 kDa for samples from March and > 1236 kDa for samples from April).*

5.6.2 Assessment of sample purity with TEM

As can be seen from negatively stained ferritin samples that had been obtained with the final isolation procedure, the samples contained sufficiently pure ferritin, as no other proteins could be observed during image acquisition. However, some of the ferritin molecules seemed to be degraded to different extents (see proteins marked with arrows in Figure 27). Although, the samples were judged to be sufficiently pure in protein context, they contained a noticeable fraction of glycerol, leading to the formation of lipid droplets on the grids (see Figure 27, left picture, arrow marked structures). Jian et al. classified the ferritin iron core morphology by their 2D projection [57]. According to their definition, we could observe a relatively high fraction of “full-rafts”, “small circles” and “crescents”, but also “doughnut” and “dumbbell” like structures appeared, even in a smaller number.

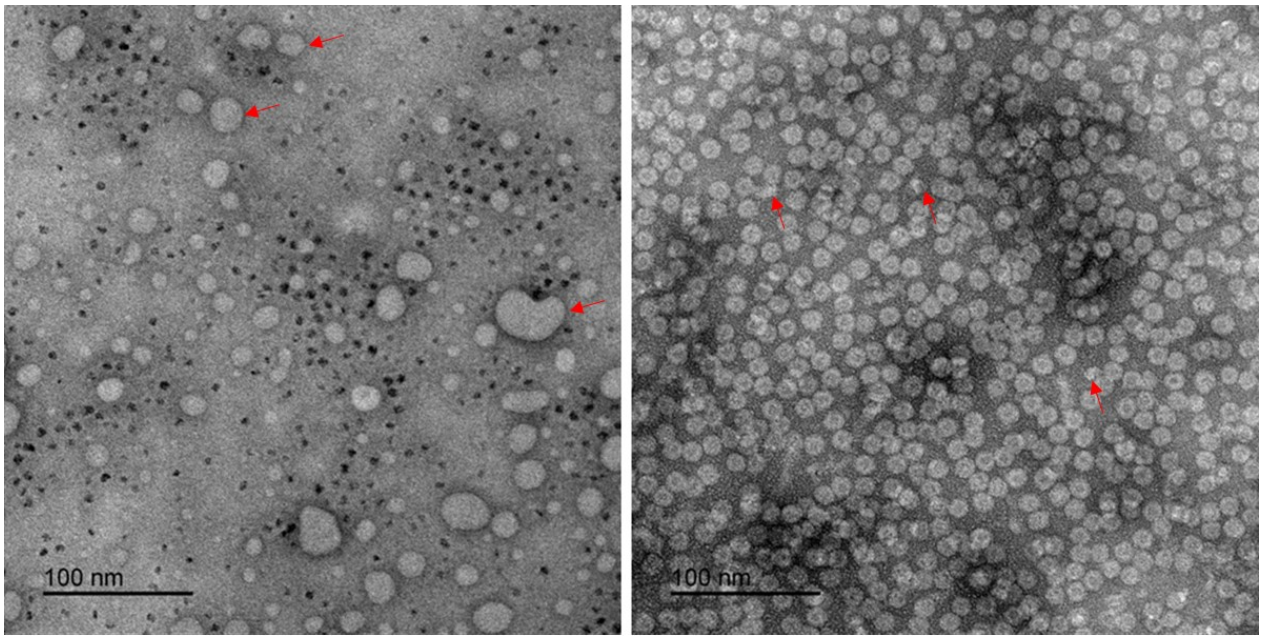

Figure 27. Evaluation of sample purity via bright field imaging and negative staining: *5 µL of the purified sample (frontal cortex, Fe230318) were applied on glow-discharged grids and either analyzed at 50 kx magnification in native state (see left picture) or after negative staining (see right picture). The sample still contained lipid droplets from the glycerol gradient, as can be seen in the left picture (= round-shaped, up to 100 nm big structures, marked with red arrows). The sample could be judged for being sufficiently pure, as no other protein structures could be observed on the negative stained grid. However, some of the ferritin molecules seemed to be degraded (see proteins marked with arrows). The results of the other samples were similar.*

5.6.3 Statistical analysis with SPSS®

Figure 28 gives an example on how well ferritin iron cores could be automatically identified with the CellProfiler™ program. Regardless of a few false-negative and -positive results, the CellProlfiler™ algorithm did a great job in recognizing ferritin iron cores (highlighted as green-framed structures), even though their borders were not well-defined. However, only about the half of the lipid droplets (red-framed structures) could be excluded from the image analysis process. Furthermore, a high number of electron dense structures being smaller than 2 nm could be observed. Since we were limited in resolution, these structures could not be assigned to ferritin with certainty and therefore were excluded from the image analysis process.

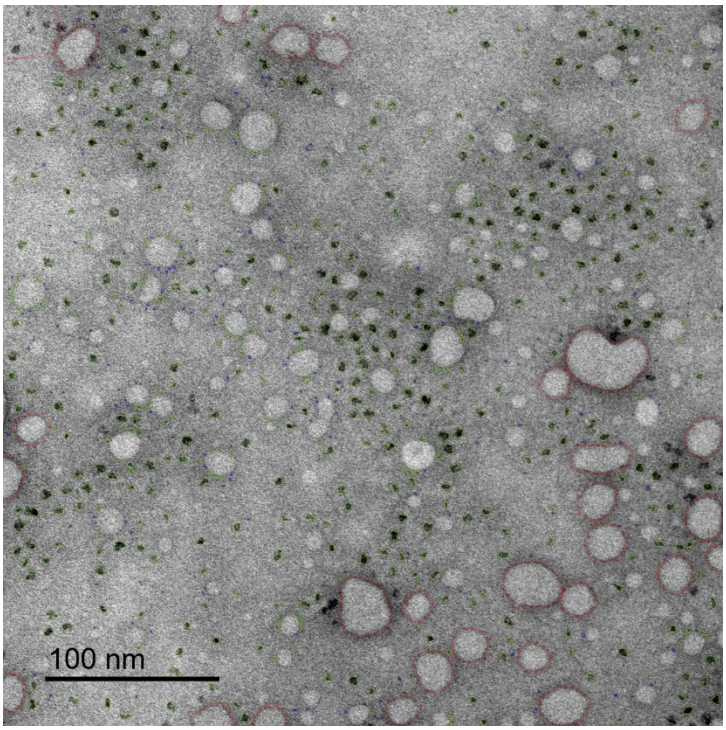

Figure 28. Overview about how well ferritin iron cores could be automatically detected with the CellProfiler™ program: *green-framed iron cores were used for statistical evaluation. Red-framed structures represent lipid droplets, excluded for evaluation. A lower cut-off of 2 nm, concerning the maximal diameter, was set to exclude particles, which could not certainly be assigned to ferritin iron cores (= blue-framed structures). Overall, the CellProfiler™ algorithm did a great job in identifying ferritin iron cores. Nevertheless, it should be mentioned, that some structures could not be identified, even though they showed iron cores with high probability. On the other hand, some structures being identified as iron cores, should be viewed skeptical.*

Once the iron cores of five randomly selected images per brain tissue sample were counted and measured for their maximum- and minimum diameter, the gathered data was analyzed with SPSS software. The figures below show the generated histograms of the analyzed iron cores. At a first glimpse, the distribution of the geometrical parameters of the iron cores were quite similar among both tissue types (occipital- and frontal cortex). But when going into further detail, the distribution of the maximum diameter of the occipital cortex related iron cores peaked at appr. 6 nm, compared to the frontal cortex iron cores, being more equally distributed. In addition to that, ferritin molecules isolated from the occipital cortex seemed to have a higher iron load, reflected by a larger mean-maximum- and also minimum diameter (5,2 ± 2,2 and 3,6 ± 1,9 nm; calculated as mean of the means) compared to the frontal cortex (4,8 ± 2,1 and 3,3 ± 1,7 nm). However, no effect on ferritin iron load distribution could be noted when comparing the same brain tissue samples with different storage lengths (brains from March and April).

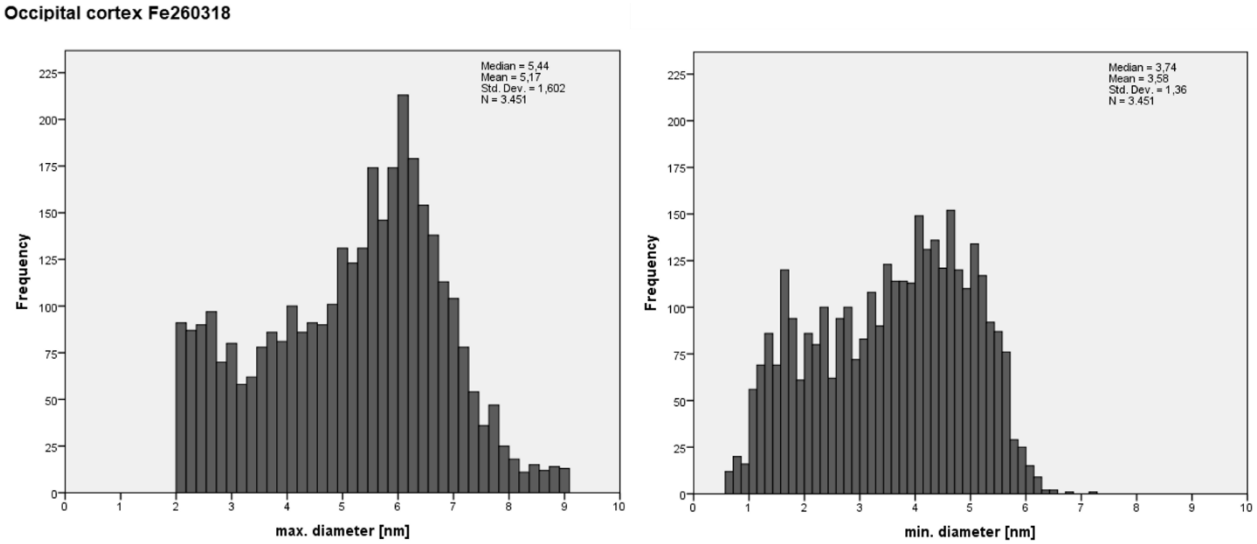

Figure 29. Observed distribution of ferritin iron load based on maximal and minimal diameter of the iron core concerning occipital cortex (Fe260318): *to ensure a representative evaluation of the sample, 5 randomly selected areas on the grid were conducted for statistical analysis, thereby reflecting approximately 3450 ferritin molecules. Ferritin iron cores were automatically detected with the CellProfiler™ program. The left histogram is showing the distribution of measured iron core maximal diameters, while the right histogram is based on the minimal diameter.*

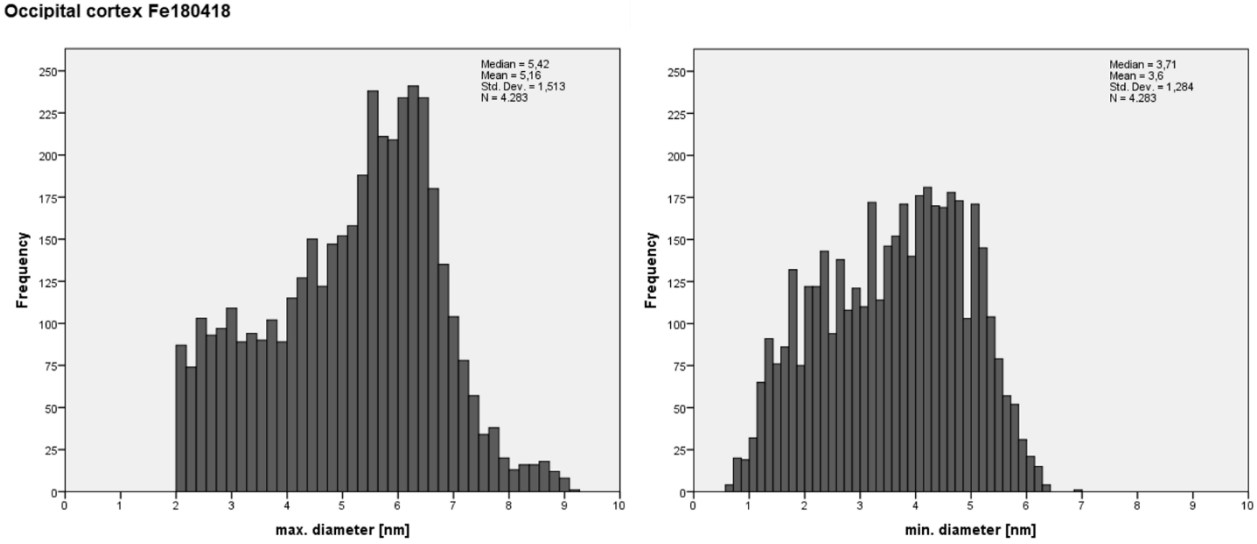

Figure 30. Observed distribution of ferritin iron load based on maximal and minimal diameter of the iron core concerning occipital cortex (Fe180418): *to ensure a representative evaluation of the sample, 5 randomly selected areas on the grid were conducted for statistical analysis, thereby reflecting approximately 4280 ferritin molecules. Ferritin iron cores were automatically detected with the CellProfiler™ program. The left histogram is showing the distribution of measured iron core maximal diameters, while the right histogram is based on the minimal diameter.*

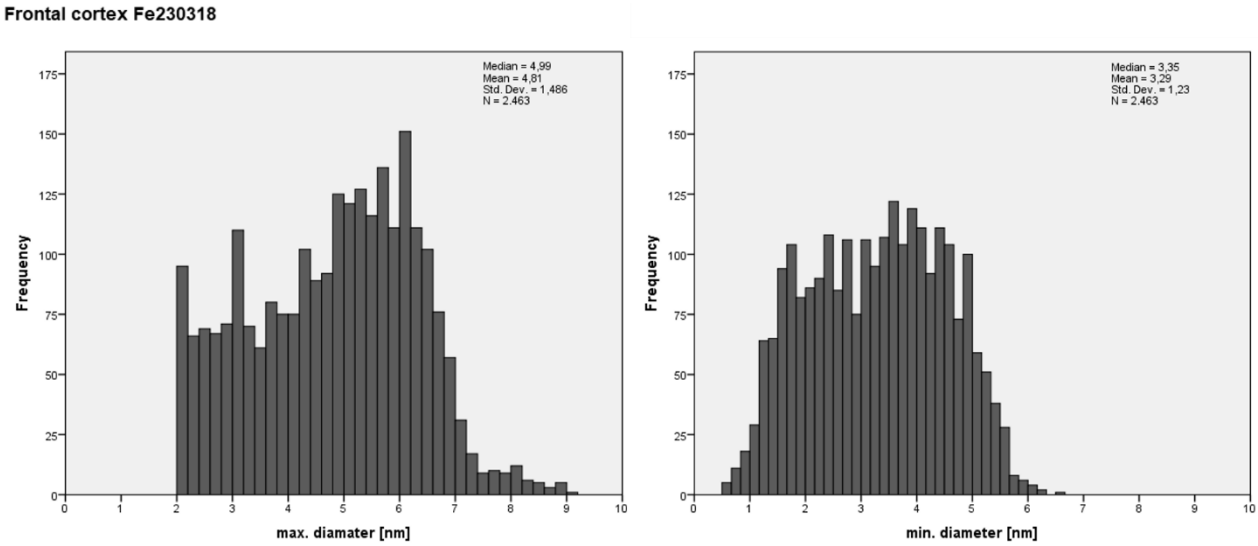

Figure 31. Observed distribution of ferritin iron load based on maximal and minimal diameter of the iron core concerning frontal cortex (Fe230318): *to ensure a representative evaluation of the sample, 5 randomly selected areas on the grid were conducted for statistical analysis, thereby reflecting approximately 2450 ferritin molecules. Ferritin iron cores were automatically detected with the CellProfiler™ program. The left histogram is showing the distribution of measured iron core maximal diameters, while the right histogram is based on the minimal diameter.*

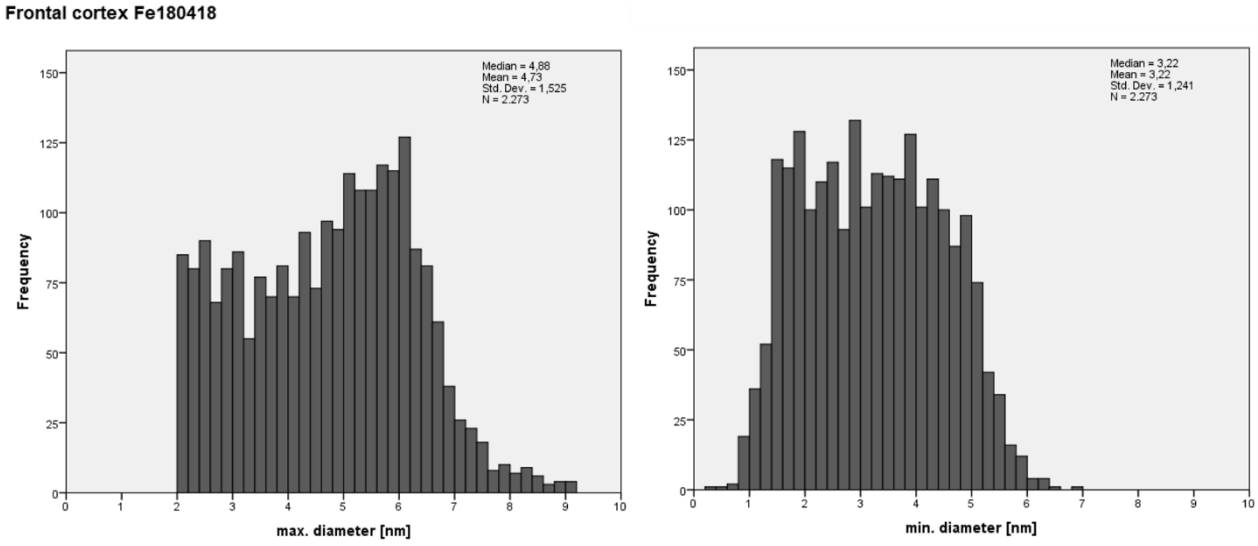

Figure 32. Observed distribution of ferritin iron load based on maximal and minimal diameter of the iron core concerning frontal cortex (Fe180418): *to ensure a representative evaluation of the sample, 5 randomly selected areas on the grid were conducted for statistical analysis, thereby reflecting approximately 2270 ferritin molecules. Ferritin iron cores were automatically detected with the CellProfiler™ program. The left histogram is showing the distribution of measured iron core maximal diameters, while the right histogram is based on the minimal diameter.*

6 Discussion & Outlook

Current research tries to elucidate the linkage of iron accumulation in certain brain regions with neurodegenerative diseases. In particular ferritin and its iron core are of special interest, as they are directly affected by rising iron levels in the cells. It is already known that ferritin isolated from different tissues has different iron loading states ranging from 0 - 5000 iron atoms [57]. However, it is unclear if there are differences in the distribution of ferritin iron levels between brain regions and if neurodegenerative diseases, like Alzheimer, are linked to an alteration of that distribution.

This master thesis provides a method for an almost comprehensive isolation of ferritin out of brain tissue samples from pig and humans. A purification method was thoroughly established with pig brains, and once it met our requirements, also applied to samples of human brain tissue. Several attempts were undertaken to further optimize the initial purification procedure aiming to maximize both ferritin purity and yield. This chapter discusses each approach regarding its capability for enriching ferritin, while at the same time maintaining a maximum yield under preservation of its native, monomeric state. As a first step in comparing the ferritin iron load of different brain regions, we analyzed isolated ferritin molecules from frontal- and occipital lobes with electron microscopic techniques.

The discussion below gives an answer to the following questions: Is the described purification procedure useful for a subsequent quantitative analysis of the distribution of ferritin iron levels with electron microscopic techniques and can we see a difference in iron load distribution regarding different brain regions?

6.1 Aiming maximum yield with the right homogenization method

Since human brain contains in average only 50 µg ferritin per g tissue [11], the aim was to maximize the yield as much as possible. Nevertheless, the chase for better yield should not impair protein stability. Time consuming methods, as well as processes that produce considerable heat must be avoided, while at the same time continuous cooling of the protein sample is essential for preserving physiological state. Therefore, the homogenization step should be performed with care, as lost protein cannot be rescued in subsequent steps. We tried two different approaches to find the best balance between maximum yield and protein stability. With added sonication the ferritin yield could be increased by 52 % compared to homogenization with Turrax Homogenizer alone. Simultaneously, total protein amount increased to a smaller extent of 39 %, indicating that some of the ferritin molecules are tightly associated with membrane structures and can be relieved by sonication. This is in good agreement with Nardi et al. [80], who came to the same conclusion. However, this result should be further evaluated, as a big proportion of the proteins could just be trapped in the tissue pellet and must not be associated with membrane structures. Thus, these trapped proteins might be easily released by re-suspending the remaining tissue pellet. For dispelling this doubt, we have undertaken a statistical evaluation comparing homogenization with Turrax

Homogenizer alone (+ re-suspending the tissue pellet) with added sonication. Similar to the previous result, the ferritin yield could be significantly increased with sonication ($p < 0,05$), while only a slight increase could be noted in case of total protein amount ($p > 0,05$). However, we decided not to use sonication, as it raises the probability for protein aggregation and produces much heat [77]. Moreover, the initial yield of ferritin was sufficient for evaluation and analysis with electron microscopic techniques.

6.2 Enhancing ferritin enrichment with combined methanol-/ heat precipitation

It is generally recommended to use as few purification steps as necessary, as the probability for protein loss decreases and time can be saved, which benefits protein stability [60]. One way to do efficient protein purification is the combination of purification steps. Here we combined methanol- with heat precipitation, which saved us one centrifugation step. Furthermore, this combination provided a harsher condition, than heat treatment alone, thus it got rid of a bulk of impurities, while ferritin was stable enough and almost unaffected. Cham et al. described a method where homogenates are heated at 75 °C for 10 min in presence of 40 % [v/v] methanol resulting in a pure ferritin fraction with 75 % yield compared to heat precipitation only [25]. Looking at the results from the sixth approach we were able to raise the proportion of ferritin from 4 - 8 % to nearly 14 %, which is still far away from being pure. This result is in good agreement with the approach of Bossoni et al., who also had a remaining bulk of impurities in the ferritin fractions after performing the same method [26]. In addition to that, the enrichment was accompanied with a significant loss of ferritin, only 15 % yield could be achieved compared to the standard approach, which was insufficient for further analysis.

6.3 Getting rid of further impurities with acidic precipitation

Several research groups included an acidic precipitation step (pH= 4,6 - 4,8) in their purification procedure [4], [11], [22]–[24], [29], since ferritin has a high stability until a pH of 3,4 (described for equine spleen ferritin) [34]. Although it seemed to be a popular method for purifying ferritin, our approach was not promising, as only 7,9 % impurities could be removed. The reason might be grounded in the buffer used for heat precipitation. The pH of Tris-HCl varies dramatically with temperature (-0,031 pK_a/ °C) [79]. Estimating a temperature increase of about 50 °C during heat precipitation, the pH of the protein solution would fall from 7,4 to 5,85. Probably, this was sufficient for removing most of the pH labile proteins. As it is advisable to aim a purification factor bigger than five [60] (also see the section Principle), we concluded to dismiss this step in further approaches.

6.4 Evaluation of ammonium sulfate precipitation

Utilization of the “salting out” method for protein purification could be traced back to around 1885 [59]. This is based on the principle that the likelihood of protein precipitation increases with increasing molecular weight [62]. Apo-ferritin has a comparably high molecular weight of 480 kDa, thus it should be possible to separate it from lighter proteins. Therefore, we tried to precipitate the whole ferritin fraction

with 50 % saturated ammonium sulfate solution, excluding most of the impurities. About 25 % more ferritin could be obtained by further increasing ammonium sulfate saturation up to 75 %. Thus, ammonium sulfate fractionation has not been the method of choice for purification purposes. This decision can be supported with the work of Russell et al., as they described an increasing precipitation probability of ferritin with increasing iron load [81]. It is highly advisable to precipitate with the highest possible ammonium sulfate concentration, since we are interested in getting insight into the iron load distribution throughout all ferritin species.

Ammonium sulfate is well known for precipitating proteins under preservation of their native states and protection of their biological activity. Furthermore, protein degradation can be avoided, as proteases also precipitate and thus have no further influence [59], [62]. Unfortunately, ammonium sulfate raises the ionic strength of the re-suspended protein solution, thereby interfering with Native-Page electrophoresis [75], even after several desalting steps by ultra-filtration. One option would have been to introduce an additional dialyzing step, but we dismissed it because it consumes much time and contributes to sample loss, so we tested protein stabilization via ammonium sulfate. As can be seen from our results (Table 16 and Table 17), ammonium sulfate had no noticeable impact ($p\sim 1$) on the final protein-/ ferritin yield, indicating that ferritin is sufficiently stable and no further stabilization agents are necessary. Hence, we decided to exclude ammonium sulfate precipitation in further approaches.

6.5 Aiming protein association and aggregation

During the method development, the Native-Page gels showed band streaking and smearing, indicating protein aggregation or association. To address this problem, we focused on parameters, like protein overload, high ionic strength, high DNA content and solid particles being present within the samples loaded in the gel pockets [75]. High ionic strength (> 50 mM ions) could be excluded as the cause, as we eliminated the ammonium sulfate precipitation step and performed several washing cycles via ultra-filtration in cases where TBS (= 150 mM NaCl) was used as buffer substance. In addition to that, we eliminated solid particles by preceding centrifugation of the applied sample. Hence, we first aimed at potentially present DNA complexes. We hypothesized that high concentrations of long DNA strands would form a complex network acting like a mesh, which impedes protein separation during electrophoresis. Therefore, we treated the samples with two different nucleases (DNase I and Benzonase®) in various amounts (4,15 - 60 U) to ensure complete fragmentation of the potentially present DNA network. Initially, both, DNase I and Benzonase® seemed to improve the band smearing problem, see Figure 17. To verify this promising result, DNase I treatment was repeated with equal and even higher amounts, but with no success. Thus, the first result was considered as being a false-positive result, with unknown cause.

Since nuclease treatment showed no effect on protein separation, we proceeded with the addition of detergents to the sample prior electrophoresis. As we hypothesized in a previous approach, some of the ferritin molecules seemed to be associated with membrane structures. Such an association could indicate the presence of hydrophobic structures. If these hydrophobic structures accompanied with some ferritin

species, got solubilized in hydrophilic environment, they would assemble to big aggregates for excluding as many water molecules as possible [50]. In order to prevent such a potential hydrophobic assembly, we added two different detergents (DDM and Digitonin) with a concentration of 1 %. However, no noticeable effect could be observed.

In the next step we provided reduced conditions during storage, by addition of 1 mM 2-mercaptoethanol. The results were promising, as ferritin molecules migrated unhindered through the Native-Page gel matrix, merging in a sharp band at appr. 480 kDa. Thus, the amount of aggregated ferritin could be reduced resulting in the formation of its monomeric state. We went a step further in the next approach, by providing not only reduced conditions during storage, but by maintaining a certain concentration of DTT through all the following purification steps. Additionally, the DTT concentration was varied to determine the maximum amount, without breaking up intramolecular disulfide-bridges. The result was again satisfying, as the higher the added DTT amount was, the more monomeric ferritin molecules could be visualized with Native-Page. This is in accordance with the research group of May et al., who could reduce the amount of aggregated protein from 54 to 13 % with increasing the amount of added DTT up to 5 mM [82]. Interestingly, the result indicated a temporal effect of the used reducing agents. The positive effect declined after several weeks (~ 4 weeks), resembling the results of previous approaches (see Figure 16 for an example). However, fresh addition of reducing agents could again produce monomeric ferritin molecules, but even higher amounts were necessary, compared to samples that were processed immediately. Since it is known, that reducing agents and chelators, such as thioglycolate, glutathione or ascorbate have the ability to solubilize the iron core of ferritin molecules in vitro [3], it was essential to test if the iron cores are effected due to the reducing agents used in our approaches. To do so, we compared samples being treated with reducing agents and a chelator (5 mM 2-mercaptoethanol, 5 mM DTT and 1 mM EDTA) with samples being untreated and evaluated them visually via TEM. No noticeable influence on the iron core structure could be observed. Thus, the reducing agents used during this master thesis either have a too low redox potential or were unable to enter the ferritin shell to directly acting on the iron core. Based on these results, we decided to increase the concentration of 2-mercaptoethanol from 1 to 5 mM as storage additive and likewise maintaining the DTT concentration at 5 mM.

6.6 Appropriate methods for determining the ferritin proportion within the sample

It is rather difficult to determine the correct ferritin amount within the samples, with a lot of other proteins present. Several reasons are given here. One approach was to measure the absorbance of each sample at 315 and 420 nm, thereby reflecting the amount of iron within the sample [83]. Eventually, the ferritin amount can be estimated by interpolation of these absorbance values with a calibration based on equine spleen- and human liver ferritin. The accuracy of this method was limited due to the fact that ferritin molecules are not equally loaded with iron, therefore samples probably have varying amounts of iron, even if the ferritin amount is the same. Furthermore, high concentrations of non-iron containing proteins also show absorption at 315 and 420 nm, even to a lower extent, as shown in Table 5. Thus, the higher the

concentration of impurities, the higher is the estimated ferritin concentration. Tissue related pigments should also be considered to interfere at this wavelength range.

Another approach aimed at a visually based, semi-quantitative determination of the ferritin proportion. Here we made use of two different electrophoresis techniques, SDS- and Native-Page, and their corresponding western blots. The use of SDS-Page enabled us to semi-quantify the amount of impurities within the tested sample. Additionally, separated protein bands should be able to be assigned to the ferritin light- and heavy-chains when compared to an appropriate reference sample (e.g. human liver- and equine spleen ferritin). In practice, other proteins possessing a similar molecular weight overlap with the ferritin bands, which makes a certain assignment and a statement about ferritin proportion almost impossible. In such a case, western blotting proved to be a suitable method. Here, we tested two different antibodies (rabbit polyclonal antibody to ferritin heavy chain from Abcam and from Bioss) to achieve highest specificity. The antibody from Abcam appeared to be the best, when used with human brain tissue samples (see Figure 25), as unspecific binding could be observed with the Bioss antibody (data not shown). However, both antibodies revealed some additional bands in case of pig brain samples (see Figure 15 for an example). Several reasons might be possible: Protein bands with molecular weights lower than expected may reflect degradation products of the ferritin heavy-chain. Or, bands that show higher molecular weight may represent various oligomeric states of the ferritin subunits (including all possible combinations of the light- and heavy-chain, even in degraded state). This would be in accordance with the work of Suryakala et al. His group showed that ferritin from different animal species can separate into more than the two common bands [28]. Nevertheless, unspecific binding of both antibodies must also be considered. Since we were interested in human brain samples, this uncertainty with pig brain samples was not further examined.

Compared to SDS-Page, the use of Native-Page electrophoresis comes along with two advantages. Ferritin bands can be specifically stained for their iron cores. This can be done with ferene-S [39] or with Prussian Blue staining [25], [29], [80]. Since we are faced with very low amounts of ferritin (~ 50 µg ferritin per g human brain tissue [11]), the sensitivity of the Prussian Blue staining protocol was enhanced with subsequent DAB treatment. In addition to that, big proteins consisting of several protein subunits are denatured during SDS-Page sample preparation. They split up into their smaller subunits covering a narrower molecular weight range than compared to their native states. Hence, the likelihood for overlapping events is higher with SDS-Page compared to Native-Page. As can be seen in Figure 16, the Coomassie Blue stained band (> 480 kDa) corresponded greatly with the brownish iron stained one, indicating that the selected band was ferritin. The capability of the Prussian Blue staining protocol for specifically staining ferritin, could be verified via western blotting. These results were really satisfying, as Prussian Blue staining (+ DAB enhancement) combines the advantages of a fast and uncomplicated Native-Page run with the specificity of western blotting.

6.7 Applicability of SEC & DGC for ferritin isolation

A big proportion of research regarding iron and its association with neurodegenerative diseases involved the isolation of ferritin from different human- and animal brain tissues [11], [19], [20], [22], [24], [26]. By considering ferritin isolation in general, regardless of the intention, most of the research groups included size exclusion chromatography in their purification procedure thereby using various column material, like Sephacryl S300 [11], [28], Sephadex G100 [4] and G200 [29], Sagavac 8F [80] and Sepharose 6B [22]–[24], [27], [29]. Apart from that, density gradient centrifugation was mostly used for investigation of ferritin`s sedimentation properties [4], [27]–[29], [82] and only one publication was found, where density gradient centrifugation was utilized for purification [30]. Since most of the purification was done with Sepharose 6B columns, we compared size exclusion chromatography with density gradient centrifugation in terms of protein separation performance.

Although protein separation through a Sepharose 6B column was the preferred purification method for many research groups, our Sepharose 6B column did not lead to a satisfying isolation of ferritin. Our protein samples separated poorly into two peaks (based on observed chromatogram, monitored at 280 nm), overlapping with each other to a big proportion, independently of applied protein amount. Thus, an exceeding of the maximum column capacity could be ruled out for being a reason. Furthermore, the peak observed with the equine ferritin reference overlapped almost completely with our sample peaks. This indicated that ferritin was distributed across all collected protein fractions, but the main proportion of ferritin should be reflected by the first peak (shown via absorption at 315 and 420 nm). These results could be verified with SDS- and Native-Page. With SDS-Page, we investigated the collected samples from the first peak in further detail, revealing that each fraction still contained impurities. However, the fractions showing the highest iron-related absorption, were pooled and concentrated to be further analyzed. Again, a big proportion of impurities smaller than 480 kDa was present in the pooled sample, as demonstrated with Native-Page.

In contrast to the size exclusion results, density gradient centrifugation was promising for ferritin isolation purpose. The monitored chromatogram (at 280 and 315 nm) showed two well separated peaks, where the ferritin fraction could be located primarily in the first peak, as shown with absorption at 315 nm. However, also the second peak had a slight elevation at exactly the same area, where the measured absorbance at 280 nm reached a maximum. That was most likely caused by the fact that highly concentrated non-iron containing proteins also show absorption at 315 nm, as described above. For verification of this initial result, the fractions from the first peak were further analyzed with SDS-Page. Here, each fraction until A12 (Figure 22; note: fractions were collected in 96-well plates) could be judged for being pure for ferritin. With this knowledge, we pooled pure ferritin fractions (= pool 1) and the remaining ones, reflecting ferritin with impurities (= initial pool 2). The second pool was forced through a filter with a molecular weight cut-off of 300 kDa, in order to further separate the remaining ferritin molecules (= new pool 2) from smaller proteins (= flow-through; should contain the main fraction of impurities). With reference to pool 1, almost all impurities being smaller than 480 kDa could be removed by density gradient centrifugation (see Figure

23, right picture). Ultra-filtration, utilizing a filter with a 300 kDa cut-off also showed the capability for isolating purely ferritin. However, most of the ferritin molecules could pass the filter, being present in the flow-through, as shown with iron staining after Native-Page electrophoresis. Thus, ultra-filtration is not suitable for isolating ferritin with high yield, at least when using a 300 kDa cut-off. It should be noted that a small proportion of ferritin molecules, presumably those with a low-iron load and thus a lower density, were excluded from the final sample (designated as pool 1), as their corresponding fractions were accompanied with impurities, even to a small amount (see Figure 22, lane B1, as example). However, density gradient centrifugation appeared to be the method of choice, as protein separation was far better as with size exclusion chromatography.

6.8 Evaluation of the final procedure & analysis of the ferritin iron load

All the results and experiences gained during the method-development with pig brains flowed into the establishment of the final purification procedure for human brain tissue. We modified the lysis buffer by reducing the Tris-HCl buffer concentration from 100 to 10 mM to minimize the possible negative effect of an uncontrolled pH decrease during heat precipitation, as discussed in subchapter 6.3. Furthermore, we provided physiological condition in the lysis buffer by addition of 150 mM NaCl in order to better stabilize the proteins. It could be shown that protein aggregation and/ or -association has a big impact on the separation process. We added further improvements concerning the avoidance of further protein aggregation and the reduction of already existing aggregates. Therefore, the sonication step was dismissed, as it is directly associated with aggregate generation and it can lead to further protein damage. We also increased the concentration 2-mercaptoethanol from 1 to 5 mM and further added 1 mM EDTA to the supernatant after heat precipitation. Providing a divalent-metal chelating agent like EDTA should further reduce the oxidative effect of free divalent metal ions, thereby acting against protein aggregation. Additionally, we added 5 mM DTT for stabilization of ferritin`s monomeric state, as 2-mercaptomethanol was washed out during ultra-filtration.

The results of the final purification procedure resembled those of the last approach concerning pig brain samples. Apparently, the above described modifications went in the right direction, as much more ferritin could be isolated than out of pig brains. However, natural differences in the ferritin amount between human- and pig brain tissue should also be considered. The higher amount of ferritin was demonstrated by a 10 times higher absorbance value at 315 nm, reflecting the iron content of the sample. In addition to that, fractions from the first peak, separated by SDS-Page electrophoresis, showed even more intense ferritin bands than compared to the pig brain tissue. However, an unknown band accompanied the two ferritin subunits, exceeding the molecular weight range of the molecular weight standard used. Since we also observed an additional band in the pooled samples with Native-Page (located between 1048 - 1236 or above 1236 kDa, depending on the storage time of the tissue sample), it was initially concluded that these bands reflect impurities of more than twice the size of ferritin. However, as can be seen in Figure 27, in the negative stained sample no proteins bigger than ferritin could be observed. Nevertheless, some smaller molecules were found that could be degradation products of ferritins as their shapes resemble

fragments of ferritin. Such fragments could aggregate in Native-Page conditions and thus form the high molecular weight bands. This would also explain the dependency of the determined molecular weights on storage duration (samples from the same month had a similar band pattern), as ferritin might be further degraded over time, even at - 20 °C. Hence, the storage conditions should be adjusted to - 80 °C, as done by other research groups working with brain tissue [11], [22], [24], [26]. Apparently, this ferritin degradation process did not concern the subunits per se, as smaller, degraded subunits could not be detected with SDS-Page. Thus, only partially dissociation of native ferritin molecules remained possible. The high molecular weight band observed with SDS-Page seemed to be un-denatured ferritin, which might be explained by their considerably high stability against various denaturizing agents [33], [37]. Overall, about 50 µg per g human brain tissue could be yielded with our purification procedure, which is in good agreement with the results of Fleming et al. [11].

Once we had enough pure ferritin, the sample could be further investigated with electron microscopic techniques (bright field imaging of native and negative stained samples). As mentioned above, the samples seemed pure when negatively stained and viewed under TEM. However, bright field imaging of unstained samples revealed that the samples are presumably contaminated with glycerin from the density gradient centrifugation, leading to the formation of lipid droplets on the sample grids. In order to avoid remaining glycerin within the protein samples, it is highly recommended to add more washing steps during ultra-filtration. Nevertheless, the sample quality was good enough for geometrical classification of the iron cores according to the definition of Jian et al. [57]. For the next step, the iron cores were automatically identified by using the CellProfiler™ program, an automatic detection system that saves time and enables further statistical evaluation of the ferritin`s iron load distribution. It should be noted however that every automatic detection is accompanied with limitations: first, the accuracy of the detection depends on properly set thresholds. Next, as can be seen in Figure 28, the background of our samples was not evenly structured in terms of grey values. Hence, in some cases it was difficult for the software to set the boundaries of the objects correctly and to distinguish between the background and a beginning object, especially in cases when ferritin molecules were loaded with a low amount of iron (less electron dense). Additionally, the lipid droplets detected in the sample contributed to a more irregular background, and only a small proportion of these droplets could be removed during image analysis using the CellProfiler™ program. Further problems were the overlapping of iron cores and sensor related artefacts. When iron cores overlapped, they appeared fused and were excluded from the object analysis because they exceeded the size limit. In the other cases, the “unevenly”-background would mimic the grey value of ferritin iron cores and therefore being identified as iron cores, which would lead to a false-positive result. Another point that should be mentioned for a proper evaluation is that we set a somewhat arbitrary cut-off for identification of iron cores of 2 nm in diameter. All these limitations under consideration, the CellProfiler™ software did a great job in identifying ferritin iron cores.

Based on the results, the ferritin molecules from the occipital cortex seemed to be more iron loaded than from the frontal cortex. We measured a higher mean-maximum and -minimum iron core diameter of 5,2 and 3,6 nm compared to 4,8 and 3,3 nm. Friedman et al. showed that human liver ferritin stores iron cores with a mean-diameter of 6 - 6,5 nm, while ferritin isolated from substantia nigra, globus pallidus and hippocampal cortex possess smaller iron cores, with mean-diameters ranging from 3,1 - 3,7 nm, based on measured maximum-diameter [19], [20]. This discrepancy can be explained by our defined cut-off of 2 nm, thereby excluding all iron cores being smaller. The usage of high-resolution electron microscopy would help for properly identification of even the smallest iron cores. Moreover, false-positive identifications related to electron dense pollution could be prevented by analyzing with energy filtered transmission electron microscopy (EFTEM). EFTEM enables for viewing only the iron atoms related information, thereby blending out possible false-positive objects. Another point contributing to this discrepancy can be found in the purification itself. Since we aimed for highest purity in the pooled ferritin samples, a small proportion was excluded from further analysis due to protein pollution. This should especially concern the lightest ferritin species (with low iron content or even missing iron core), as the fractions of lower glycerin density were found to be polluted and excluded from the analysis (see DGC results, Figure 25).

6.9 Conclusion & Outlook

The purification procedure established during this master thesis provides a fast and efficient method for isolating ferritin out of human brain tissue. Isolated ferritin was proved to be suitable for a TEM analysis with high reliability in combination with the CellProfiler™ program, which enables time efficient iron core identification, count, and geometric measurements. However, even though we could isolate almost the whole ferritin population with only one density gradient centrifugation run, the lightest ferritin species were excluded, due to protein pollution. It should be tested if a low amount of impurities would impair automatic identification of ferritin iron cores with particle analysis software. There is also still potential for optimizing the density gradient for a better separation. Moreover, the pixel resolution of the EM images prevented us from detecting particles smaller than 2 nm with certainty. This could be circumvented by using high-resolution electron microscopic techniques.

When the method is optimized towards complete isolation of ferritin or an independent identification of its iron core, different brain regions, especially those which are associated with neurodegenerative diseases, could be compared for their ferritin iron load distribution. Once enough information of the healthy control is available, the results can be compared with AD samples by comparing specimens of different Braak stages.

Bibliography

[1] G. Cairo, F. Bernuzzi, and S. Recalcati, “A precious metal: Iron, an essential nutrient for all cells,” *Genes Nutr.*, vol. 1, no. 1, pp. 25–39, Mar. 2006.

[2] B. Silva and P. Faustino, “An overview of molecular basis of iron metabolism regulation and the associated pathologies,” *Biochim. Biophys. Acta - Mol. Basis Dis.*, vol. 1852, no. 7, pp. 1347–1359, Jul. 2015.

[3] A. La *et al.*, “Mobilization of iron from ferritin: new steps and details,” *Metallomics*, vol. 10, no. 1, pp. 154–168, Jan. 2018.

[4] D. J. Price and J. G. Joshi, “Ferritin. Binding of beryllium and other divalent metal ions.,” *J. Biol. Chem.*, vol. 258, no. 18, pp. 10873–80, Sep. 1983.

[5] M. C. Linder, “Mobilization of stored iron in mammals: a review.,” *Nutrients*, vol. 5, no. 10, pp. 4022–50, Oct. 2013.

[6] A. Sfera, K. Bullock, A. Price, L. Inderias, and C. Osorio, “Ferrosenescence: The iron age of neurodegeneration?,” *Mech. Ageing Dev.*, vol. 174, pp. 63–75, Sep. 2018.

[7] M. K. Georgieff, “The role of iron in neurodevelopment: fetal iron deficiency and the developing hippocampus.,” *Biochem. Soc. Trans.*, vol. 36, no. Pt 6, pp. 1267–71, Dec. 2008.

[8] B. Todorich, J. M. Pasquini, C. I. Garcia, P. M. Paez, and J. R. Connor, “Oligodendrocytes and myelination: The role of iron,” *Glia*, vol. 57, no. 5, pp. 467–478, Apr. 2009.

[9] B. Hallgren and P. Sourander, “THE EFFECT OF AGE ON THE NON-HAEMIN IRON IN THE HUMAN BRAIN,” *J. Neurochem.*, vol. 3, no. 1, pp. 41–51, Oct. 1958.

[10] P. Hogarth, “Neurodegeneration with brain iron accumulation: diagnosis and management.,” *J. Mov. Disord.*, vol. 8, no. 1, pp. 1–13, Jan. 2015.

[11] J. Fleming and J. G. Joshi, “Ferritin: isolation of aluminum-ferritin complex from brain.,” *Proc. Natl. Acad. Sci. U. S. A.*, vol. 84, no. 22, pp. 7866–70, Nov. 1987.

[12] D. F. Wallace, “The Regulation of Iron Absorption and Homeostasis.,” *Clin. Biochem. Rev.*, vol. 37, no. 2, pp. 51–62, May 2016.

[13] Y. Funauchi *et al.*, “Regulation of iron homeostasis by the p53-ISCU pathway.,” *Sci. Rep.*, vol. 5, p. 16497, Nov. 2015.

[14] N. Singh *et al.*, “Brain Iron Homeostasis: From Molecular Mechanisms To Clinical Significance and Therapeutic Opportunities,” *Antioxid. Redox Signal.*, vol. 20, no. 8, pp. 1324–1363, Mar. 2014.

[15] M. Mehlenbacher *et al.*, “Iron Oxidation and Core Formation in Recombinant Heteropolymeric Human Ferritins,” *Biochemistry*, vol. 56, no. 30, pp. 3900–3912, Aug. 2017.

[16] Y.-H. Pan *et al.*, “3D morphology of the human hepatic ferritin mineral core: New evidence for a subunit structure revealed by single particle analysis of HAADF-STEM images,” *J. Struct. Biol.*, vol. 166, no. 1, pp. 22–31, Apr. 2009.

[17] C. Pozzi, F. Di Pisa, C. Bernacchioni, S. Ciambellotti, P. Turano, and S. Mangani, “Iron binding to human heavy-chain ferritin,” *Acta Crystallogr. Sect. D Biol. Crystallogr.*, vol. 71, no. 9, pp. 1909–1920, Sep. 2015.

[18] A. Treffry *et al.*, "Defining the roles of the threefold channels in iron uptake, iron oxidation and iron-core formation in ferritin: a study aided by site-directed mutagenesis.," *Biochem. J.*, vol. 296 (Pt 3), pp. 721–8, Dec. 1993.

[19] A. Friedman, P. Arosio, D. Finazzi, D. Koziorowski, and J. Galazka-Friedman, "Ferritin as an important player in neurodegeneration," *Parkinsonism Relat. Disord.*, vol. 17, no. 6, pp. 423–430, Jul. 2011.

[20] J. Galazka-Friedman, E. R. Bauminger, K. Szlachta, and A. Friedman, "The role of iron in neurodegeneration—Mössbauer spectroscopy, electron microscopy, enzyme-linked immunosorbent assay and neuroimaging studies," *J. Phys. Condens. Matter*, vol. 24, no. 24, p. 244106, Jun. 2012.

[21] M. C. Linder and H. N. Munro, "Metabolic and chemical features of ferritins, a series of iron-inducible tissue proteins.," *Am. J. Pathol.*, vol. 72, no. 2, pp. 263–82, Aug. 1973.

[22] D. J. Dedman *et al.*, "Iron and aluminium in relation to brain ferritin in normal individuals and Alzheimer's-disease and chronic renal-dialysis patients.," *Biochem. J.*, vol. 287 (Pt 2), no. 2, pp. 509–14, Oct. 1992.

[23] P. Arosio, T. G. Adelman, and J. W. Drysdale, "On ferritin heterogeneity. Further evidence for heteropolymers.," *J. Biol. Chem.*, vol. 253, no. 12, pp. 4451–8, Jun. 1978.

[24] T. Sakamoto, Y. Ogasawara, K. Ishii, H. Takahashi, and S. Tanabe, "Accumulation of aluminum in ferritin isolated from rat brain," *Neurosci. Lett.*, vol. 366, no. 3, pp. 264–267, Aug. 2004.

[25] B. E. Cham, H. P. Roeser, A. Nikles, and K. Ridgway, "A procedure for the purification of ferritin from human liver by heating a methanol-treated homogenate," *Anal. Biochem.*, vol. 151, no. 2, pp. 561–565, Dec. 1985.

[26] L. Bossoni *et al.*, "Human-brain ferritin studied by muon spin rotation: a pilot study," *J. Phys. Condens. Matter*, vol. 29, no. 41, p. 415801, Oct. 2017.

[27] A. Bomford, C. Conlon-Hollingshead, and H. N. Munro, "Adaptive responses of rat tissue isoferritins to iron administration. Changes in subunit synthesis, isoferritin abundance, and capacity for iron storage.," *J. Biol. Chem.*, vol. 256, no. 2, pp. 948–55, Jan. 1981.

[28] S. Suryakala and V. Deshpande, "Purification and Characterization of Liver Ferritins from Different Animal Species," *Vet. Res. Commun.*, vol. 23, no. 3, pp. 165–181, 1999.

[29] M. Worwood, W. Aherne, S. Dawkins, and A. Jacobs, "The characteristics of ferritin from human tissues, serum and blood cells.," *Clin. Sci. Mol. Med.*, vol. 48, no. 5, pp. 441–51, May 1975.

[30] J. J. Winzerling, P. Nez, J. Porath, and J. H. Law, "Rapid and efficient isolation of transferrin and ferritin from Manduca sexta," *Insect Biochem. Mol. Biol.*, vol. 25, no. 2, pp. 217–224, Feb. 1995.

[31] B. S. Kim, C. S. Lee, C. Y. Yun, S. M. Yeo, W. M. Park, and H. R. Kim, "Characterization and immunological analysis of ferritin from the hemolymph of Galleria mellonella.," *Comp. Biochem. Physiol. A. Mol. Integr. Physiol.*, vol. 129, no. 2–3, pp. 501–9, Jun. 2001.

[32] S. Stefanini *et al.*, "Thermal Stability of Horse Spleen Apoferritin and Human Recombinant H Apoferritin," *Arch. Biochem. Biophys.*, vol. 325, no. 1, pp. 58–64, Jan. 1996.

[33] P. Santambrogio *et al.*, "Evidence that a salt bridge in the light chain contributes to the physical stability difference between heavy and light human ferritins.," *J. Biol. Chem.*, vol. 267, no. 20, pp. 14077–83, Jul. 1992.

[34] M. Kim *et al.*, "pH-Dependent Structures of Ferritin and Apoferritin in Solution: Disassembly and

Reassembly," *Biomacromolecules*, vol. 12, no. 5, pp. 1629–1640, May 2011.

[35] A. MAZUR, I. LITT, and E. SHORR, "Chemical properties of ferritin and their relation to its vasodepressor activity.," *J. Biol. Chem.*, vol. 187, no. 2, pp. 473–84, Dec. 1950.

[36] R. R. Crichton and C. F. Bryce, "Subunit interactions in horse spleen apoferritin. Dissociation by extremes of pH.," *Biochem. J.*, vol. 133, no. 2, pp. 289–99, Jun. 1973.

[37] I. Listowsky, G. Blauer, S. Englard, and J. J. Betheil, "Denaturation of horse spleen ferritin in aqueous guanidinium chloride solutions," *Biochemistry*, vol. 11, no. 11, pp. 2176–2182, May 1972.

[38] P. Wang *et al.*, "Mitochondrial Ferritin Deletion Exacerbates β-Amyloid-Induced Neurotoxicity in Mice," *Oxid. Med. Cell. Longev.*, vol. 2017, pp. 1–10, 2017.

[39] D. Fei *et al.*, "Isolation of ferritin and its interaction with BmNPV in the silkworm, Bombyx mori," *Dev. Comp. Immunol.*, vol. 86, pp. 130–137, Sep. 2018.

[40] L. A. Cohen *et al.*, "Serum ferritin is derived primarily from macrophages through a nonclassical secretory pathway," *Blood*, vol. 116, no. 9, pp. 1574–1584, Sep. 2010.

[41] "Human iron metabolism," 2015. [Online]. Available: https://en.wikipedia.org/wiki/Human_iron_metabolism. [Accessed: 15-Jan-2019].

[42] D. Gelvan, E. Fibach, E. G. Meyron-Holtz, and A. M. Konijn, "Ferritin uptake by human erythroid precursors is a regulated iron uptake pathway.," *Blood*, vol. 88, no. 8, pp. 3200–7, Oct. 1996.

[43] M. Gryzik *et al.*, "Expression and characterization of the ferritin binding domain of Nuclear Receptor Coactivator-4 (NCOA4)," *Biochim. Biophys. Acta - Gen. Subj.*, vol. 1861, no. 11, pp. 2710–2716, Nov. 2017.

[44] N. Abbaspour, R. Hurrell, and R. Kelishadi, "Review on iron and its importance for human health.," *J. Res. Med. Sci.*, vol. 19, no. 2, pp. 164–74, Feb. 2014.

[45] D. H. Manz, N. L. Blanchette, B. T. Paul, F. M. Torti, and S. V. Torti, "Iron and cancer: recent insights," *Ann. N. Y. Acad. Sci.*, vol. 1368, no. 1, pp. 149–161, Mar. 2016.

[46] I. G. Mollet *et al.*, "Low Dose Iron Treatments Induce a DNA Damage Response in Human Endothelial Cells within Minutes," *PLoS One*, vol. 11, no. 2, p. e0147990, Feb. 2016.

[47] J. Shen *et al.*, "Iron Metabolism Regulates p53 Signaling through Direct Heme-p53 Interaction and Modulation of p53 Localization, Stability, and Function," *Cell Rep.*, vol. 7, no. 1, pp. 180–193, Apr. 2014.

[48] Á. Sturm, Z. Ivics, and T. Vellai, "The mechanism of ageing: primary role of transposable elements in genome disintegration," *Cell. Mol. Life Sci.*, vol. 72, no. 10, pp. 1839–1847, May 2015.

[49] W. C. Orr, "Tightening the connection between transposable element mobilization and aging," *Proc. Natl. Acad. Sci.*, vol. 113, no. 40, pp. 11069–11070, Oct. 2016.

[50] H. Lodish *et al.*, *Molecular Cell Biology*, 8th Ed. New York: W. H. Freeman and Company, 2016.

[51] S. Paillusson *et al.*, "There's Something Wrong with my MAM; the ER–Mitochondria Axis and Neurodegenerative Diseases," *Trends Neurosci.*, vol. 39, no. 3, pp. 146–157, Mar. 2016.

[52] G. Premasekharan, K. Nguyen, J. Contreras, V. Ramon, V. J. Leppert, and H. J. Forman, "Iron-mediated lipid peroxidation and lipid raft disruption in low-dose silica-induced macrophage cytokine production," *Free*

Radic. Biol. Med., vol. 51, no. 6, pp. 1184–1194, Sep. 2011.

[53] J. Wong-ekkabut, Z. Xu, W. Triampo, I.-M. Tang, D. Peter Tieleman, and L. Monticelli, "Effect of Lipid Peroxidation on the Properties of Lipid Bilayers: A Molecular Dynamics Study," *Biophys. J.*, vol. 93, no. 12, pp. 4225–4236, Dec. 2007.

[54] J.-H. Park, J. Zhuang, J. Li, and P. M. Hwang, "p53 as guardian of the mitochondrial genome," *FEBS Lett.*, vol. 590, no. 7, pp. 924–934, Apr. 2016.

[55] L. Buizza *et al.*, "Conformational Altered p53 as an Early Marker of Oxidative Stress in Alzheimer's Disease," *PLoS One*, vol. 7, no. 1, p. e29789, Jan. 2012.

[56] P. Davalli, T. Mitic, A. Caporali, A. Lauriola, and D. D'Arca, "ROS, Cell Senescence, and Novel Molecular Mechanisms in Aging and Age-Related Diseases," *Oxid. Med. Cell. Longev.*, vol. 2016, pp. 1–18, 2016.

[57] N. Jian, M. Dowle, R. D. Horniblow, C. Tselepis, and R. E. Palmer, "Morphology of the ferritin iron core by aberration corrected scanning transmission electron microscopy," *Nanotechnology*, vol. 27, no. 46, p. 46LT02, Nov. 2016.

[58] D. W. Burden, "Guide to Homogenization of Biological Samples," *Random Prim.*, 2008.

[59] F. Lottspeich, "Protein Purification," in *Bioanalytics: Analytical Methods and Concepts in Biochemistry and Molecular Biology*, F. Lottspeich and J. Engels, Eds. Weinheim: Wiley-VCH Verlag, 2018, pp. 1–22.

[60] H. Rehm and T. Letzel, *Der Experimentator: Proteinbiochemie/ Proteomics*, 7. Auflage. Berlin, Heidelberg: Springer Verlag, 2016.

[61] GE Healthcare, "Strategies for Protein Purification: Handbook," *GE Healthc.*, 2010.

[62] P. Wingfield, "Protein precipitation using ammonium sulfate.," *Curr. Protoc. protein Sci.*, vol. Appendix 3, p. Appendix 3F, May 2001.

[63] R. Boysen, "Chromatographic Separation Methods," in *Bioanalytics: Analytical Methods and Concepts in Biochemistry and Molecular Biology*, F. Lottspeich and J. Engels, Eds. Weinheim: Wiley-VCH Verlag, 2018, pp. 219–242.

[64] E. Rodahl, "Ultracentrifugation," *Encyclopedia of Immunology*. Elsevier Ltd., pp. 2446–2448, 1998.

[65] L. Fischer and T. Stressler, "Protein determination," in *Bioanalytics: Analytical Methods and Concepts in Biochemistry and Molecular Biology*, F. Lottspeich and J. Engels, Eds. Weinheim: Wiley-VCH Verlag, 2018, pp. 23–34.

[66] R. Westermeier and A. Görg, "Electrophoretic Techniques," in *Bioanalytics: Analytical Methods and Concepts in Biochemistry and Molecular Biology*, F. Lottspeich and J. Engels, Eds. Weinheim: Wiley-VCH Verlag, 2018, pp. 243–274.

[67] H. Schägger and G. von Jagow, "Blue native electrophoresis for isolation of membrane protein complexes in enzymatically active form," *Anal. Biochem.*, vol. 199, no. 2, pp. 223–231, Dec. 1991.

[68] T. Mahmood and P.-C. Yang, "Western blot: technique, theory, and trouble shooting," *N. Am. J. Med. Sci.*, vol. 4, no. 9, pp. 429–34, Sep. 2012.

[69] E. C. Jensen, "The Basics of Western Blotting," *Anat. Rec. Adv. Integr. Anat. Evol. Biol.*, vol. 295, no. 3, pp. 369–371, Mar. 2012.

[70] R. P. Linke, “Immunological Techniques,” in *Bioanalytics: Analytical Methods and Concepts in Biochemistry and Molecular Biology*, F. Lottspeich and J. Engels, Eds. Weinheim: Wiley-VCH Verlag, 2018, pp. 63–106.

[71] H. Engelhardt, “Electron Microscopy,” in *Bioanalytics: Analytical Methods and Concepts in Biochemistry and Molecular Biology*, F. Lottspeich and J. Engels, Eds. Weinheim: Wiley-VCH Verlag, 2018, pp. 485–518.

[72] S. Aryal, “Differences between Light Microscope and Electron Microscope,” 2015. [Online]. Available: https://microbiologyinfo.com/differences-between-light-microscope-and-electron-microscope/. [Accessed: 06-Jan-2019].

[73] S. De Carlo and J. R. Harris, “Negative staining and cryo-negative staining of macromolecules and viruses for TEM,” *Micron*, vol. 42, no. 2, pp. 117–131, Feb. 2011.

[74] “Ammonium Sulfate Calculator from EnCor Biotechnology Inc.,” 2018. [Online]. Available: http://www.encorbio.com/protocols/AM-SO4.htm. [Accessed: 30-Mar-2018].

[75] “NativePAGE™ Novex® Bis-Tris Gel System: A system for native gel electrophoresis,” Carlsbad, 25-0894, 2012.

[76] E. Wiberg, N. Wiberg, and A. F. Holleman, *Inorganic chemistry*. San Diego, Berlin, New York: Academic Press, 2001.

[77] P. B. Stathopulos, G. A. Scholz, Y.-M. Hwang, J. A. O. Rumfeldt, J. R. Lepock, and E. M. Meiering, “Sonication of proteins causes formation of aggregates that resemble amyloid,” *Protein Sci.*, vol. 13, no. 11, pp. 3017–3027, Dec. 2008.

[78] “ProductInformation: Deoxyribonuclease I from Bovine Pancreas,” Saint Louis, 98–CKV, 2005.

[79] N. E. Good, G. D. Winget, W. Winter, T. N. Connolly, S. Izawa, and R. M. Singh, “Hydrogen ion buffers for biological research.,” *Biochemistry*, vol. 5, no. 2, pp. 467–77, Feb. 1966.

[80] G. Nardi, E. O. Muzii, and M. Puca, “Ferritin in the hepatopancreas of octopus vulgaris Lam.,” *Comp. Biochem. Physiol. Part B Comp. Biochem.*, vol. 40, no. 1, pp. 199–202, Sep. 1971.

[81] S. M. Russell and P. M. Harrison, “Heterogeneity in horse ferritins. A comparative study of surface charge, iron content and kinetics of iron uptake.,” *Biochem. J.*, vol. 175, no. 1, pp. 91–104, Oct. 1978.

[82] C. A. May, J. K. Grady, T. M. Laue, M. Poli, P. Arosio, and N. D. Chasteen, “The sedimentation properties of ferritins. New insights and analysis of methods of nanoparticle preparation.,” *Biochim. Biophys. Acta*, vol. 1800, no. 8, pp. 858–70, Aug. 2010.

[83] S. Bejjani, R. Pullakhandam, R. Punjal, and K. M. Nair, “Gastric digestion of pea ferritin and modulation of its iron bioavailability by ascorbic and phytic acids in caco-2 cells.,” *World J. Gastroenterol.*, vol. 13, no. 14, pp. 2083–8, Apr. 2007.

Appendix

Table 19. Overview about used chemicals

Chemical	Company	Identification Number
Homogenization		
Tris(hydroxymethyl)aminomethane	Merck	1.08382.2500
Sodium chloride	Merck	1.06404.1000
Protease inhibitor cocktail set III, EDTA-free - Calbiochem	Merck	Cat. No. 539134
Heat-, Acidic- & Ammonium sulfate precipitation		
Methanol ≥99,9 %	Roth	Art. No. 4627.5
Citric acid monohydrate	Merck	1.00244.1000
Ammonium sulfate	Merck	Art. No. 1217
Size Exclusion Chromatography & Density Gradient Centrifugation		
Sepharose CL-6B		
Sodium dihydrogen phosphate monohydrate	Merck	1.06346.1000
di-Sodium hydrogen phosphate dodecahydrate	Merck	1.06579.1000
Tris(hydroxymethyl)aminomethane	Merck	1.08382.2500
Sodium chloride	Merck	1.06404.1000
Glycerin 86 %	Lactan	-
NanoDrop® measurement & Lowry Assay		
Albumine Bovine Serum	VWR Chemicals	Prod. No. 421501J
Native human ferritin from liver	Bio-Rad	4420-4804
Ferritin from equine spleen, type I, saline solution	Sigma	F4503
Solution A: 2 % Na_2CO_3 in 0,1 M NaOH		
Solution B: 1 % $CuSO_4$ * 5 H_2O		
Solution C: 2 % $KNOC_4H_4O_8$ * 4 H_2O		
Folin Ciocalteu`s phenol reagent	Merck	1.09001.0500
Electrophoresis		
NuPAGE® LDS Sample Buffer (4x)	Invitrogen	Cat. No. NP0007
NuPAGE® Sample Reducing Agent (10x)	Invitrogen	Cat. No. NP0009
NativePAGE™ 4x Sample Buffer	Invitrogen	Part. No. BN20032
NativePAGE™ 5 % G-250 Sample Additive	Invitrogen	Part. No. BN20041
10 % DDM	Invitrogen	Part. No. BN20051
5 % Digitonin	Invitrogen	Part. No. BN20061
Trichloroacetic acid ≥99,0 %	Merck	Cat. No. T6399
Tris(hydroxymethyl)aminomethane	Merck	1.08382.2500

NuPAGE® MES SDS Running Buffer (20x)	Novex by life technologies	Cat. No. NP0002
NativePAGE™ 20x Running Buffer	Novex by life technologies	Cat. No. BN2001
NativePAGE™ 20x Cathode Buffer Additive	Invitrogen	Cat. No. BN2002
NuPAGE™ 4-12 % Bis-Tris Gel, 1,0mm * 10 well	Invitrogen	Cat. No. NP0321BOX
NativePAGE™ 3-12 % Bis-Tris Gel, 1,0mm * 10 well	Invitrogen	Cat. No. BN2011BX10
PageRuler™ Plus Prestained Protein Ladder	Thermo Scientific	Product# 26619
NativeMark™ Unstained Protein Standard	Invitrogen	Cat. No. LC0725
MagicMark™ XP Western Standard	Invitrogen	Cat. No. LC5603
SimplyBlue™ SafeStain	Invitrogen	Cat. No. LC6060
Potassium ferricyanide (II)	Merck	339A754584
Hydrochloric acid 37 %	Roth	Art. No. X942.1
3,3`-Diaminobenzidine tetrahydrochloride hydrate	Sigma	D5637
Hydrogen peroxide 30 %	Merck	1.07210.0250
WesternBlotting		
NuPAGE® Transfer Buffer (20x)	Novex by life technologies	Cat. No. NP0006-1
Methanol ≥99,9 %	Roth	Art. No. 4627.5
Ponceau S solution	Sigma	P7170
Acetic acid glacial 100 %	Merck	913K11680363
Powdered milk, blotting grade	Roth	Art. No. T145.2
Tris(hydroxymethyl)aminomethane	Merck	1.08382.2500
Sodium chloride	Merck	1.06404.1000
Tween® 20	Merck	8.22184.0500
Rabbit polyclonal Antibody to Ferritin Heavy Chain	Abcam	ab81444
Rabbit polyclonal Antibody to Ferritin Heavy Chain	Bioss	bs-5907R
Goat Anti-Rabbit IgG (H+L)-HRP Conjugate	Bio-Rad	Cat. No. 170-6515
WesternBright™ Quantum	Advansta	R-03026-C10
WesternBright™ Peroxidase	Advansta	R-03025-C10
Restore™ Western Blot Stripping Buffer	Thermo Scientific	Cat. No. 21059
DNase, Reducing- & Chelating Agents		
DNase I from Bovine Pancreas	Sigma	D4513
Benzonase® Nuclease	ChemCruz	Sc-202391
2-mercaptoethanol 99 %	Roth	Art. No. 4227.1
DL-Dithiothreitol ≥ 98 %	Sigma	D0632
Ethylenedinitrilotetraacetic acid, disodium salt	Merck	1.08418.0250

Table 20. Overview about used devices and material

Device or Material	Company	Designation
Homogenization		
Ultra-Turrax®	IKA® Labortechnik	T10 basic
Sonifier 250	Branson	250 W output
Sonication probe	Branson	102C
Heat-, Acidic- & Ammonium sulfate precipitation		
Heating plate	IKA® Labortechnik	Typ RET
pH-Meter	Mettler Toledo	SevenMulti
Size Exclusion Chromatography & Density Gradient Centrifugation		
fraction collector	ISCO	Foxy Jr.
UV/ VIS detector	ISCO	UA-6
96-well deep well plates	Ritter	riplate® SW
NanoDrop® measurement & Lowry Assay		
NanoDrop® Spectrophotometer	Peqlab, Biotechnology GmbH	ND-1000
Plate reader	Anthos	2010
96-well plates	Thermo Scientific	Nunclon™ Delta Surface
Electrophoresis & Western Blotting		
Thermomixer	Eppendorf	compact
Power-supply	Bio-Rad	PowerPac™ HC, 300 W
Power-supply	Consort	EV231
Transfer tank	Bio-Rad	Mini Protean II™
Blotting Filter Paper, 2,5 mm thick	Invitrogen	Cat. No. LC2008
Nitrocellulose Blotting Membrane, Amersham™ Protan™, 0,45 µm	GE Healthcare Life science	Cat. No. 10600002
PVDF/ Filter Paper, 0,45 µm	Invitrogen	Cat. No. LC2007
Plate-shaker	Heidolph	Polymax 2040
FluorChem® Q	Alpha Innotech	MultiImage® III
Bright Field Imaging & Negative Staining		
transmission electron microscope	Fei company	Tecnai G20
grids	EMResolutions	400 mesh Copper with carbon film
Glow discharger	Pelco	easiGlow, Model 91000
Centrifugation, Scales, etc.		
Centrifuge	Beckman	Avanti™ 30
Fixed-Angle Rotor	Beckman	C0650
Fixed-Angle Rotor	Beckman	C1015
Ultracentrifuge	Beckman	Optima™ LE-80K
Swinging-Bucket Rotor	Beckman	SW45Ti
scale	Kern	GS, d= 0,01 g
Analytical scale	Sartorius	Secura, d= 0,01 mg